Heterologous production and characterization of selected G-protein-coupled receptors and G-proteins for structural and functional studies

Dissertation

zur Erlangung des Doktorgrades der Naturwissenschaften

vorgelegt beim Fachbereich 14 für Biochemie, Chemie und Pharmazie
der Johann Wolfgang Goethe-Universität
in Frankfurt am Main

von
Aditya Prasad Patra

aus Konark, Indien

Frankfurt am Main, 2023
(D30*)*

vom Fachbereich 14 für Biochemie, Chemie und Pharmazie der Johann Wolfgang Goethe-Universität als Dissertation angenommen

Dekan: Prof. Dr. Clemens Glaubitz

Gutachter: Prof. Dr. Clemens Glaubitz

Gutachter: Prof. Dr. Dr. h.c. Hartmut Michel

Datum der Disputation:

Diese Dissertation wurde unter der Leitung von Prof. Dr. Dr. h.c. Hartmut Michel in der Abteilung Molekulare Membranbiologie am Max Planck Institut für Biophysik in Frankfurt am Main bis Februar 2023 durchgeführt.

Eidesstattliche Erklärung

Hiermit versichere ich, dass ich die vorliegende Arbeit selbstständig angefertigt und keine anderen, als die angegebenen Hilfsmittel und Quellen verwendet habe.

_____

(Aditya Prasad Patra)

Frankfurt am Main, den ……

TABLE OF CONTENTS

.

List of abbreviation

Ab	antibody	DDM	n-dodecyl-β-D-maltoside
ACE	angiotensin-converting enzyme	Dntp	deoxyribonucleoside
ACEIs	angiotensin-converting enzyme inhibitors	Dpm	decays per minute
		DQ-SQ	double quantum-single quantum
AcP	acetyl phosphate	DTT	dithiothreitol
ATP	adenosine-5‘-triphosphate	ECL	extracellular loop
AP	alkaline phosphatase	EDTA	ethylenediamine-tetra-acetate
βMe	β-mercaptoethanol	ERK	extracellular-signal-regulated kinase
B1 R	bradykinin 1 receptor	E64	(1S,2S)-2-(((S)-1-((4 Guanidinobutyl)amino)-4 methyl-1- oxopentan-2yl)carbamoyl) cyclo propanecarboxylic acid
B2 R	bradykinin 2 receptor		
BCIP	5-bromo-4-chloro-3-indolyl phosphate		
BCA	bicinchoninic acid		
Bmax	maximal binding	Fos12	fos choline-12
BSA	bovine serum albumin	FBS	fetal bovine serum
BN-PAGE	blue native- polyacrylamide gel electrophoresis	FDI	free induction decay
		FDA	food and drug administration
cAMP	cyclic adenosine monophosphate	FM	feeding mix
CaSR	calcium-sensing receptor	GDP	guanosine diphosphate
cDNA	complementary deoxyribonucleic acid	G_{α}	α subunit of heterotrimeric G-protein
CHS	cholesteryl hemisuccinate	G_{β}	β subunit of heterotrimeric G-protein
CMC	critical micellar concentration		
CsA	chemical shift anisotropy	G_{γ}	γ subunit of heterotrimeric G-protein
CTP	cytidine-5‘- triphosphate		
CV	column volume	GIRK	G protein-coupled inwardly-rectifying potassium channel
DAG	diacylglycerol		
DAKD	desArg10 -kallidin	GPCR	G protein-coupled receptor
DALK	desArg10 -Leu 9 -kallidin	G-protein	Guanine nucleotide binding protein
DDM	n-dodecyl ß-D-maltoside		
DEER	double electron-electron resonance	GRK	G protein receptor kinase
DHB	2,5-dihydroxybenzoic acid	GTP	guanosine-5‘-triphosphate
DMF	dimethylformamide	Hepes	4-(2-hydroxyethyl)-1-piperazineethanesulfonic acid
DMSO	dimethyl sulfoxide		
DNA	deoxyribonucleic acid		
DNP	dynamic nuclear polarization		
DM	n-decyl-β-D-maltoside		

ICL	intracellular loop	PCR	polymerase chain reaction
IMAC	immobilized metal ion affinity chromatography	PDB	protein data bank
		PEG	polyethylene glycol
IP 3	inositol-1,4,5-triphosphate	PEI	polyethylenimine
IPTG	isopropyl-ß-D-1-thiogalactopyranoside	Pfu	plaque forming units
KD	dissociation constant	PKC	proteinkinase C
KDa	kiloDalton	PLC	phospholipase C
Kan	kanamycin	PMSF	phenylmethylsulfonyl fluoride
K_I	inhibition constant	PVDF	polyvinylidene fluoride
LB	Luria Broth medium	Rmsd	root mean square deviation
MALDI-TOF	matrix-assisted laser desorption ionisation-time of flight	Rpm	rounds per minute
		RT	room temperature
MALS	multiangle light scattering	SDS	sodium dodecylsulfate
MAP	mitogen-activated protein	Sf 9	spodoptera frugiperda cell line 9
MAS	magic angle spinning	ssNMR	solid state nuclear magnetic resonance spectroscopy
MD	molecular dynamics		
MES	2-(N-morpholino)ethanesulfonic acid	SMA	styrene-maleic anhydride
MOI	multiplicity of infection	SPA	single particle analysis
MW	molecular weight	TCID 50	50% response
MWCO	molecular weight cut off	TMH	transmembrane helix
NCBI	National Center for Biotechnology Information	TPPM	two-pulse phase-modulated
Ni-NTA	nickel-nitrilotriacetic acid	SEM	standard error of the mean
OD	optical density	UTP	uridine-5‘-triphosphate
P3IK	phosphoinositid- 3-kinase	UV	ultraviolet light
PAGE	polyacrylamide gel electrophoresis	v/v	volume per volume
PBS	phosphate buffered saline	w/v	weight per volume
		YNB	yeast nitrogen base

List of Figures

Summary

G-protein-coupled receptors (GPCRs) are the largest family of receptors in the human body. They contain seven transmembrane helices. There are roughly 800-900 GPCR genes expressed in humans encoded by 4-5% of the human genome. These receptors are the most important signal transducers and play a crucial role in cell physiology and pathology, by using various extracellular stimuli to start complex intracellular signaling. GPCRs interact with a wide variety of stimuli from small molecules (photons, ions, amines) to large molecules (peptides, small proteins), and trigger downstream cascade effects by interacting with G-proteins, GPCR kinases, and β-arrestin. Because of their crucial roles in many cellular functions, GPCRs are the most important drug targets for the pharmaceutical industry. Approximately 30% of the clinically approved drugs available in the market are against GPCRs.

GPCRs can be classified into 6 classes depending on their sequence similarities such as Rhodopsin-like, glutamate, adhesion, frizzled/taste2, and secretin receptors. The intracellular domain of a GPCR undergoes a conformational change after interaction with its ligand, eventually triggering the binding of a heterotrimeric G-protein. G-proteins consist of three subunits, G_{α}, G_{β}, and G_{γ} where $G_{\beta\gamma}$ exists as a stable heterodimer. There are 21 different types of $G\alpha$ subunits found in mammals which can be broadly classified into four classes depending on their structural and functional similarity, for example, $G_{\alpha s}$, $G_{\alpha I}$, $G_{\alpha q}$, and $G_{\alpha 12/13}$. Depending on the G-protein-receptor interaction distinct intercellular signalling cascades are activated by different secondary messenger molecules (cAMP, IP3, DAG, RhoGTPase).

In the last decade, many structures of GPCRs in complex with G-proteins have been published, leading to a better understanding of their molecular mechanism of the active and inactive state, ligand interaction, and allosteric modulations. The first GPCR structure was published in 2007 after decades of extensive work in developing new innovative crystallization techniques. Since then, nearly 150 GPCR structures have been determined and nearly 95 of them are unique. The

availability of high-resolution structures of GPCRs creates a strong urge for other advanced techniques like HDX-MS, solid or solution-state - NMR, to gain a better understanding of its structural plasticity, molecular dynamics, ligand-receptor interaction, and allosteric modulations. Despite significant advancements in the structure elucidation of GPCRs in recent years, little is known regarding the mechanisms of ligand selectivity and its binding modulation with respect to allosteric modulators. The allosteric modulators' interaction with GPCRs could enhance or weaken endogenous ligand binding with receptors is called either positive allosteric modulators (PAMs) or negative allosteric modulators (NAMs) respectively. GPCRs' involvement in various biological processes plays a crucial role and makes GPCRs important targets for structural and therapeutic studies. But there still exists a significant hurdle to generating drugs for these targets. In the case of subtypes of GPCRs or closely related GPCRs that share common or highly similar orthosteric ligand binding sites, the situation is even more difficult.

This work achieved successful expression and purification of GPCRs from class-C and class-A families. Combined with biochemical experiments, DNP-ssNMR, and molecular simulation helped to decipher the mechanism of crosstalk between the allosteric modulator, and the orthosteric binding sites of the peptide receptor. The main findings and major highlights of this dissertation are outlined in the following paragraphs.

The calcium-sensing receptor (CaSR) belongs to the GPCR class-C family and contains a large extracellular domain. This receptor regulates Ca^{2+} homeostasis in blood and its absorption in the kidney and bone. To understand the molecular and structural mechanisms of these receptors their cDNAs were cloned into the pPICZ and pOET1 vectors to express them in *Pichia pastoris* and in *Sf9* insect cells respectively. The CaSR was successfully expressed heterologously in *Pichia pastoris* and in the insect cell with high yield. The CaSR in styrene maleic anhydride (SMA) purified from both *Pichia* and *Sf9* indicates the aggregation of the receptor. The receptor was purified further in LMNG detergent in a three-step purification process, 1- immobilized

metal ion affinity chromatography (IMAC) using Ni-NTA resin, 2- followed by the flag-affinity chromatography using M2-resin, and 3- size exclusion chromatography (SEC) steps. The purified receptor shows no aggregation in a monomeric state. Further optimization was performed to use it for cryo-EM sample preparation and structure determination.

The binding of endogenous ligands to GPCRs causes a conformational change in the intracellular domain leading to interactions with G-proteins. In the last decade, nearly 200 agonist-bound and 95 unique GPCRs-G-protein complex structures were reported. However, challenges still exist in obtaining active GPCR structures due to the instability of G-protein or G-protein-bound receptors. In this work, different mini G_α (mini G_s, mini G_i, mini G_{qs}, and mini Gsi) DNA constructs were made and expressed in *E. coli*. All mini-G proteins were purified using immobilized metal ion affinity chromatography using Ni-NTA and then size exclusion chromatography. The chimera mini-G-protein-maltose binding protein (MBP) was cloned and expressed in *E. coli* and purified with a His-trap column with high purity.

In the last part of the thesis, to decipher the mechanism of allosteric modulation of orthosteric binding sites in the bradykinin receptor was produced and characterized in insect cells. The human bradykinin receptor is a class-A (rhodopsin-like) peptide receptor GPCR, and there are two subtypes of it (B_1R and B_2R) in humans. The human B_1R responds to endogenous peptide hormones such as kallidin (KD) and des-Arg10-kallidin (DAKD) whereas the human B_2R responds to bradykinin. These receptors are involved in a variety of cellular functions such as inflammation, pain, brain function, and blood vessel dilation. Many studies indicate that antagonists of the bradykinin receptors act as potential drugs against inflammation and analgesics. Deactivation of this receptor happens through the degradation of the peptide ligand at the pro7-phe8 amide bond by the angiotensin I converting enzyme (ACE). While the majority of earlier studies concentrated on the orthosteric ligands of this receptor, it has been shown that ACE inhibitors (ACEIs) may be able to bind to the hB1R allosterically. Angiotensin I converting enzyme inhibitors (ACEIs), are very important drugs and are widely used for the

treatment of hypertension, congestive heart failure, and diabetic neuropathy. These drugs target primarily the catalytic zinc center of the ACE. It has been shown that enalaprilat, a well-known ACEI, binds to a proposed zinc-binding site on hB1R and even directly activates the receptor. To obtain information on the influence of ACEIs on the receptor-peptide complex, and to have a better understanding of the molecular mechanism and structural plasticity of the bradykinin receptor and PAM, we used the three commercially available ACEIs captopril, enalaprilat, and lisinopril for our studies.

To investigate the impact of Zn^{2+} on the orthosteric binding pockets of the hB1R receptor, radioactive competitive binding assays were used in the presence of varying concentrations of zinc. The results of the experiments with radioligands indicate that the affinity of the endogenous ligand DAKD to hB1R is enhanced by 10 to 15-fold in the presence of 1mM Zn^{2+}. These findings indicate that Zn^{2+} acts as a weak PAM of hB1R, whereas it doesn't show any effects on B2R. In-silico studies of hB1R and ACEIs suggest that the ACEIs interact with the sequence region 195HEAWH199 (Zn^{2+} binding site) of the extracellular loop (ECL)-2 of the receptor. The Zn^{2+} binding site in this region is specific to hB1R and does not exist in hB2R. A mutation in this region leads to a reduction of the pharmacological effects of Zn^{2+} on the hB1R. Zn^{2+} and ACEI show complex and cooperative interactions with the orthosteric binding pockets of hB1R. In the presence of Zn^{2+}, the structurally relevant ACEIs have relatively distinct allosteric effects on orthosteric agonists, probably due to their various binding poses to the Zn^{2+} site. The drugs enalaprilat and captopril act as PAM, enhancing endogenous ligand affinity ~50-fold, whereas lisinopril acts as NAM.

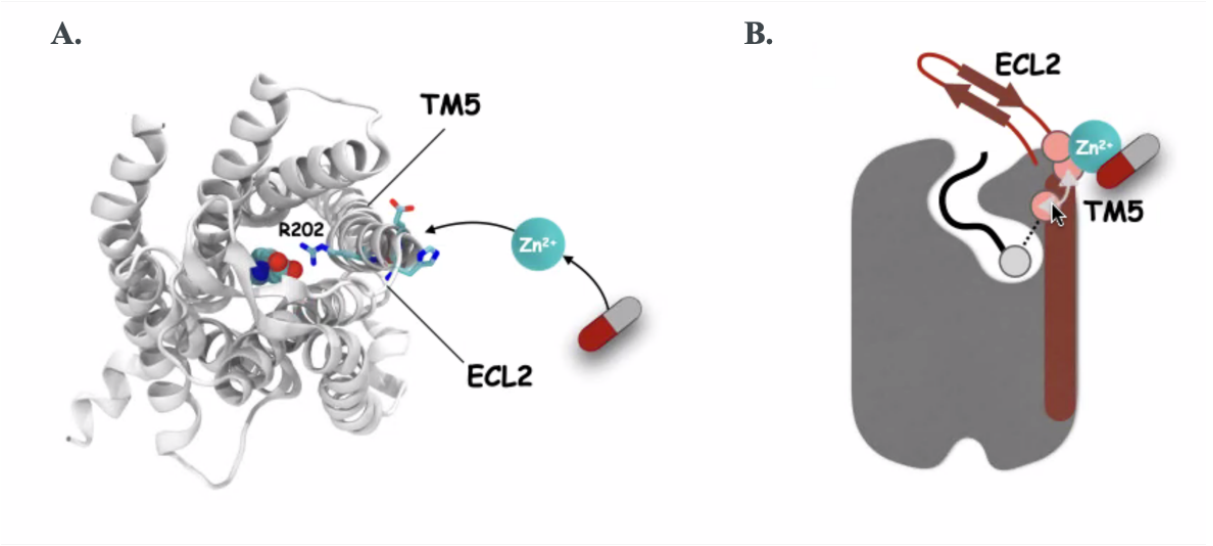

Figure I-1: Overall structural mechanism of interaction of Zn^{2+} and ACEI with hB1R: A) Top view of the B1R, depicting the interaction of zinc and ACEI at the H195 and E196 position of the ECL2 region of the receptor. B) Depicting possible mechanisms of structural rearrangements within the orthosteric binding pocket of hB1R receptors upon binding of ACEI and Zn^{2+}.

To identify any conformational change in the orthosteric binding pockets of the receptor, an isotopically labeled peptide (agonist) was used as an NMR reporter to probe the structural perturbation in the orthosteric binding site upon binding to three allosteric modulators. DNP-ssNMR spectrum data suggest that there is a possibility of three-distinct structures of the peptide in presence of three different ACEIs. These findings agreed well with our biochemical assays. Molecular dynamic (MD) simulations of the cryo-EM structure of hB1R-DAKD (Yin *et al.,* 2021) reveal a structural polymorphism in the peptide structure which is unique to the DAKD peptide in contrast to the bradykinin peptide.

An important result of this thesis is that though enalaprilat, captopril, and lisinopril all have similar functional properties in humans, each one regulates the orthosteric binding site of hB1R in a unique way. These findings provide atomic insights into the allosteric modulation of the bradykinin receptor. This study along with the effects of ACEI on the binding sites of receptors also deciphers the effects of the Zn^{2+} as well as the crosstalk between zinc binding sites and ACEI compounds. The binding of allosteric modulators induces distinct endogenous binding, which might aid in creating new possibilities in the pharmaceutical field.

Zusammenfassung

Die G-Protein-n Rezeptoren (GPCRs) bilden die größte Rezeptorfamilie des Menschen. Sie besitzen sieben Transmembranhelices. Beim Menschen gibt es etwa 800-900 GPCRs, die von 4-5 % des menschlichen Genoms kodiert werden. Diese Rezeptoren sind die wichtigsten Signalüberträger und spielen eine entscheidende Rolle in der Zellphysiologie und -pathologie, indem sie verschiedene endogene extrazelluläre Stimuli in komplexe intrazelluläre *Downstream*-Signale umwandeln. Sie interagieren mit einer Vielzahl von Reizen, von kleinen Molekülen (Ionen, Amine) und Licht bis hin zu großen Molekülen (Peptide, kleine Proteine), und lösen durch Interaktion mit G-Proteinen, GPCR-Kinasen und Arrestin nachgeschaltete Kaskadeneffekte aus. Aufgrund ihrer entscheidenden Rolle bei vielen Zellfunktionen sind GPCRs die wichtigsten Zielstrukturen für Arzneimittel in der Pharmaindustrie. Etwa 30 % der auf dem Markt befindlichen, klinisch zugelassenen Arzneimittel richten sich gegen sie.

GPCRs können je nach ihren Sequenzähnlichkeiten in 6 Klassen eingeteilt werden, z. B. in Rhodopsin-ähnliche, Glutamat-, Adhäsions-, Frizzled/Taste2- und Sekretin-Rezeptoren. Die intrazelluläre Domäne des Rezeptors erfährt nach der Interaktion mit seinem Liganden eine Konformationsänderung, die schließlich die Bindung eines heterotrimeren G-Proteins an ihn auslöst. Das G-Protein besteht aus drei Untereinheiten, G_{α}, G_{β} und G_{γ}, wobei $G_{\beta\gamma}$ als stabiles Heterodimer vorliegt. Bei Säugetieren gibt es fast 21 verschiedene Arten von G-Untereinheiten, die je nach ihrer strukturellen und funktionellen Ähnlichkeit grob in vier Klassen eingeteilt werden können, zum Beispiel G_s, G_I, G_q und $G_{12/13}$. Abhängig von der Interaktion zwischen G-Protein und Rezeptor werden verschiedene intrazelluläre Signalkaskaden durch unterschiedliche sekundäre Botenmoleküle (cAMP, IP3, DAG, Rho-GTPase) aktiviert.

In den letzten zehn Jahren wurden viele Strukturen von GPCRs im Komplex mit G-Proteinen veröffentlicht, was zu einem besseren Verständnis der molekularen Mechanismen des aktiven

und inaktiven Zustands, der Liganden interaktion und der allosterischen Modulationen führte. Die erste GPCR-Struktur wurde 2007 nach jahrzehntelanger intensiver Arbeit an der Entwicklung neuer innovativer Kristallisationsverfahren veröffentlicht. Seitdem sind fast 150 GPCR-Strukturen gelöst worden, von denen fast 95 einzigartig sind. Die Verfügbarkeit hochauflösender GPCR-Strukturen macht den Einsatz anderer fortschrittlicher Techniken wie HDX-MS, Festkörper- oder Lösungs-NMR erforderlich, um ein besseres molekulares Verständnis der strukturellen Plastizität, der molekularen Dynamik, der Ligand-Rezeptor-Interaktion und der allosterischen Modulationen zu erlangen. Trotz erheblicher Fortschritte bei der Strukturaufklärung von GPCRs in den letzten Jahren ist nur wenig über die atomaren Mechanismen der Ligandenselektivität und deren Bindungsmodulation durch allosterische Modulatoren bekannt. Die Interaktion der allosterischen Modulatoren mit GPCRs könnte die Bindung des endogenen Liganden an die Rezeptoren verstärken oder abschwächen und diese werden entweder als positive allosterische Modulatoren (PAMs) oder negative allosterische Modulatoren (NAMs) bezeichnet. Die Beteiligung von GPCR an verschiedenen biologischen Prozessen spielt dabei eine entscheidende Rolle und macht sie zu einem wichtigen Ziel für strukturelle und therapeutische Studien. Es gibt jedoch immer noch erhebliche Hürden bei der Entwicklung von Medikamenten für diese Zielstrukturen. Im Falle von Subtypen von GPCRs oder eng verwandten GPCRs, die gemeinsame oder sehr ähnliche orthosterische Ligandenbindungsstellen haben, ist die Situation noch schwieriger.

Der Calcium-Rezeptor gehört zur Klasse-C-Familie der GPCR, die eine große extrazelluläre Domäne enthält. Dieser Rezeptor reguliert die Ca^{2+}-Homöostase im Blut und die Aufnahme von Ca^{2+} in Niere und Knochen. Um die molekularen und strukturellen Mechanismen des Rezeptors zu verstehen, klonierten wir seine cDNA in die Vektoren pPICZ und pOET1, um sie in *Pichia pastoris* bzw. in der Insektenzelle Sf9 zu exprimieren. Es gelang uns, den CaSR mit hoher Ausbeute in *Pichia pastoris* und in der Insektenzelle *Sf9* zu erhalten. Der CaSR in Styrol-

Maleinsäureanhydrid (SMA), das sowohl aus *Pichia* als auch aus *Sf9* gereinigt wurde, zeigt die Aggregation des Rezeptors an. Der Rezeptor wurde in LMNG-Detergens in einem dreistufigen Reinigungsverfahren gereinigt: 1. immobilisierte Metallionen-Affinitätschromatographie (IMAC) mit Ni-NTA-Harz, 2. gefolgt von der Flaggen-Affinitätschromatographie mit M2-Harz und 3. zuletzt Größenausschlusschromatographie (SEC). Der Rezeptor zeigte keine Aggregation, wenn er in monomerem Zustand gereinigt wurde. Weitere Optimierungen wurden durchgeführt, so dass er für die Kryo-EM-Probenpräparation und Strukturbestimmung geeignet war.

Die Bindung von endogenen Liganden an GPCRs führt zu einer Konformationsänderung in der intrazellulären Domäne, die zu Interaktionen mit G-Proteinen führt. In den letzten zehn Jahren wurden fast 200 an Agonisten gebundene und 95 einzigartige GPCRs-G-Protein-Komplexstrukturen beschrieben. Aufgrund der Instabilität von G-Protein oder G-Protein-gebundenen Rezeptoren ist es jedoch nach wie vor schwierig, aktive GPCR-Strukturen zu erhalten. In dieser Arbeit wurden cDNAs für vier verschiedene Mini-G-Konstrukte (Mini-Gs, Mini-Gi, Mini-Gqs und Mini-Gsi) kloniert und in *E. coli* exprimiert. Alle mini-G-Proteine wurden mit immobilisierter Metallionen-Affinitätschromatographie (IMAC) unter Verwendung von Ni-NTA und anschließender Größenausschlusschromatographie (SEC) gereinigt. Das Konstrukt für ein chimäres Mini-G-Protein-MBP Fusionsproteinwurde kloniert, in *E. coli* exprimiert und das Fusionsprotein mit einer His-Trap-Säule hochgradig gereinigt.

Im letzten Teil der Arbeit soll der molekulare Mechanismus der allosterischen Modulation der orthosterischen Bindungsstellen im Bradykinin rezeptor entschlüsselt werden. Der menschliche Bradykinin rezeptor ist ein Peptidrezeptor der Klasse A (Rhodopsin-ähnlich), und es gibt zwei Subtypen von Bradykinin rezeptoren (B_1R und B_2R), die beim Menschen vorkommen. Der menschliche B_1R reagiert auf endogene Peptidhormone wie Kallidin (KD) und Des-Arg10-Kallidin (DAKD), während der menschliche B_2R auf Bradykinin reagiert. Diese Rezeptoren

sind an einer Vielzahl zellulärer Funktionen wie Entzündung, Schmerz, Gehirnfunktion und Blutgefäßerweiterung beteiligt. Viele Studien deuten darauf hin, dass der Bradykinin-Rezeptors ein potenzieller Angriffspunkt für Entzündungs- und Schmerzmittel durch Antagonisten ist. Die Deaktivierung dieses Rezeptors erfolgt durch den Abbau des Peptids an der Pro7-Phe8-Amidbindung durch das Angiotensin-I-Converting-Enzym (ACE). Während sich die meisten früheren Studien auf die orthosterischen Liganden dieses Rezeptors konzentrierten, hat sich gezeigt, dass Inhibitoren des *angiotensin-I- converting enzyme* (ACE) in der Lage sein können, allosterisch an hB_1R zu binden. *Angiotensin-I-Converting*-Enzym-Inhibitoren (ACEIs) sind sehr wichtige therapeutische Arzneimittel und werden häufig zur Behandlung von Bluthochdruck, Herzinsuffizienz und diabetischer Neuropathie eingesetzt. Diese Medikamente zielen in erster Linie auf das katalytische Zinkzentrum des ACE ab. Es hat sich gezeigt, dass Enalaprilat, ein bekannter ACEI, an eine vorgeschlagene Zink-Bindungsstelle am hB_1R bindet und den Rezeptor sogar direkt aktiviert. Um Informationen auf molekularer Ebene über den von ACE-Hemmern beeinflussten Rezeptor-Peptid-Komplex zu erhalten und ein besseres Verständnis des molekularen Mechanismus und der strukturellen Plastizität des Bradykinin-Rezeptors und des positive allosterische Modulatoren (PAM) zu erlangen, wurden für unsere Studien die drei handelsüblichen ACE-Hemmer Captopril, Enalaprilat und Lisinopril verwendet.

Um die Auswirkungen von Zn^{2+} auf die orthosterischen Bindungstaschen des hB_1R-Rezeptors zu untersuchen, haben wir kompetitive Bindungstests mit radioaktiven Liganden in Gegenwart unterschiedlicher Zinkkonzentrationen durchgeführt. Die Experimente zeigen, dass die Affinität des endogenen Liganden DAKD gegenüber hB_1R in Gegenwart von 1mM Zn^{2+} um das 10- bis 15-fache erhöht ist. Diese Ergebnisse deuten darauf hin, dass Zn^{2+} als schwacher PAM in hB1R wirkt, während es keine Auswirkungen auf den B_2R-Subtyp zeigt. *In-silico*-Studien von hB_1R und ACEIs legen nahe, dass die ACEIs mit dem Peptid 195HEAWH199

(Zn^{2+}-Bindungsstelle) der ECL2-Regionen des Rezeptors interagieren. Die Zn^{2+}-Bindungsstelle in dieser Region ist spezifisch für den hB_1R und kommt im hB_2R nicht vor. Eine Mutation in dieser Region führt zu einer Verringerung der pharmakologischen Wirkung von Zn^{2+} auf den hB_1R. Zn^{2+} und ACEI zeigen eine komplexe und kooperative Interaktion mit den orthosterischen Bindungstaschen von hB_1R. In Gegenwart von Zn^{2+} haben die strukturell relevanten ACEIs relativ unterschiedliche allosterische Wirkungen auf orthosterische Agonisten, was wahrscheinlich auf ihre unterschiedlichen Bindungspositionen an der Zn^{2+}-Stelle zurückzuführen ist. Die Medikamente Enalaprilat und Captopril wirken als PAM und erhöhen die Affinität des endogenen Liganden um das 50-fache, während Lisinopril als negative allosterische Modulatoren (NAM) wirkt.

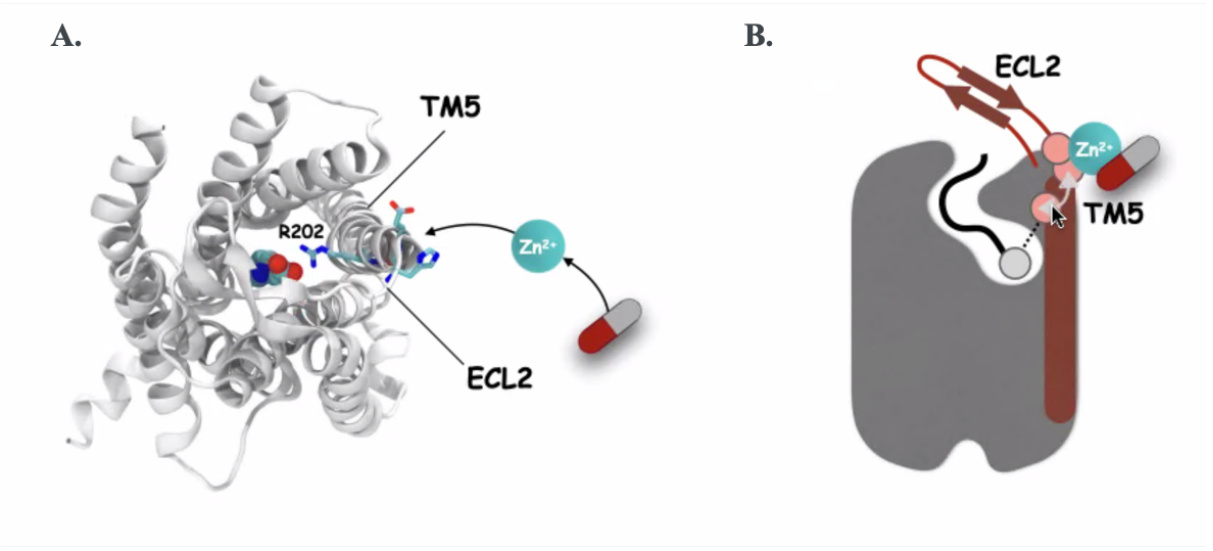

Abbildung II-1: Struktureller Gesamtmechanismus der Interaktion von Zn^{2+} und ACEI mit hB1R: A) Draufsicht auf den B1R, Darstellung der Interaktion von Zink und ACEI an den Positionen H195 und E196 der ECL2-Region des Rezeptors. B) Darstellung möglicher Mechanismen der strukturellen Umstrukturierung innerhalb der orthosterischen Bindungstasche von hB1R-Rezeptoren bei Bindung mit ACEI und Zn^{2+}.

Um eine Konformationsänderung in den orthosterischen Bindungstaschen des Rezeptors nachzuweisen, wird ein mit isotopen markiertes Peptid (Agonist) als NMR-Reporter verwendet, um die strukturelle Störung in der orthosterischen Bindungsstelle bei der Bindung mit drei

allosterischen Modulatoren zu untersuchen. Die DNP-ssNMR-Spektraldaten deuten darauf hin, dass das Peptid in Gegenwart von drei verschiedenen ACEIs eine dreifach unterschiedliche Konformation aufweisen könnte. Diese Ergebnisse stimmten gut mit unseren biochemischen Tests überein. Eine Molekular dynamisbimulation der Kryo-EM-Struktur von hB1R-DAKD (Yin *et al.,* 2021)(1) zeigt den strukturellen Polymorphismus in der Peptidstruktur, der für das DAKD-Peptid im Gegensatz zum Bradykinin-Peptid einzigartig ist.

In dieser Arbeit wurde entdeckt, dass Enalaprilat, Captopril und Lisinopril zwar alle ähnliche funktionelle Eigenschaften in Zellen haben, aber jeder von ihnen reguliert die orthosterische Bindungsstelle des menschlichen Bradykinin-1-Rezeptors auf einzigartige Weise. Diese Ergebnisse geben einen Einblick in die allosterische Modulation des Bradykininrezeptors. Diese Studie entschlüsselt neben den Auswirkungen von ACEI auf die Bindungsstellen von Rezeptoren auch den Einfluss von Zn^{2+}. Diese Ergebnisse können neue Möglichkeiten im pharmazeutischen Bereich eröffnen.

Chapter – 1: Introduction

1. Introduction

Cells are the basic units of living organisms, whether they belong to single-celled (e.g. bacteria), or multicellular organisms (e.g. humans). In gist, "*the cell is an organized and highly concentrated protoplasm surrounded by a protective and permeable membrane*". It is interesting to note that different types of cells in multicellular organisms perform diverse roles despite having a similar basic architecture. Cells can change their fate depending on their potency. A totipotent cell can give rise to whole organisms from a single cell. Internally cells have microscopic compartments that are made up of various organelles that perform a wide range of functions (2). From unicellular to multicellular animals, organelles' complexity, structures, and topology had evolved exponentially. The communication between cells is a crucial process in unicellular and multicellular organisms. They must communicate with each other in order to grow, migrate, survive, divide, and differentiate. In this chapter, I shall describe the importance of membrane proteins and their involvement in various biological processes in detail.

1.1 Biological Membranes:

The protoplasm of the cells is separated from the external aqueous milieu by a semi-permeable lipid bilayer, which is called a cell membrane or plasma membrane. The plasma membrane is one of the most complicated and dynamic structures of the cell. It is composed of lipids, proteins, and polysaccharides. The most groundbreaking and acceptable cell theory was coined as the "fluid mosaic model" proposed by Singer and Nicolson in 1972 (3). According to it, membranes do not have a single uniform lipid bilayer, instead, they are composed of lipids and proteins in a mosaic manner. Proteins are icebergs inside the sea of lipids, and they can be present on both inside or on the outer sides of the lipid bilayer. These proteins are called "membrane proteins", which connect the exterior and inner parts of the cells. The outer and

inner surface of the lipid bilayer of the membrane is made up of lipid head groups that are hydrophilic in nature. In contrast, the inside of the lipid bilayer membrane is made up of the fatty acyl tails, which is hydrophobic or lipophilic in nature. The hydrophilic head group of the membrane is in contact with the external milieu of the solvent, and the hydrophobic tail region of the membrane prevents hydrophilic molecules from passing across the bilayer. Later after a plethora of research over the last three decades the "fluid mosaic model" was complemented by the "*lipid raft"* model (4-6). According to the lipid raft model, biological membranes are heterogeneous and dynamic microscopic assemblies of lipids, carbohydrates, and proteins that aid in the segregation of cellular functions within the membrane. There is a high degree of structural diversity and complexity associated with membrane proteins and the surrounding environment. Deciphering the structural complexity of membrane proteins and their mechanisms of action will provide us with a better understanding of the biophysical and biochemical processes of cell activity.

Due to its quasifluid nature, biological membranes are associated with various essential cellular functions such as energy conservation, cell-cell interactions, cellular structure, cell motility, and transport of ions or small molecules. The lipid bilayer of the cell membrane mainly consists of glycerophospholipids, which provide a core sn-glycerol-3-phosphate backbone esterified to two fatty acid chains at positions C-1 and C-2. These phospholipids mainly possess hydrophilic tail regions bound to the hydrophilic glyceryl moiety and the phosphate head group (7).

1.1.1 Membrane proteins:

Membrane proteins are types of proteins that are integrated or associated with biological membranes. The transmembrane part of membrane proteins is hydrophobic which allows the protein to integrate into the lipophilic part of the membrane. Nearly 20-30% of the human genome encodes membrane proteins (8,9). These proteins are highly organized and involved

in regulating and facilitating various crucial cellular functions with high precision (10,11). Membrane proteins serve as a connecting link between intracellular and extracellular milieus, and any changes in the outside environment are sensed by membrane proteins. From a pharmacological point of view, membrane proteins are important targets for drug development, because of their involvement in many biological processes. Nearly 60% of marketed drugs act against membrane proteins, reiterating the importance of research on membrane proteins and their involvement in various cellular processes (12,13). Michel and coworkers published the first high-resolution crystal structure of a membrane protein (photosynthetic reaction center) in 1985 (14).

Membrane proteins can be mainly classified into two types depending on their interaction with biological membranes and their localization: 1- peripheral membrane proteins and 2-integral membrane proteins. Peripheral membrane proteins are bound to the surface of membranes mainly via polar hydrophobic interaction. In comparison, integral membrane proteins, also known as transmembrane proteins, are a part of the biological membrane where the hydrophobic region of the protein is embedded into the lipid bilayer. It can be either an integral polytopic or an integral monotopic protein. Most integral membrane proteins can be classified into a α-helical or β-barrel type depending on their secondary structure. Apart from structure-based classification, membrane proteins can be further classified based on their functions, such as enzymes, ion channels, transporters, receptors, and anchors/linkers.

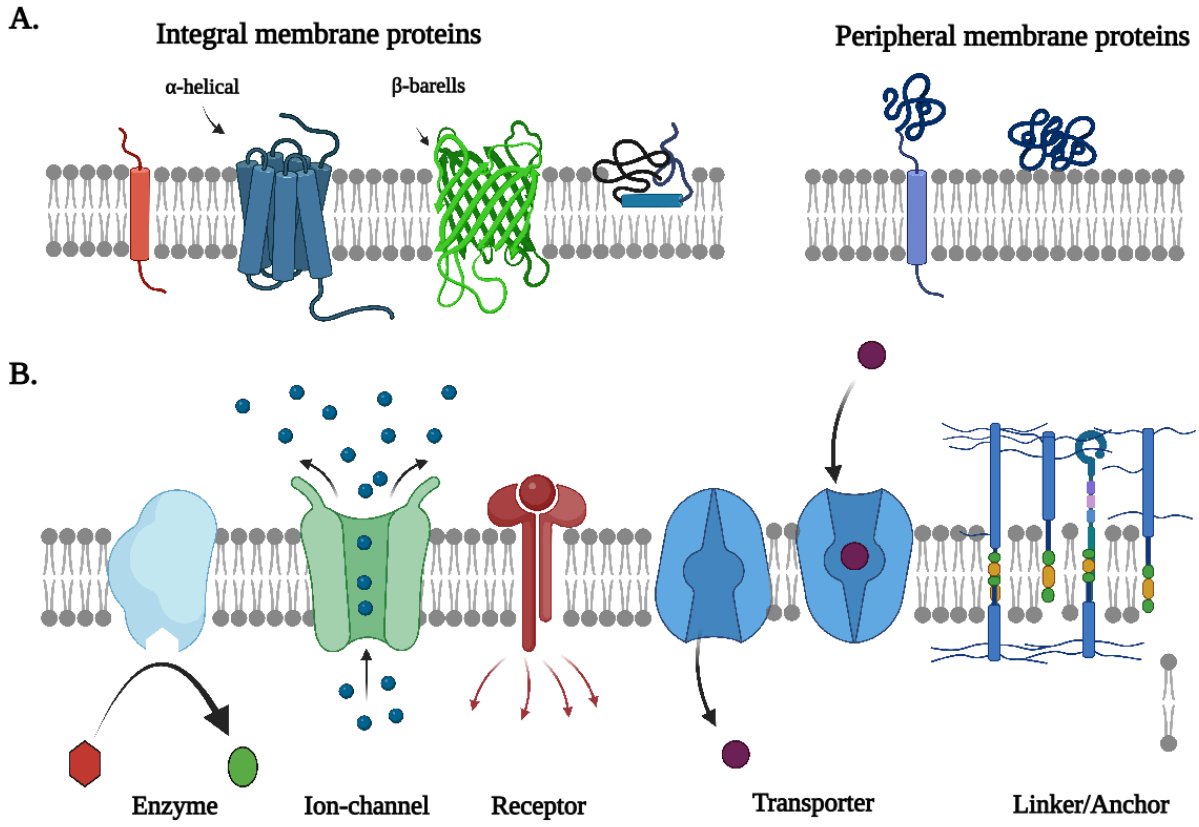

FIGURE 1.1: Schematic representation of membrane protein types: A) depending on their interaction with the membrane they can be classified into two types; integral membrane proteins and peripheral membrane proteins. B) these proteins are associated with various crucial biological processes. therefore, depending on their function, they can be classified into enzymes, ion channels, receptors, transporters, and linkers/anchors.

1.2 Cellular signaling:

It is a crucial process for both unicellular and multicellular organisms to communicate with the environment for their proliferation and survival (15). Cellular signaling is the process where the cells communicate with the environment or themselves. The external signals can be physical (Mechanical force, pressure, temperature, light) or chemical (small or large molecules). These signals are transmitted across the cell membrane by activating various chemical events in the cells. In this process, the external stimulus is sensed and detected by a cell receptor on the surface causing a signal, which is the signal later transmitted to the cell through a specific signal cascade (16). Receptors are essential in cell signaling because they can detect or sense physical stimuli or chemical signals. A particular receptor only interacts with a certain kind of

signaling molecule, which translates to downstream cellular signaling i.e., a signaling molecule can only influence target cells that contain the specific cell surface receptor. The particular receptor and ligand interaction cause specific downstream signaling. Each cell is programmed to respond to a certain type of external stimuli and it is an essential feature for cell growth, proliferation, immunity, and cell death. Any error in interactions between receptors and signaling molecules can lead to diseases.

The signal molecules can be classified by their chemical properties as amino acids, lipids, phospholipids, proteins, and glycoproteins. Depending on the physiochemical properties, they can be divided into lipophilic (steroids, thyroid hormones, prostaglandins) and hydrophilic ones (insulin, glucagon, adrenaline, histamine). The lipophilic molecules (steroids, thyroid hormones) can directly diffuse through the cell membrane and reach the cytosolic or nuclear compartments. Contrarily, signaling by the large lipophilic (prostaglandins) or hydrophilic (insulin, glucagon) signal molecules relies on the presence of their receptor in the membrane.

Cell signals can be transmitted over a short or long distance from its effector, depending on the range of effects, which can be categorized into four categories, e.g. autocrine, juxtacrine, intracrine, endocrine, or paracrine. In autocrine signaling, the signal molecule is generated by the cell, which binds to the receptor located on the same cell surface, whereas in the case of paracrine signaling, the cells target nearby cells that are not connected by any gap junctions (figure 1.2). The paracrine molecules diffuse only over a small distance. Direct proximity between the signal and the target cell is essential for juxtacrine signaling. Juxtacrine signaling molecules are membrane-bound in contrast to the freely diffusible paracrine signaling molecules. The signal molecules with long-range effects are hormones secreted from endocrine cells called “endocrine” signals. The hormones can reach distant target cells within the body after being released by the endocrine gland. Specific cells can only respond to particular types of hormones.

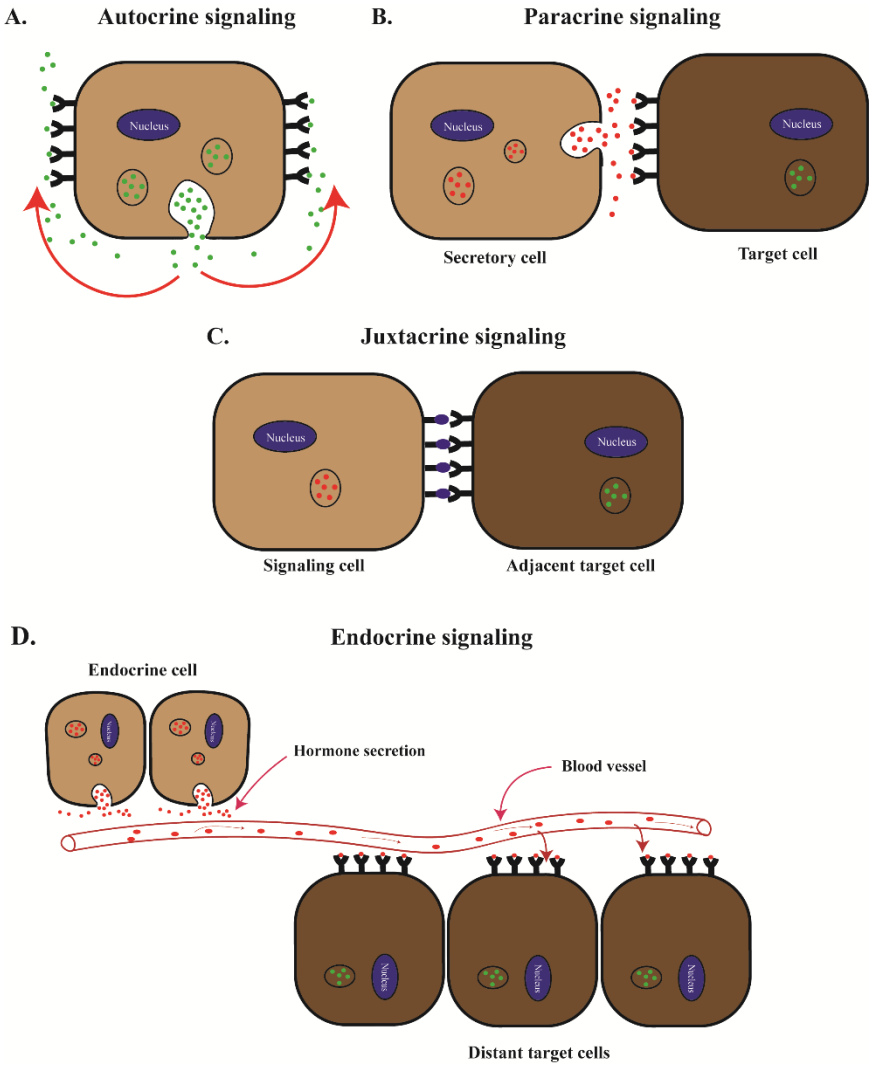

FIGURE 1.2: Schematic representation of different types of cellular signaling inside the body: cells communicate with each other through cellular signaling, depending on the location of the receptor and distance traveled by signal molecules, it can broadly be classified into 4-classes: A) autocrine signaling (self-induction of the cell), B) paracrine signaling (locally induce signaling in neighboring cells), C) juxtacrine signaling (signaling that requires direct contact between cells) and D) endocrine (long-range signaling).

1.3 Different types of receptors and their functions:

Receptors are a class of proteins that receive signals from their environment or another cell and cause a cellular response inside the cell (16). The mechanism of the receptor's actions can be described in three steps: receiving the signal, amplifying it, and lastly causing a response. Depending on the location, receptors can be broadly classified into cell surface receptors and intracellular receptors (cytosolic receptors). Cell surface receptors are transmembrane proteins

present on the plasma membrane. Whereas, "cytosolic receptors" are present inside the cells either in the cytoplasm or nucleus. The intracellular receptors respond to small hydrophobic ligand molecules that can pass through the plasma membrane. The key characteristic of the nuclear or cytosolic receptors is that they can directly interact with the DNA and control the cell's transcription.

There are various types of receptors, which can be mainly classified into the following types.

I -*Ligand-gated ion channels (Ionotropic Transport):* These are transmembrane ion channel proteins that allow the transport of ions like Na^+, K^+, Ca^{2+}, or Cl^- across the plasma membrane. Upon binding of the agonist to the receptor undergoes conformational changes, which leads to ion translocation, resulting in the change of the electrochemical properties of the cell. These receptors have two distinct domains: an extracellular domain that contains a ligand-binding (agonist) site and a transmembrane domain that contains pore-forming transmembrane helices. These receptors respond to signals in milliseconds, which is faster than that of other types of receptors (17). Examples are the nicotinic acetylcholine receptor, NMDA and non-NMDA glutamate receptors, and GABA.

II-*G-protein Coupled Receptors (GPCRs):* GPCRs form the largest class of receptors and contain seven transmembrane helices (18). Extracellular binding of an agonist to the receptor induces intracellular binding of a heterotrimeric guanine nucleotide protein (G-protein) and its activations (19). Activated G-proteins influence the synthesis of secondary signaling molecules, which amplify the signal exponentially. There are various types of GPCRs with different functions and mechanisms, which are explained later in detail.

III- *Enzyme-linked or related receptors*: These types of transmembrane receptors become enzymatically active upon binding the external signal molecules. These enzyme-linked receptors can be further subcategorized into two classes, receptor tyrosine kinases, and kinase-linked receptors. In the case of the receptor tyrosine kinases, activation of the receptor leads to

its dimerization which further activates cytosolic tyrosine kinases. Tyrosine kinases later also phosphorylate tyrosine residues of the receptor (20). These receptors have both catalytic and receptor functions (21).

IV- *Nuclear Receptors*: These receptors are found within cells and are typically triggered by steroid hormones like estrogen and progesterone and other hydrophobic molecules like e.g., thyroid hormones and retinoic acid (22). Upon ligand binding, they move to the nucleus of the cell (23). These receptors consist of a core DNA-binding domain, a C-terminal binding site, and N-terminal regions. In contrast to other cellular signaling pathways, which are triggered via cell surface receptors, the nuclear receptors interact with the ligands which can permeate through the plasma membrane. These receptors regulate gene transcription in cells when they are activated, which is why they are also referred to as "transcription factors" (24,25). These receptors are involved in various biological processes such as cell proliferation, metabolism, development, and apoptosis.

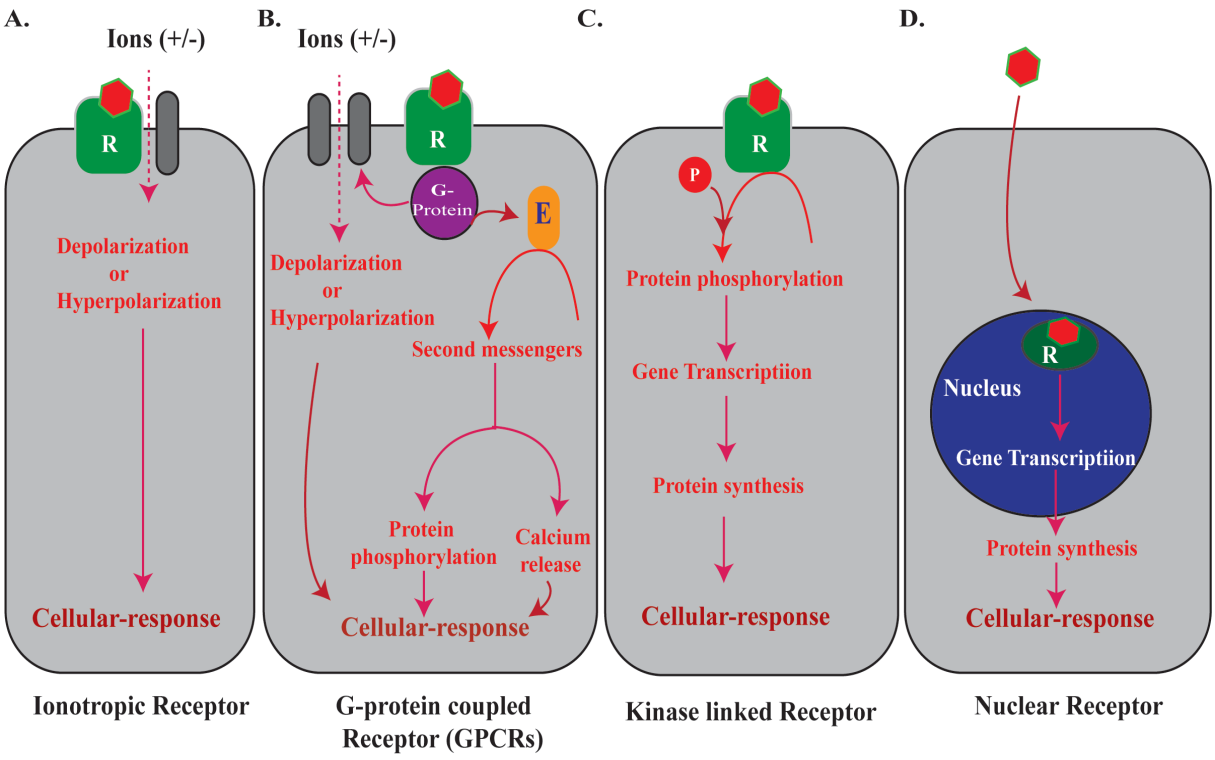

Figure 1.3: Schematic representation of different types of receptors and their general functions: A) Ionotropic receptor, B) G-protein coupled receptor, C) Kinase linked receptor, and D) Nuclear Receptor (adopted from Goodman and Gilman et al., 2018)

1.4 G-Protein Coupled Receptors (GPCRs):

The cell membrane of a eukaryotic cell contains many distinct G-protein-coupled receptors (GPCRs), which are responsible for various physiological processes in cells. GPCRs, which form the largest family of cell-surface receptors in the higher eukaryotes, contain seven transmembrane helices (18,19). These receptors are the most important signal transducers and play a crucial role in cell physiology by converting diverse extracellular signals into complex intracellular downstream responses (26,27). 4-5% of the human genome encodes GPCRs, and nearly ~ 900 different GPCRs are found in humans (28). GPCRs are associated with a diverse range of functions and are widely expressed in phylogenetically distinct eukaryotes from yeasts to mammals (29). They are activated by a wide variety of stimuli from ions and small molecules to large molecules (lipids, peptides, small proteins), and trigger downstream signalling by activating heterotrimeric G-proteins. Due to their high importance in various cell functions, they are considered to be the most important drug targets. Approximately 30% of the marketed or clinically approved drugs act on the GPCRs (12,30).

1.4.1 GPCR-Classification

Depending on the characteristics of ligand binding or structural similarity of GPCRs, they are broadly classified into 6 classes namely- class-A (Rhodopsin-like), 2- class B (secretin), 3- class-C (metabotropic glutamate/pheromone), 4- class D (fungal-mating), 5- class E (cyclic AMP) and 6-class F (frizzled/smoothened). This A-F classification includes all GPCRs expressed in eukaryotes, from vertebrates and non-vertebrates. There are ~800 GPCRs found in humans majorly from classes A, B, C, and F but there are no human GPCRs from classes D and class E.

1- Class-A (Rhodopsin-like): It is the largest class consisting of nearly ~80 -85% of all GPCRs. This class contains rhodopsin, olfactory, peptide, hormone, nucleotide-like, and cannabinoid-to-glycoprotein receptors (31-33). Class-A can be further classified into 19 sub-classes depending on their structural similarity and on phylogenetic analyses (34). Although, members of this class display diverse functions, there are some amino acids which are highly conserved and form a disulfide bridge connecting loop I and loop III. The palmitoylation at the C-terminal tail of GPCRs at the cytoplasmic part of the receptor is another common feature among members of the class-A GPCRs (35,36). These posttranslational modifications regulate structural and cellular signaling inside the cell (37,38). Class-A GPCRs get deactivated upon phosphorylation of residues (serine or threonine) at the C-terminus by G-protein kinases. Phosphorylated GPCRs show a high affinity towards β-arrestin, which deactivates the receptor upon binding and leads to its internalization (39,40).

2- Class-B GPCRs: This class is also called the secretin receptor family. These receptors are expressed only in plants, fungi, and prokaryotes. As other GPCRs, they also contain seven transmembrane helices, their arrangements are different. This class of GPCRs has a unique and long extracellular N-terminal domain. They specifically interact with peptide hormones (ligands) such as calcitonin, secretin, and parathyroid hormones. You can further subdivide this group into three subfamilies, B1-B3 (41).

3- Class-C GPCRs: This class contains the so-called metabotropic receptors. These GPCRs are mainly expressed in the peripheral and central nervous system (42). Members of this family are characterized by large N-terminal and C-terminal domains. The extracellular loops II and IV are connected by a disulfide bridge. Some of the common examples of receptors of this class are metabotropic glutamate receptors (mGluR), receptors for pheromones, GABA-B, the calcium-sensing receptor (CaSR), and taste receptor (T1R).

4- Class-D GPCRs: Receptors of this class are also referred to as fungal mating receptors. They are mainly expressed in *Saccharomyces* and consist of receptors for mating pheromones of yeast. This class of receptors plays a crucial role in response to yeast mating factors (43). The receptors of this family are fungal pheromone-A factors-STE2, STE3, and fungal pheromone B factors like – BAR, BBR, RCB, and PRA(44-46).

5- Class-E GPCRs: Members of this class are also known as cyclic AMP receptors, mainly expressed in the amoeba *Dictyostelium discoideum,* and are responsible for chemotaxis and other cellular processes (47,48).

6- Class-F GPCRs: This class contains the frizzled or smoothened receptors. They play a crucial role in *Wnt* and Hedgehog signaling pathways in *Drosophila* and are responsible for the dorsal closure of the larva (49,50).

To classify the GPCRs from human, Fredriksson *et al.,* (51) developed a classification method like GRAFS, which classify human GPCRs according to their sequence similarity in the transmembrane region of the receptors. The GRAFS classification of the human GPCRs lists five subfamilies [glutamate (G), rhodopsin-like (R), adhesion (A), frizzled/taste2 (F), and smoothened (S)]. There are many GPCRs that are unexplored and their physiological function and natural ligands are still unknown. They are called “orphan GPCRs”. Studying these types of GPCRs and discovering their natural ligand and functions are called “deorphanization” (52). They may become crucial targets for pharmaceutical industries.

1.4.2 General features of GPCR

GPCRs, as already stated, contain seven membrane-spanning helices, they are therefore also known as 7-TM receptors. These seven transmembrane helices are connected by three intercellular loops (ICL 1-3) and three extracellular loops (ECL 1-3), The C-terminus (carboxy-terminus) of the receptor faces the intracellular space and the N-terminus is exposed to the extracellular space. The seven transmembrane helices, which constitute the receptor's structural

core region, aid in converting extracellular signals into intracellular signals by structural and conformational rearrangement upon ligand interaction. While the extracellular region of the receptor is primarily responsible for ligand binding, the intracellular region interacts with downstream signaling partners such as cytosolic G-proteins, arrestins, and G-protein coupled receptor kinases. Interestingly, the seven transmembrane helices of GPCRs share the least sequence homology with each other. Up to 30% of the sequence similarities between GPCRs were identified in the transmembrane region of the receptor. The C-terminal region, the N-terminal region, and ICL-3 (connecting helices V and VI of the receptor) are the most variable regions of GPCRs and do not possess any sequence similarity with other GPCRs (18,53,54). The lengths of the N- and C-termini of receptors vary significantly. Class-A (rhodopsin-like) GPCRs have a shorter N-terminal (10-50 aa) and shorter C-terminal region than the other GPCRs whereas Class-C (glutamate receptor) possess a longer N-terminal (500-600 aa) and C-terminal region (18,51). In the transmembrane part of the receptor, helices-V and VI are longer than the other ones by 1-2 helical turns towards the intracellular space. In the case of class-A receptors, the intracellular loop ICL3 of the receptor is longer than the other loops. Helices V and VI, as well as ICL3 are responsible for binding G-proteins, G-protein coupled receptor kinases (GRKs), and β-arrestin (55,56).

GPCRs share conserved structural features despite their wide range of ligands and different activities. The majority of the rhodopsin-like GPCRs have an additional helix VIII which has a highly conserved [F(RK)xx(FL)xxx] amphipathic sequence motif. In contrast to the seven transmembrane helices, helix VIII is found parallel to the membrane bilayer on the intracellular side. Most rhodopsin-like GPCRs have two distinctive amino acid motifs that act as microswitches to control activation and G protein coupling. One such conserved sequence, the D[E]RY motif, which is involved in a salt bridge with a D/E sequence of helix VI, is present in helix III. This salt bridge also called “ionic lock”, is the characteristic feature of inactive

GPCRs, and prevents the receptor from interacting with G-proteins (57). Another conserved motif [NPxxY] is present in helix VII and also plays a crucial role in the activation of the receptor. In addition to the conserved motif in the transmembrane region of the receptor, the extracellular domains of the GPCRs also exhibit certain structural similarities. Most prevalent is the disulfide bridge between ECL2 and helix III, which is found in the majority of rhodopsin GPCRs. This disulfide linkage stabilizes the extracellular domain which is crucial for the interaction with ligands (58). The highest structural homology was observed in the transmembrane part of the receptors, where they exhibit unique tilts and turns which contribute to their different interactions with various ligands (especially the ligand-binding pocket region of the receptor) (59).

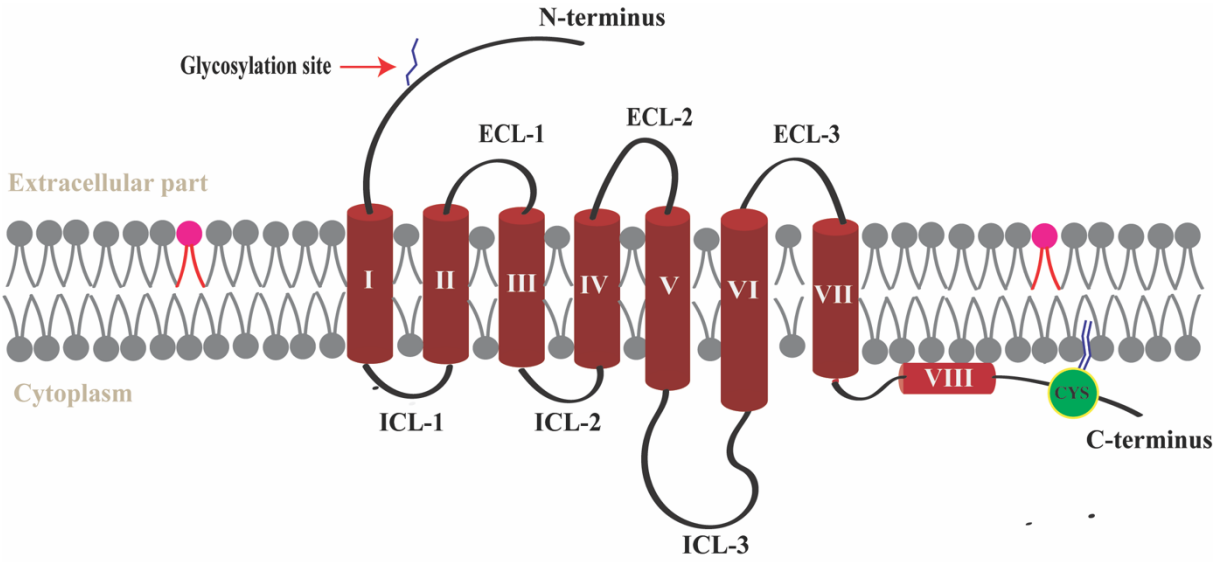

Figure 1.4: Schematic representation of the general topology of G-protein coupled receptors (GPCRs): GPCRs contain 7 transmembrane helices which are connected by 3 extracellular loops (ECL) and 3 intracellular loops (ICL). The N-terminal part of the GPCRs faces toward the extracellular and the C-terminal part towards the intercellular side of the cell. Most of the GPCRs contain an N-glycosylation site in the N-terminal and in some ECL regions of the receptor. Helix-V and VI and the intracellular domain-3 (ICL3) are longer than the other helices and loops due to their involvement in G-protein binding. The majority of the rhodopsin-like GPCRs from class-A feature palmitoylated cysteine residues at the C-terminus and an additional amphipathic helix VIII that is parallel to the membrane.

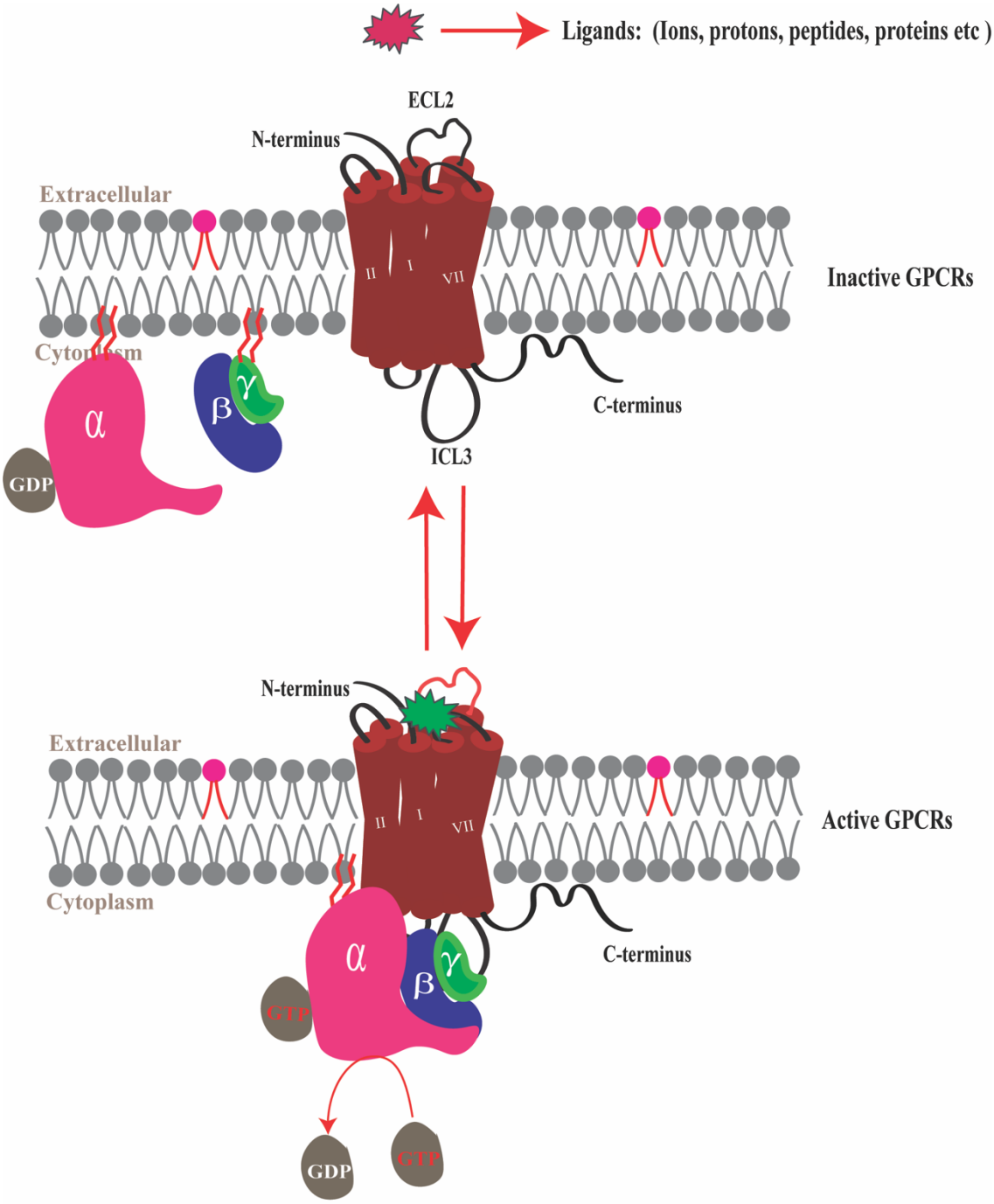

Figure 1.5: Schematic representation of G-protein coupled receptors (GPCRs) and their activation: The scheme depicts the activation of GPCRs through G-protein coupling. Inactive GPCRs get activated by binding endogenous ligands (red), ligand binding leads to a conformational change in the intracellular part of the receptor, which in turn leads to the binding of a heterotrimeric G-protein which is a reversible process. Then the exchange of GDP-bound to G_{α} for GTP leads to the dissociation of the G-protein.

1.5 G-protein coupling:

The so-called G-proteins got their names because of the bind guanine nucleotides. They consist of three subunits, the large alpha (α)-subunit of ~40 kDa, a beta (β) -subunit of ~35 kDa, and a γ-subunit of ~8 kDa. Heterotrimeric G-proteins are highly conserved from yeasts and plants to humans and are members of the GTPase superfamily (60). Signal transduction by GPCRs is majorly transmitted into the cell via heterotrimeric G-proteins. The alpha subunit of G-proteins consists of two distinct domains: a unique α-helical domain and a Ras-like GTPase domain. The G_{β}- subunit of G-proteins is a β- sheet-rich protein with several β-sheets forming a propeller. The G_{γ}-subunit is the smallest subunit consisting of two elongated helical motifs (61). GPCRs respond to a variety of signals and are responsible for various cellular signal transduction events inside the cell. The intracellular signaling cascade and secondary signaling molecules are induced majorly by different G_{α} proteins. G_{α} proteins of eukaryotes show a high structural and functional similarity. Depending on their functions and sequence homology, Gα proteins can be classified into 4-major classes: $G_{\alpha S}$, $G_{\alpha q}$, $G_{\alpha i}$, and $G_{\alpha 12/13}$ (60,62). 21 different types of G_{α} subunits have been identified in mammals. They can hetero-trimerize with five different types of G_{β} and twelve G_{γ} subunits. Once the receptor binds its ligand, a conformational change in the intracellular domain leads to the binding of a heterotrimeric G-protein complex.

The $G\alpha_S$- family ($G\alpha_S$, $G\alpha_{olf}$, $G\alpha_{SXL}$) members activate adenylyl cyclases which lead to an increase in the production of cAMP (2^{nd} messenger). Increased cAMP triggers cAMP-dependent pathways, where it binds and activates a protein kinase (PKA). The $G\alpha_i$- family ($G\alpha_{i(1-3)}$, $G\alpha_z$, $G\alpha_o$) members inhibit the activation of adenyl cyclases and decrease the level of cAMP (2^{nd} messenger) (63). $G\alpha_q$ family members activate protein kinase (PKC), phospholipase C (PLC), and calcium channels. $G\alpha_{12/13}$ family members are involved in the activation of

mitogen protein kinases (MAPK) and Rho family GTPase signaling pathways. $G\alpha_{12/13}$ family members are associated with pathways related to cytoskeleton rearrangement and cell motility (64).

The G_{β}- subunit and G_{γ}-subunit form a stable heterodimer. Five G_{β}subunits-are found in mammals they are named $G_{\beta 1 \text{ to } 5}$, Except $G\beta_{5,}$ rest of them exhibit high structural identity (~80 %) among with each other.

G_{β} contains seven β sheets which form one seven-bladed propeller. Each propeller blade of the protein consists of a 4-stranded antiparallel β-sheet with seven centrals Trp-Asp (WD) repeats (65). The G_{γ}-subunits show less structural identity to each other and contain a conserved C-terminal CAAX (A: aliphatic amino acids and X: leucine/ serine) motif. The protein is post-translationally modified by prenylation (geranylgeranyl or farnesyl group) of the C-terminal region at position X (66).

G-proteins can interact with GPCRs by two different mechanisms: "collision coupling" and "physical scaffolding". In collision coupling, the GPCRs interact with heterotrimeric G-proteins or downstream effector molecules by simple diffusion of molecules within the cell.In “physical scaffolding”, the GPCRs and the downstream molecules exist within a distinct compartment within the cell, allowing a quick signal transduction (67,68).

G-protein subclasses	*Target protein*	*Second messenger*	Subtype (expression in human)
$G\alpha_S$	adenylyl cyclase, Ca^{2+}-channel	cAMP Ca^{2+} potential	$G\alpha_S$, GαsXL, Gαolf
$G\alpha_i$	adenylyl cyclase, *Ca^{2+}-channel*	cAMP *Ca^{2+}*	Gαi1, Gαi2, Gαi3 Gαgust, Gαo, Gαz, Gαt-r , Gαt-c
Gαq	Phospholipase C	Ip3, DAG	Gαq, Gα11, Gα14, Gα15/16

Gα12/13	Rho-GTPase	Rho and MAPK	Gα12, Gα13
Gβγ	Phospholipase C adenylyl cyclase	Ip3, DAG Ca^{2+}	Gβ1 to Gβ5, Gγ1 to Gγ15, Gγ-rod and Gγ-cone

Table T-1: **Effectors for different G protein subunits expressed in mammals**

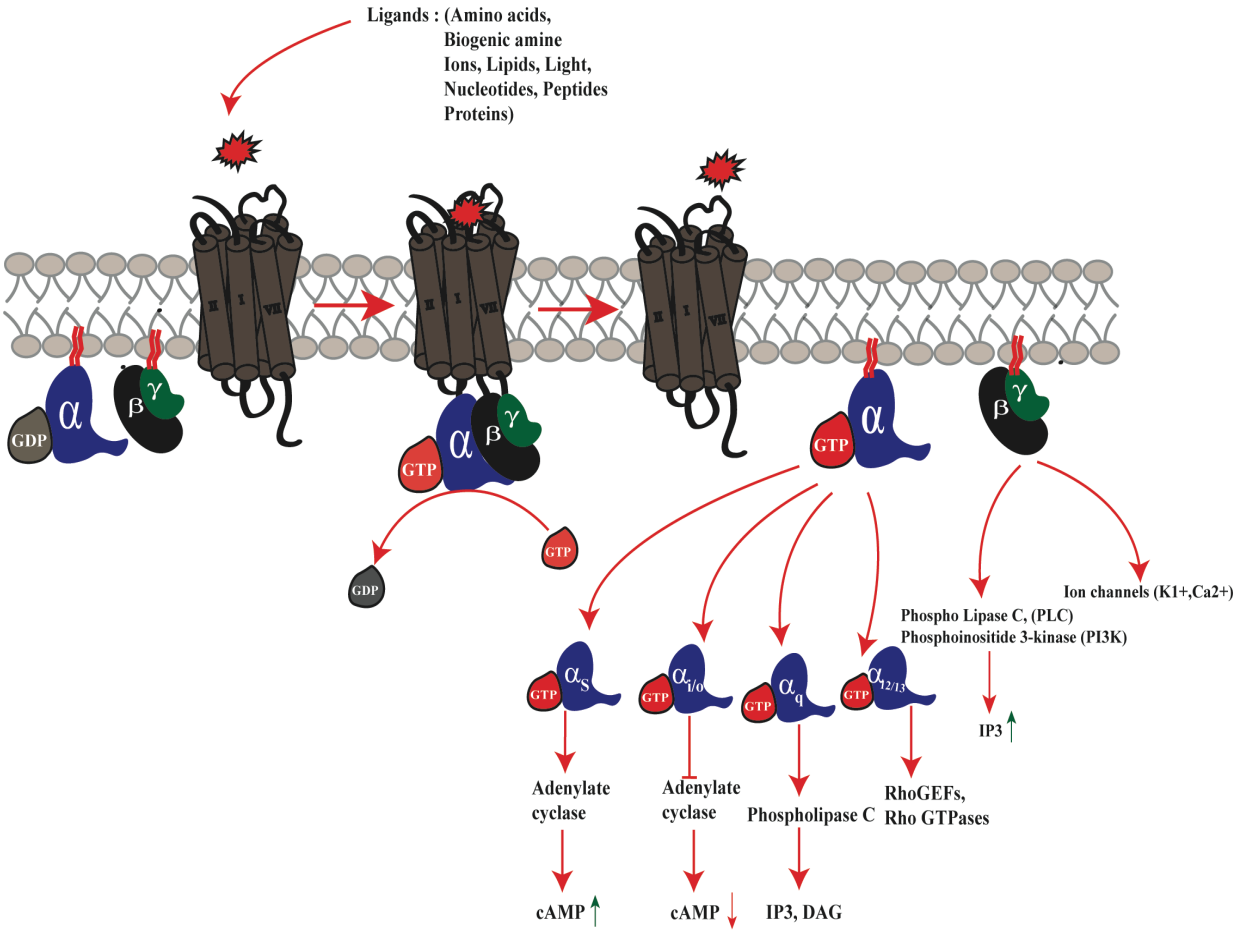

Figure 1.6: Schematic representation of signal transduction triggered by GPCRs and G-protein coupling: The heterotrimeric G-protein consists of three subunits, a GDP-bound membrane-anchored G_α (blue), G_β (black), and G_γ (green) subunits. G_β and G_γ form a stable $G_{\beta\gamma}$ heterodimer which is membrane-anchored by the Gγ subunits. Once a GPCR gets activated by binding an endogenous ligand (red), a conformational change in the intracellular part of the receptor occurs, which in turn binds a heterotrimeric G-protein. A GTP and GDP exchange in the G_α subunit leads to the dissociation of the heterotrimeric G-protein and interaction with downstream signaling molecules. Depending on the type of the G_α - subunit ($G_{\alpha s}$, $G_{\alpha I}$, $G_{\alpha q}$, and $G_{\alpha 12/13}$) different downstream signaling cascades are activated. The $G_{\alpha s}$-subunit activates the adenyl cyclase leading to an increase in cAMP production whereas $G_{\alpha I}$ inhibits the function of adenylate cyclase leading to a decrease in cAMP production. $G_{\alpha q}$ activates phospholipase-C which in turn generates the secondary messenger inositol-1,4,5-triphosphate (IP3) and

di-acylglycerol (DAG) in the cell. $G_{\alpha 12/13}$ activates Rho family members of GTPases in cells and is responsible for various cytoskeleton rearrangements. The Gβγ heterodimer leads to the activation of ion channels and is also responsible for the activation of certain enzymes like phospholipase-C(PLC) and phosphoinositide-3-kinase (PI3K).

1.5.1 Desensitization and Arrestin recruitment

A weakened cellular response to the signal transmission caused by prolonged stimulation of receptors is known as the desensitization of receptors. In cases of diseases, where the receptor is constitutively active, desensitization of receptors is an essential mechanism for cells to modulate cellular activity. The dissociation of G-proteins from GPCRs activates a cascade of events inside the cell. These G-proteins can again bind to the receptor if it constitutively binds its ligand. In that case, deactivation of GPCRs is achieved by the binding of GRK kinase, which sterically hinders the binding of G-proteins (69,70). The binding of GRK to GPCRs leads to the phosphorylation of specific serine and threonine residues of intracellular loop (ICL) regions or C-terminal regions of the receptor (71-75). Once a GPCR is phosphorylated, it shows a high affinity to β-arrestin (76). The clathrin endocytic machinery interacts with the receptor-bound arrestin complex to internalize it for endocytosis (77). The desensitized and dephosphorylated receptor in the endosome is either recycled and transported back to the membrane or carried to a lysosome for its destruction (78,79). β-arrestin-bound receptors also activate the MAP (mitogen-activated protein) kinase signalling pathway (80).

There are mainly four different kinds of β-arrestin expressed in humans. Two β-arrestins are expressed in photoreceptor cells whereas the other two β-arrestins (1 and 2) are ubiquitously expressed in all cells (81). Arrestin-1 (visual arrestin) is expressed in rod cells and arrestin-4 (cone arrestin) is expressed in cone cells Both arrestins are responsible for the termination of visual signals by interaction with rhodopsin or color opsin. The two non-visual arrestins interact with many GPCRs in a non-specific manner (81).

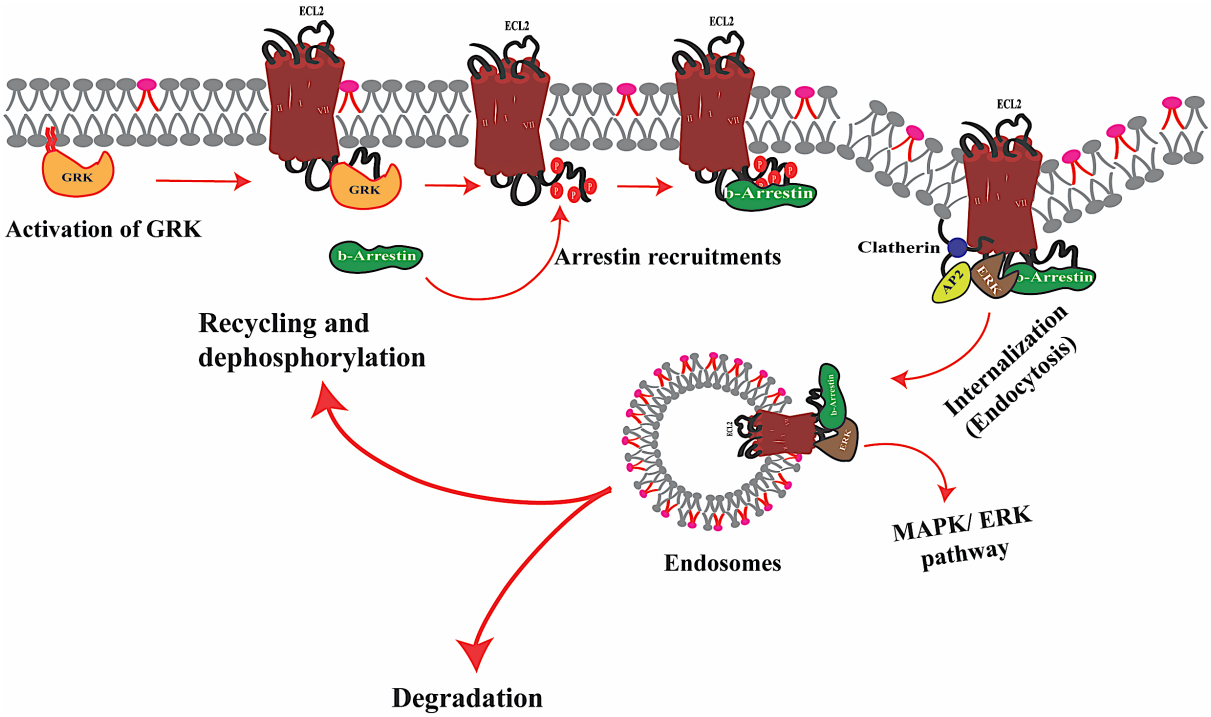

Figure 1.7: Schematic representation of G-protein coupled receptors' (GPCRs) phosphorylation and arrestin binding: After the dissociation of the heterotrimeric G-protein from a GPCR, the G-protein coupled receptor kinase (GRK) binds to the activated GPCRs and phosphorylates the C-terminal region of the receptor. The binding of GRK leads to the deactivation of the receptor by sterically hindering G-protein binding and promoting arrestin recruitment to the receptor. Phosphorylation of GPCRs by GRK kinase leads to the recruitment of β-arrestin, which initiates internalization of the receptor by clathrin-dependent endocytosis. An internalized receptor is subsequently carried to endosomes, where it is either degraded in the lysosome or is recycled and transported back to the membrane. (Adopted from Weis and Kobilka et al., 2019 (82))

1.6 Allosteric modulation of GPCRs and its importance:

An allosteric modulator is a ligand that binds to different (allosteric) positions on the receptor that is both topologically and spatially distinct from the endogenous ligand (orthosteric) binding site of the receptor (33,83). Allosteric modulation in proteins was first discovered in enzymes, but later it was found in all proteins including GPCRs. GPCRs form the largest cell surface receptor family and are ubiquitously expressed in all types of cells. Compared to other cell receptors, GPCRs can receive various different types of external stimuli which cause downstream signalling inside the cell. There are usually multiple binding sites present in GPCRs, including one specific orthosteric binding site and one distinct, less conserved

allosteric secondary binding site (84,85). The allosteric binding site in GPCRs can be found both in the intracellular and extracellular parts of the receptor. Several of these binding sites are well separated from the orthosteric binding site (OBP), whereas in some cases, like the 5-Hydroxytryptamine receptor 4 (5-HT4), it may have an extended binding pocket-like characteristic. If the binding of a modulator at the allosteric binding site in GPCRs enhances the effects of the orthosteric ligand, it is a called positive allosteric modulator (PAM), if it decreases the effects, is called a negative allosteric modulator (NAM) (86,87).

As compared to orthosteric binding pockets, the allosteric binding pockets are more receptor-specific and less conserved within subtypes of GPCRs. Designing specific compounds which activate only one GPCR subtype can be difficult due to sharing conserved binding pockets and limited pharmacokinetics of endogenous ligands. The binding site of the allosteric modulator can be a promising drug target site causing fewer side effects and a higher GPCR subtype-selectivity (30,88,89). The allosteric properties of GPCRs are not only relevant for the drug industry but is also important for structure-function investigations of GPCRs to understand their mechanism of action.

1.7 Pharmacological importance of GPCRs:

GPCRs are the 2nd most important pharmaceutical target family after enzymes due to its involvement with various biological processes. They are widely expressed in different organs and tissues in humans (12,30). GPCRs are crucial membrane protein receptors that are involved in various biological processes and responsible for many downstream signals inside the cells. There is a vast number of cellular functions which are regulated by GPCR signaling, for example, cell growth, immune response, cell organization, homeostasis, and cell death, among many others. Any dysfunction or loss of function of GPCRs can lead to acute or chronic diseases in humans. like asthma/ hypertension (caused by β_2-andrenergic receptors), cardiovascular disease or heart failure (caused by β1-andrenergic receptors), anxiety/depression (dopamine

receptors), and heart strokes (A_2A-adenosine receptors)(90-93). Mutations of GPCRs can also lead to various diseases in humans such as infertility in females (follicle-stimulating hormone receptors (FSHR)), nephrogenic diabetes insipidus (vasopressin receptors (V2R)), retinitis pigmentosa (rhodopsin receptors), whim syndrome (CXCR4), familial exudative vitreoretinopathy (frizzled receptor (FZD4)), and sporadic hypoparathyroidism (calcium-sensing receptor (CaSR) (94).

It has been shown that in the development of cancer, metastasis is due to the overexpression of certain GPCRs. These distinct GPCRs are over-expressed in different types of cancer cells in humans such as breast, prostate, and gastric cancer, lung cancer (prostaglandin E2 receptor), melanoma [chemokine receptor 4 (CXC4)], B-cell lymphoma (smoothened receptor) and head and neck squamous carcinoma (bradykinin receptor and chemokine receptor-2)(95-98). In addition to the human GPCRs, there are also reports about several viral GPCRs have a role in viral infection or pathogenesis as well as virus-induced oncogenesis in humans (99,100). For instance, human herpes virus-8, which regulates the production of viral GPCR, ORF74 upon infection, is responsible for "Kaposi's sarcoma" in humans (97,98).

GPCRs play a significant role in numerous essential biological processes as well as numerous clinical disorders affecting humans, making them excellent candidates for drug discovery. The GPCRs' position in the cellular membrane provides special pharmacological access to these proteins, and the effectors and signaling pathways systems linked to the receptors enable effective drug action. Nearly one-third of the FDA approved drugs target GPCRs, but only a few GPCRs (~25 of the ~800 known GPCRs) are targeted by these drugs (12,101). As a result, enormous effort is put into finding novel GPCR-targeted drugs.

A thorough understanding of the mechanisms of GPCR action and structure will enable the development of more specific drugs which will help in therapies (84). There are still many GPCRs, whose functions and mechanisms of action are not known. They are referred to as orphan GPCRs.

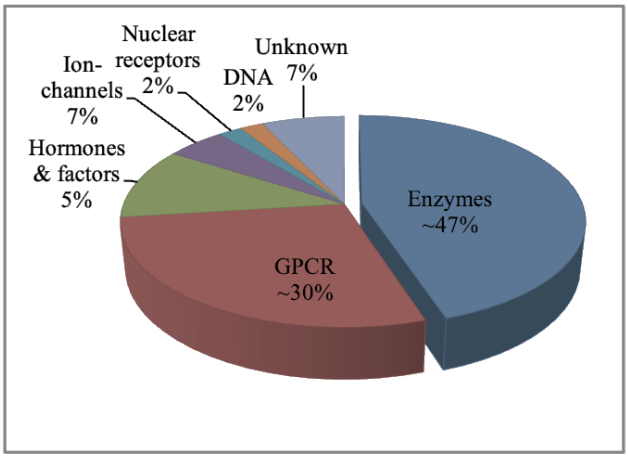

Figure 1.8: Pie-chart representation of FDA-approved marketed drugs against different target molecules in humans: The pie-chart depicts the percentage of marketed drugs against different targets in the human body. Out of all these drugs, ~ 47% are targeted against enzymes and ~ 30% are against GPCRs (adopted from (30)).

1. 8 Structural biology techniques for protein structure determination and dynamics studies:

Proteins are responsible for regulating various complex cellular functions inside the cells. A well-defined and high-resolution 3D structure of proteins is required to understand their mechanism of action. The biological functions of proteins depend on the local and global conformational dynamics of their structures. The atomic structure and the dynamics of the protein can be studied by using several biophysical techniques such as X-ray crystallography, electron cryo-microscopy, nuclear magnetic resonance (NMR), and fluorescence resonance energy transfer **(**FRET). The first atomic structure of a protein, namely that of myoglobin was determined by John Kendrew in 1960, at the same time, Max Perutz published the structure of hemoglobin at 5.5 Å resolution. For their contributions, Max-Perutz, and John Kendrew received the Nobel Prize in Chemistry, in 1962. Kurt Wüthrich and co-workers published the first NMR structure of a protein, namely that of the “bull seminal protease inhibitor” in 1984, followed by a PSTI (porcine pancreatic secretory trypsin inhibitor) structure that resembled its crystal structure. He received the Nobel Prize in Chemistry for his working 2010 (102-104).

Membrane proteins are the most difficult targets for structural studies, because of their hydrophobic nature. The first X-ray crystal structure of a membrane protein or of a membrane protein complex, namely of a "photosynthetic reaction center" was published in 1985. Hartmut Michel, together with Johann Deisenhofer and Robert Huber, received the Nobel Prize in Chemistry of 1988 (14) for structure determination. From pharmacological perspective membrane proteins are key targets due to their involvement in numerous crucial biological processes. Due to the importance of membrane protein, today there are ~1200 structures from distinct membrane proteins submitted to the Protein Data Bank (PDB).

1.8.1 Electron cryo-microscopy (Cryo-EM)

There are challenges and obstacles have gradually emerged after studying membrane protein structure by X-ray crystallography. These challenges are mainly associated with the nature of membrane proteins rather than with X-ray technology. For example, obtaining high-yield (milligram amounts), pure, active, and stable membrane protein samples, not to mention getting well-diffracting crystals are essential for obtaining high-resolution X-ray structures. All of these factors make it challenging for studying membrane protein's structure using X-ray crystallography, especially mammalian membrane proteins.

The field of structural biology has undergone a major transformation in recent years due to the discovery and advancement of electron cryo-microscopy (cryo-EM). Structural research on membrane proteins is significantly enhanced and facilitated by the use of single particle analysis (SPA) cryo-EM, a non-crystallographic technique that deals with randomly oriented single protein molecules. Recently, the development in cryo-EM technology especially in direct electron detectors (DED), whose detective quantum efficiency (DQE) has greatly improved, facilitated membrane protein structure determination to a great extent. In addition to

technology, the introduction of better and more efficient data analysis software using artificial intelligence (AI), and deep learning, helps in getting high-resolution structures.

In SPA, the biological samples were rapidly vitrified with the help of liquid ethane or propane on top of cryo-EM grids. Rapid vitrification aids in preserving the biological samples in their native state and allowing the samples to be distributed uniformly in an amorphous thin layer of ice. The samples were exposed to the high-voltage electron beam. As an electron beam passes through the samples embedded in a thin ice layer, it gets diffracted which is later recorded as multi-frame movies with the help of a camera. To minimize radiation damage to the sample, low dose imaging strategy was used. This strategy creates a high background noise, which can be overcome by aligning and averaging many 2D classes of the particle with distinct orientations. The SPA approach is based on a large collection of images obtained from a variety of angles while looking at the same molecules. 3D structure of the molecules is reconstructed by using 2D class averages with the help of mathematical algorithms based on Fourier slice theorem. Further iterative improvement of the 2D average classes can result in the generation of high-resolution 3D maps (105,106). SPA offers a significant benefit over crystallography for examining membrane protein structure since it only requires relatively small quantity of sample (0.1 mg) and does not require protein crystallization, which was previously the most challenging step for membrane protein structural studies (107-109).

1.8.2 Solid-state nuclear magnetic resonance spectroscopy (ssNMR)

Nuclear magnetic resonance spectroscopy is a powerful technique for studying molecular structure and dynamics at the atomic level (110,111). Nuclei with non-zero spin quantum numbers in target molecules can be probed by this technique. In NMR experiments, samples are placed in an external static magnetic field, while radio-frequency pulses are applied to the nuclei. The detected radio-frequency NMR signals are then collected by the signal receiver,

digitalized, and processed for further analysis. The energy difference between two spin-states is dependent on the external magnetic field (B) and the angular moment (μ).

$$\boldsymbol{E = -\mu * B_0 = -\gamma P * B_0 = -(m_i * h\gamma B_0)}$$

"B_0" is the static magnetic field whereas "$\boldsymbol{m_i}$" is the magnetic quantum number and "γ" is the gyromagnetic ratio of nuclei (characteristic property of a distinct nucleus).

In Fourier transform NMR the time-domain RF signals, so-called free induction decays (FIDs), are recorded and are Fourier transformed to the frequency-domain spectra by Fourier transformation.

A number of NMR interactions can be probed via specific NMR methods. The isotopes that are most often used to study biomacromolecules are ^{1}H, ^{13}C, ^{15}N, ^{19}F, and ^{31}P, the spin quantum number of which is (+/-)1/2. A number of NMR interactions involving these spins contribute to the resulting NMR spectra: chemical shifts, chemical shift anisotropy, dipole coupling, J-coupling, and quadrupole coupling. The isotropic chemical shift indicates that the nuclear spin's resonance frequency is affected by its chemical and electronic environment. In the case of chemical shift anisotropy (CSA), it depends on the anisotropic arrangement of electrons surrounding the nuclei. In the case of "dipole coupling," the magnetic moment of one nuclei spin interacts with the dipole of other nuclei in its surrounding through space.

"J-coupling" describes the interaction between two nuclear spins when they are connected by a chemical bond. "Quadrupole coupling" occurs in nuclei with I>1/2, which contain two different spin states with opposite charge distributions. The isotropic chemical shift and J-coupling are isotropic parameters independent of the nuclei orientations inside the magnetic field. In the case of chemical shift anisotropy (CSA), dipole-coupling and quadrupolar coupling depend on nuclei orientations as well as dynamics. CSA and quadrupolar coupling can provide knowledge about the electrical structure and chemical bonding, dipolar coupling is especially capable of providing information about inter- and intramolecular distances of molecules.

In solution NMR, molecular tumbling averages out anisotropic interactions, which permits to resolve NMR signals. But for large biomacromolecules, slow tumbling also leads to rapid transverse relaxation, which causes the broadening of spectral lines. Solid-state NMR can be applied to molecules in solids or in general in sample forms in which molecular motions are restricted. A molecule's mobility is typically restricted in the solid state. As a result most anisotropic interactions, (e.g., dipole coupling, chemical shift anisotropy, and quadrupolar coupling) can be characterized by ssNMR (112).

In solid-state NMR these anisotropic interactions result in the broadening of spectra. To minimize the effects of anisotropy interaction in line broadening and low resolution, magic angle spinning (MAS) is widely used in ssNMR, where the samples are spun at high speeds about an axis at the magic angle of 54.74° with respect to the external magnetic field B_0 (113,114). Most anisotropic interactions can be efficiently averaged when the MAS frequency is greater than the NMR interaction, resulting in well-resolved SSNMR signals. MAS ssNMR has been developed extensively during the last decades, which enables the extraction of desired structural information while offering great spectral resolution in the ssNMR (115). Applying MAS to ssNMR, anisotropic interactions are averaged for improving the spectral resolution. But this feature also leads to the loss of important structural and electronic structural information. To recover such lost information, recoupling schemes are often applied in ssNMR spectroscopy, which allows to establish of, for example, the correlations between ^{13}C and ^{15}N. An example of such recoupling schemes is the transferred echo double resonance (TEDOR) (116,117).

Cross polarization is the method to overcome the problem associated with low sensitivity and low abundance of low-gamma nuclei by transferring the nuclear magnetization from the high-gamma therefore highly polarized nuclei (e.g. ^{1}H) to low-gamma nuclei. The magnetization transfer is accomplished by applying external RF pulses under Hartmann-Hahn conditions (118).

Considering that protein backbones and side chains are composed largely of C and N, the ssNMR technique focuses primarily on nuclei like ^{13}C and ^{15}N to obtain crucial structural information from protein samples. However, ^{13}C and ^{15}N spins are of low gamma and exhibit long T1 relaxation times, which are not favorable for sensitivity. In contrast, the high-gamma ^{1}H in a biological sample is highly abundant and shows a fast T1 relaxation. ^{1}H signals are difficult to be resolved in ssNMR due to the strong homonuclear dipolar interactions in solids but can be used to amplify the signal for low gyromagnetic ratios like ^{13}C and ^{15}N by transferring magnetization from ^{1}H via cross-polarization.

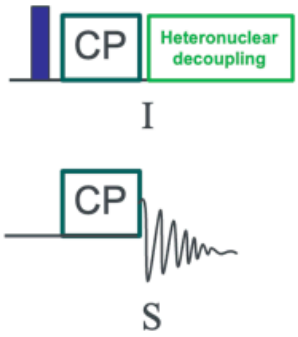

Figure 1.9: Graphical representation of a typical cross-polarisation experiment: The magnetization of a proton (I), radiofrequency was applied to two nuclei for cross-polarization (CP) (in green) The signal from the low magnetization nucleus (S) can be detected after heteronuclear decoupling.

2-Dimensional NMR: In biological samples, 2D NMR plays an important role in resolving overlapping signals of complex molecules. The preparation phase of a 2D ssNMR experiment begins with a $\pi/2$ pulse, which is followed by a CP step. During the evolution period t1, chemical shift information is encoded. In mixing time "t_m" inter-nuclei magnetization transfer occurs. The experiment ends with a detection period and the following inter-delay. The 2D spectrum is reconstructed by combining multiple 1D spectra collected with varied t_1 intervals and plotted into two frequency axes. In the case of single quantum-single quantum (SQ-SQ) homonuclear 2D NMR, the diagonal peak of the two axes corresponds to two frequencies of 1D spectra collected at different time points of the same nuclei, whereas other peaks are

considered to be cross-peaks. In the case of heteronuclear 2D-NMR, the frequency axis corresponds to two different nuclei, either ^{1}H and ^{13}C or ^{15}N, and the peaks are associated with chemical changes of associated spins.

Transferred Echo Double Resonance (TEDOR): In biological samples, ^{13}C – ^{15}N distances, which contain valuable structural information, can be measured via TEDOR which reintroduces heteronuclear dipolar couplings. TEDOR is based on rotating echo double resonance (REDOR). It enables the detection of correlations between ^{13}C and ^{15}N spins and even quantitative measurements of their internuclear distances (119). Generally, in REDOR experiments, a set of MAS-synchronized RF pulses are used to transfer the magnetization between ^{13}C and ^{15}N. In comparison to 15N-13C double CP, TEDOR-based magnetization transfer is more robust against missing RF power and RF inhomogeneity, therefore it is used in our case while conventional double CP cannot be optimized due to the low sensitivity (120).

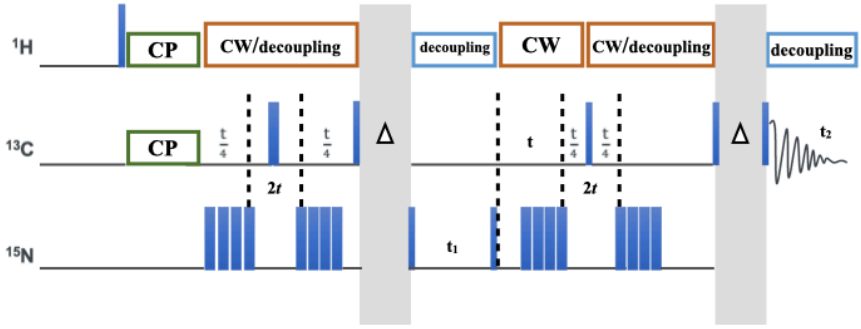

Figure 1.10: Graphical representation of typical TEDOR experiments: It depicts the typical pulse sequence of TEDOR experiment to introduce dipolar couplings between the ^{13}C and ^{15}N using ^{1}H. where Δ = z-filter period, CP=cross polarisation, CW=continuous wave, adopted from (121).

DNP-enhanced ssNMR spectroscopy: NMR is often a technique with low sensitivity. ssNMR studies on membrane proteins, such as GPCRs, require large quantities of high-quality samples, which are difficult to obtain. By making use of the highly polarized electron spins, the gyromagnetic ratio, which is over 600 times of 1h spins, dynamic nuclear polarization (DNP)

improves NMR signals drastically (122). In DNP experiments, the polarization of unpaired electrons is transferred to nuclear spins. Electrons exhibit a far higher level of polarization in an external magnetic field than nuclei because of their large intrinsic magnetic moment. Upon microwave saturation of electron Zeeman transitions, the NMR signals can be amplified through various DNP mechanisms. The DNP enhancement can be defined as

$$E = \frac{I_{on}}{I_{off}}$$

where I_{on} = the signal intensity when the microwave is turned on

I_{off} = The signal intensity when the microwave is turned off

and E = signal enhancement

DNP experiments are often performed at low temperatures, where the extended electron relaxation times permit better saturation of electron spins. Both endogenous and exogenous species might provide unpaired electron spins for DNP. Usually, synthetic biradicals like AMUPol are tailor designed for efficient cross-effect DNP on biological samples (123). To prevent the broadening and quenching of the NMR signals due to paramagnetic broadening, the concentration of unpaired electrons must be kept under control.

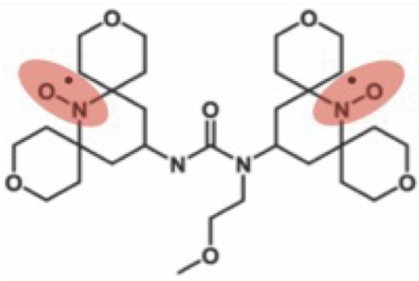

Figure 1.11: Chemical formula of the biradical reagent AMUPol, which is used in DNP-ssNMR as a polarizing agent (123).

1.9 Aim of the study:

GPCRs are involved in various biological processes within the body and they are crucial targets for therapeutic drug development. There are more than 150 high-resolution GPCR structures published from 2007 until now. Despite the plethora of research in understanding the structural and chemical properties of GPCRs, very little is known regarding the mechanisms of ligand selectivity, biased signaling, and its binding modulation with respect to allosteric modulators.

The first aim of this thesis was to heterologously express and purify the calcium-sensing receptor (CaSR) from class-C GPCRs in *Pichia pastoris* and insect cells (*Sf9*). This task included the optimization of the solubilization and purification of the CaSR receptor for structural and functional studies. The second aim of this thesis was to heterologously express and purify mini G_{α} proteins in *E. coli* for getting an active GPCR-mini G protein complex for structural and functional studies of GPCRs. The last aim of the thesis was to decipher the structural and functional impacts of the allosteric modulator on the orthosteric binding pocket of the bradykinin receptor, a class-A GPCR.

Chapter – 2: Materials and Methods

2. Materials and Methods

2.1 Materials

2.1.1: Chemicals and kits used

The Chemicals and kits used in this study was listed below in detail.

Table 2.1: List of suppliers of general chemicals and kits.

Chemicals	Suppliers
2-Propanol	Carl Roth, Karlsruhe, Germany
Bromophenol blue (3',3,5',5-tetrabromo-phenolsulfonphthalein)	Carl Roth, Karlsruhe, Germany
Acetic acid	Carl Roth, Karlsruhe, Germany
Agarose (Roti®garose NEEO)	Carl Roth, Karlsruhe, Germany
Ampicillin	AppliChem, Darmstadt, Germany
Aprotinin	Carl Roth, Karlsruhe, Germany
BCIP (5-bromo-4-chloro-3-indolyl phosphate)	Life Technologies, Darmstadt, Germany
Chloramphenicol	Carl Roth, Karlsruhe, Germany
complete protease inhibitors EDTA-free	Roche Applied Science, Mannheim, Germany
Cholesteryl hemisuccinate	Anatrace, Maumee, USA
dimethylformamide	Carl Roth, Karlsruhe, Germany
d-desthiobiotin	Sigma Aldrich, Steinheim, Germany
Dithiothreitol	Carl Roth, Karlsruhe, Germany
n-Dodecyl-ß-D-maltoside	Glycon Biochemicals GmbH, Germany
Ethanol analytical grade	Merck, Darmstadt, Germany
Ethidium bromide	Carl Roth, Karlsruhe, Germany
E64	AppliChem, Darmstadt, Germany
Ethylenediaminetetraacetic acid (EDTA)	Carl Roth, Karlsruhe, Germany
Glycerol	Carl Roth, Karlsruhe, Germany

Hepes (4-(2-hydroxyethyl)-1-piperazine-ethane-	Carl Roth, Karlsruhe, Germany
Hydrochloric acid	Fluka/Sigma Aldrich, Steinheim, Germany
Imidazole	Merck, Darmstadt, Germany
Isopropyl b-D-1-thiogalactopyranoside (IPTG)	Carl Roth, Karlsruhe, Germany
Kanamycine	Gerbu, Heidelberg, Germany
Leupeptin	Carl Roth, Karlsruhe, Germany
Magnesium chloride	Merck, Darmstadt, Germany
Magnesium sulphate	Merck, Darmstadt, Germany
MES (2-(N-morpholino)ethanesulfonic acid)	Carl Roth, Karlsruhe, Germany
Methanol	Carl Roth, Karlsruhe, Germany
MOPS (3-(N-morpholino)propanesulfonic acid)	Carl Roth, Karlsruhe, Germany
NBT (nitrotetrazolium blue chloride)	Life Technologies, Darmstadt, Germany
Pepstatin A	Carl Roth, Karlsruhe, Germany
Phenylmethanesulfonylfluoride (PMSF)	Carl Roth, Karlsruhe, Germany
Polyethyleneimine (PEI)	Sigma Aldrich, Steinheim, Germany
Potassium chloride	Merck, Darmstadt, Germany
Rotiszint ecoPlus	Carl Roth, Karlsruhe, Germany
Sodium chloride	Merck, Darmstadt, Germany
SDS (sodium dodecylsulphate)	Carl Roth, Karlsruhe, Germany
Sodium hydroxide	Gerbu, Heidelberg, Germany
Tris (2-Amino-2-hydroxymethyl-propane-1,3-diol)	Roth, Karlsruhe, Germany
Tween-20	Gerbu, Heidelberg, Germany
PierceTM BCA Protein Assay Kit	Life Technologies, Darmstadt, Germany

Table 2.2: List of suppliers of protein purification resins.

Resins	Supplier
Histrap HP	GE Healthcare, Munich, Germany

Histrap FF	GE Healthcare, Munich, Germany
StrepTactin FF	GE Healthcare, Munich, Germany
MBP trap HP	GE Healthcare, Munich, Germany
Anti-Flag™ M2 Affinity Gel	Sigma-Aldrich Chemie GmbH, Deisenhofen
Monomeric Avidin Gel	Pierce, Rockford, USA
Ni-NTA® Agarose	Qiagen GmbH, Hilden, Germany
Strep-Tactin®-Agarose	IBA BioTAGnology, USA
Superdex 200 PC 3.2/30	Amersham Pharmacia Biotech, Freiburg
Q-Sepharose	Sigma-Aldrich Chemie GmbH, Deisenhofen

Table 2.3: List of suppliers of laboratory equipment.

Instruments	Supplier Name
Äkta purifier and basic FPLC systems	GE Healthcare, Munich, Germany
Infors shaker incubator	Infors, Bottmingen, Switzerland
Molecular Imager Gel DocXR system	Bio-Rad, München, Germany
Nanodrop ND-1000 spectrophotometer	Peqlab, Erlangen, Germany
Parr bomb high pressure vessels (50 and 600 ml)	Parr Instrument Company, Moline, USA
Thermomix	Eppendorf, Hamburg, Germany
Tristar LB941 microplate reader	Berthold Technologies, Bad Wildbad, Germany
Ultracentrifuge Optima LE90-K	Beckman Coulter, Krefeld, Germany

Table 2.4: List of suppliers of enzymes, chemicals and kits used for molecular biology.

Chemicals	Supplier Name
Hot start polymerase	New England Biolabs, Frankfurt, Germany
BamHI, HindIII-HF, NdeI, NotI-HF,	New England Biolabs, Frankfurt, Germany
KpnI, NcoI, XhoI	Life Technologies, Darmstadt, Germany
T4 DNA ligase	New England Biolabs GmbH, Schwalbach
bovine serum albumine	New England Biolabs, Frankfurt, Germany
Benzonase	Merck KgaA, Darmstadt, DE
EndoH	New England Biolabs GmbH, Schwalbach

PNGaseF	New England Biolabs, Frankfurt, Germany
6x DNA loading dye	Life Technologies, Darmstadt, Germany
10 kb DNA marker	Life Technologies, Darmstadt, Germany

Table 2.5: List of suppliers of materials and reagents used for cell culture.

Chemicals	Supplier Name
TNM-FH medium	c.c.pro, Oberdorla, Germany
Insect-Xpress	Lonza,
Cellfectin	Life Technologies, Darmstadt, Germany
Fetal bovine serum (FBS)	BioWest, Nuaillé, France
Vitamin B12	Sigma Aldrich, Steinheim, Germany
Pluronic F68	AppliChem, Darmstadt, Germany
L-glutamine	c.c.pro, Oberdorla, Germany
Gentamicine	Life Technologies, Darmstadt, Germany
58Lashback kit	Oxford Expression Technologies, Oxford, UK

Table 2.6: Cell culture Flask and general materials

Materials	Supplier Name
Nunclon Delta T25, T75, T17	Thermo Scientific, Dreieich, Germany
Nunclon Delta 96-well plates	Thermo Scientific, Dreieich, Germany
Nunclon Delta 6-well plates	Thermo Scientific, Dreieich, Germany
Nunclon Delta 10 mm dishes	Thermo Scientific, Dreieich, Germany

Table 2.7: SDS PAGE, and Western blot

Materials	Supplier Name
NuPAGE Bis-Tris gels	Thermo Scientific, Dreieich, Germany
PageBlue Protein Staining Solution	Thermo Scientific, Dreieich, Germany
NuPAGE Native-PAGE	Thermo Scientific, Dreieich, Germany

Table 2.8: Antibodies used in these studies

Materials	Supplier Name
Anti-flag M1 antibody	Sigma-Aldrich Chemie GmbH, Deisenhofen
Anti-flag M2-AP conjugate	Sigma-Aldrich Chemie GmbH, Deisenhofen
Anti-polyhistidine antibody	Sigma-Aldrich Chemie GmbH, Deisenhofen
Anti-polyhistidine-AP conjugate	Sigma-Aldrich Chemie GmbH, Deisenhofen
Anti G α i antibody	Calbiochem, MerckKGaA, Darmstadt
Anti G β antibody	Calbiochem, Merck KgaA, Darmstadt
Anti-Mouse IgG, AP conjugate	Sigma-Aldrich Chemie GmbH, Deisenhofen

Table 2.9: Kits used for the study

Materials	Supplier Name
Qiagen Plasmid miniprep kit	Qiagen GmbH, Hilden
QIA quick Gel Extraction kit	Qiagen GmbH, Hilden
QIA quick PCR Purification Kit	Qiagen GmbH, Hilden
BCA Protein Assay Kit	Pierce, Rockford, USA

Table 2.10: Detergents

Materials	Supplier Name
n-Dodecyl- β -D-maltoside (LM)	Glycon Biochemicals, Luckenwalde, DE
n-Decyl- β -D-maltoside (DM)	Glycon Biochemicals, Luckenwalde, DE
Digitonin	Sigma-Aldrich Chemie GmbH, Deisenhofen
Deoxycholate, sodium salt	Sigma-Aldrich Chemie GmbH, Deisenhofen
CHAPS	Calbiochem, Merck KgaA, Darmstadt
N-Dodecylphoscholine (Fos12)	Anatrace, Maumee, USA
N-Tetradecylphoscholine (Fos14)	Anatrace, Maumee, USA
N-Hexadecylphoscholine (Fos16)	Anatrace, Maumee, USA
n-Octyl- β -D-glucopyranoside (OG)	Glycon Biochemicals, Luckenwalde, DE
n-Octyl- β -D-maltoside (OM)	Glycon Biochemicals, Luckenwalde, DE
SDS	Carl Roth GmbH & Co. KG, Karlsruhe
LMNG	Anatrace, Maumee, USA
SMA	Anatrace, Maumee, USA

Table 2.11: Technical Equipment used in this study.

Devices	**Manufacturer Name**
Centrifuges	
4K15 centrifuge	Sigma Labcentrifuge GmbH, Germany
Avanti™ J-20 XPI	Beckman Coulter, USA
HERAEUS Fresco21 Centrifuge	Thermo Electron Corporation, USA
Optima™ LE80K Ultracentrifuge	Beckman Coulter, USA
Centrifuge 5418	Eppendorf, Germany
Optima™ MAX Ultracentrifuge	Beckman Coulter, USA
Sorvall® RC-5B	Du Pont Instruments, USA
Rotors	
Thermo Scientific™, USA	Thermo Scientific™, USA
24 X 1,5/2,0 ml	Eppendorf, Germany
JLA 8.1000	Beckman Coulter, USA
Sorvall® GS-3	Du Pont Instruments, USA
Swing-out rotor 11140	Sigma Laborzentrifugen GmbH, Germany
Swing-out rotor 11150	Sigma Laborzentrifugen GmbH, Germany
TLA55 (Serial No. 02-E-3831)	Beckman Coulter, USA
Type 45 Ti (Serial No. 8E 965)	Beckman Coulter, USA
Type 70 Ti (Serial No. 98E 2714)	Beckman Coulter, USA
Pumps	
Peristaltic Pump P-1	Pharmacia / Cytiva, USA
Peristaltic Pump VL500	Verder, Netherlands
Vacuum Pump MP40	Biometra GmbH, Germany
Spectrophotometers	
BioMate 3 UV-Visible Spectrophotometer	Thermo Spectronic, USA
Nano-Drop® ND-1000 Spectrophotometer	peqlab Biotechnologie GmbH / VWR International, USA
SpectraMax M2 Plate reader	Molecular Devices, USA
Incubation devices	
Lab incubator	Memmert GmbH + Co. KG, Germany
Multi-tron incubator shaker	INFORS HT, Switzerland

Thermomixer compact	Eppendorf, Germany
Insect cell incubator	Eppendorf, Germany
Cooling devices	
Circulation Thermostat C1	Haake / Thermo Fisher Scientific, USA
Circulation Thermostat D8	Haake / Thermo Fisher Scientific, USA
Waterbath G	Haake / Thermo Fisher Scientific, USA
Watherbath K20	Haake / Thermo Fisher Scientific, USA
Cloning and transformation	
Concentrator 5301 (Speed Vac)	Eppendorf, Germany
T-Gradient PCR cycler	Biometra GmbH, Germany
Gene Pulser® II	Bio-Rad Laboratories, USA
Homogenisation and cell Lysis	
PARBOMB	
Desintegrator 6 Bead mill	BIOmatik GmbH, Germany
TurboMix™	Scientific Industries, Inc™, USA
Ultra-Turrax T15	IKA®-Labortechnik, Janke & Kunkel GmbH & CO.KG, Germany
Protein Purification Systems	
ÄKTAbasic	Amersham Biosciences / Cytiva, USA
ÄKTAmicro	GE Healthcare / Cytiva, USA
ÄKTAPurifier	Amersham Biosciences / Cytiva, USA
ÄKTAPure	GE Healthcare / Cytiva, USA
SMART system	Pharmacia Biotech / Cytiva, USA
Protein detection	
Bio-Dot® Microfiltraton Apparatus	Bio-Rad Laboratories, USA
Electrophoresis Power Supply EPS 600	Pharmacia Biotech / Cytiva, USA
iBlot™ Device	Invitrogen™/ Thermo Fisher Scientific, USA
Xcell SureLock™ Mini-Cell	Novex / Thermo Fisher Scientific, USA
Electron microscopy	
PELCO easiGLOW™ Glow Discharge Cleaning System	PELCO/ Ted Pella Inc, USA
Vitrobot IV	FEI / Thermo Fisher Scientific, USA

Tecnai Spirit BioTWIN	FEI / Thermo Fisher Scientific, USA
Titan Krios G3i	Thermo Fischer Scientific, USA

General	
BH-2 Microscope	Olympus Corp., Japan
Vortex Genie 2™	Bender & Hobein AG, Switzerland
HERAEUS LaminAir® Bench	Thermo Scientific™, USA
IKAMAG® Reo magnetic stirrer	IKA®-Labortechnik, Janke & Kunkel GmbH & CO.KG, Germany
pH-Meter 765 Calimatic	Knick Elektronische MessgeräteGmbH & Co. KG, Germany
Prometheus NT.48 nanoDSF	NanoTemper Technologies GmbH, Germany

2.1.2 Media and buffer compositions

Agarose gel (1%)	1 g agarose in 100 ml 1X TAE buffer
Ampicillin Stock solution (1000x)	150 mg/ml in sterile water (-20ºC)
Aprotinin (1000x)	10 mg/ml in water (-20ºC)
AP-buffer	100 mM Tris/HCl, (pH 9,5), 100 mM NaCl and 5 mM MgCl2
BCIP solution	50 mg/ml in DMF (-20ºC)
Destaining solution	100 ml methanol, 200 ml acetic acid mixed with 700 ml water
HEPES buffer	20 mM HEPES, pH 7,4 100 mM NaCl 12 mM $MgCl_2$
Membrane Buffer	20 mM Tris, pH 8 120 mM NaCl, 2mM EDTA 10% (v/v) Glycerin
PBS buffer	13,7 mM NaCl 2,7 mM KCl 1,5 mM KH_2PO_4

	13 mM Na_2HPO_4
PMSF (200x)	200 mM in DMSO
dNTP mix	dNTP mix (10x) 8 mM (2 mM each dATP, dCTP, dGTP, dTTP)
E64 (10000x)	3.5 mg/ml 50% ethanol (-20ºC)
Kanamycin stock (1000x)	40 mg/ml in water (-20ºC)
Leupeptin(2000x)	10 mg/ml in water (-20ºC)
NBT solution	50 mg NBT/ml in 70% DMF in water (-20ºC)
TAE buffer (50x) pH 7.4	2M Tris
	1 M acetic acid
	50 mM EDTA
TBS buffer	50 mM Tris/HCl, pH 7.4
	150 mM NaCl
Radioligand binding buffer	20 mM Tris/HCl pH 7.4
	100 mM NaCl
	5 mM $MgCl_2$
	1 mM EDTA
	1% BSA
	APS 10% (w/v) in water
TBST-Buffer	10 mM Tris/HCl, (pH 8,0)
	150 mM NaCl
	0,05% Tween 20
Media used for E.coli	
LB Medium	1% (w/v) Bacto™ Tryptone, 0.5% (w/v) yeast extract , and 1% (w/v) NaCl
LB-Agar	1% (w/v) Bacto™ Tryptone, 0.5% (w/v) yeast extract, and 1% (w/v) NaCl and 1.5 % (w/v) agar
SOC	0.5% (w/v) Bacto™ Yeast extract, 2% (w/v) Bacto™ Tryptone, 10 mM NaCl, 2.5 mM KCl, 10 mM MgCl2, 10 mM $MgSO_4$, 20 mM dextrose
Low salt LB	1% (w/v) Bacto™ Tryptone, 0.5% (w/v) Bacto™ yeast extract, 0.5%
	(w/v) NaCl, pH 7.5

Low salt LB-Agar	1% (w/v) Bacto™ tryptone, 0.5% (w/v) Bacto™ yeast extract, 0.5% (w/v) NaCl, 2% (w/v) Bacto™ agar, pH 7.5
Media used for *P. pastoris*	
YPD	1% (w/v) Bacto™ yeast extract, 2% (w/v) peptone, 2% (w/v) dextrose
YPD-agar	1% (w/v) Bacto™ yeast extract, 2% (w/v) peptone, 2% (w/v) dextrose, 2% (w/v) Bacto™ agar
YPDS	1% (w/v) Bacto™ yeast extract, 2% (w/v) peptone, 2% (w/v) dextrose, 1 M sorbitol
YPDS-Agar	1% (w/v) Bacto™ Yeast extract, 2% (w/v) peptone, 2% (w/v) dextrose, 1 M sorbitol, 2% (w/v) Bacto™ agar
BMGY	100 mM potassium phosphate pH 6, 1%(w/v) Bacto™ yeast extract, 2% (w/v) peptone, 1.34% (w/v) Difco™ yeast Nitrogen Base W/O amino acids, 0.00004% (w/v) biotin, 1% (w/v) glycerol
BMMY	100 mM potassium phosphate pH 6, 1% (w/v) Bacto™ yeast extract, 2% (w/v) peptone, 1.34% (w/v) Difco™ yeast nitrogen Base W/O amino acids, 0.00004% (w/v) biotin, 0.5 – 1% (v/v) methanol
BMMY-Agar	100 mM potassium phosphate pH 6, 1% (w/v) Bacto™ yeast extract,2% (w/v) peptone, 1.34% (w/v) Difco™ yeast nitrogen base W/O amino acids, 0.00004% (w/v) biotin, 2% (v/v) methanol, 2% (w/v) Bacto™ agar

2.1.4 Software, servers, and databases

The software and databases used in this study was listed below in detail.

Table 2.11: Software:

Software	Version	Application
ChimeraX	1.2.3	Structure visualization
Chimera	1.14	Structure modelling
SnapGene	5.2.4	DNA cloning
Unicorn	5.11	Protein purification
cisTEM	1.0.0-beta	EM data processing
Leginon	3.2	EM data acquisition
EPU Krios	2.9	EM data acquisition
RELION	3.1	Cryo-EM data processing
CryoSparcs		
MicroWin	4.41	Protein concentration determination

2.2 Methods

2.2.1 Molecular cloning

The cloning of all constructs used in this study, for insect cells, yeast, and *E. coli* strains is described in this section. For the experiments, sterile conditions were maintained throughout e.g. all tips had been autoclaved, and autoclaved Milli-Q water was used. All clones used in our studies were cloned into the different vectors by using restriction enzyme-free cloning (124). The megaprimer for cloning was designed and used to clone different constructs into the vectors. The PCR experiments were carried out by using the Phusion DNA polymerase enzyme (Thermo Fisher Scientific, Germany), and the T Gradient thermocycler from Biometra (Germany). Overlap extension cloning is a PCR-based, restriction enzyme-free method that allows the cloning of the gene of interest into a plasmid without any homologous recombination

site or any restriction enzyme site. To achieve this, we had to design a custom-built hybrid megaprimer that contains part of the plasmid vector and part of the insert DNA construct. These hybrid primers were synthesized and received from Eurofins Genomics (France). The composition of the medium used for the PCR reaction in our studies is mentioned in the following table:

Composition	Volume (Reaction volume 50 µl)	Final concentration
5x Phusion HF buffer	10 µl	1x
10 mM dNTPs	1 µl	200 µM
10 µM reverse primer	2.5 µl	0.5 µM
10 µM forward primer	2.5 µl	0.5 µM
Template cDNA		50ng
Nuclease-free water	Final volume to 50 µl	-
Phusion DNA polymerase (2 Units/µl)	0.5 µl	1 Unit per reaction

Table 2. 16: Set up for PCR-reactions.

1st PCR

step	time	temperature	cycle
Initial denaturation	1 min	98 °C	1
Denaturation	15 sec	98 °C	
Annealing	30 sec	50-65 °C	30
Extension	1 min	72 °C	
Final extension	10 min	72 °C	1
Hold		4 °C	1

After the first PCR reaction, the sample containing the amplified DNA was checked and purified by agarose gel electrophoresis. The PCR samples were run in a 1% agarose gel in 1X Tris-acetate-EDTA (TAE) running buffer (40 mM Tris, pH 8.3, 20 mM acetate, 10 mM EDTA) at 80 V for approximately 1 hr. The agarose gel was stained using an aqueous EtBr (Thermo Fisher, Germany) solution (0.002% w/v). The binding of EtBr to double-stranded DNA enables

UV-light imaging of DNA fragments with the help of a UV transillumination gel doc (Biorad). The desired DNA band was scraped out with a scalpel and DNA was purified by the QIAquick gel extraction kit (Qiagen) using the manufacturer's protocol. Then the concentration of the gel-extracted DNA was measured using a nanodrop photometer. The purified DNA from the agarose gel was used as a megaprimer for the second PCR. The overhanging part of the megaprimer contains the complementary stand for vector plasmids to anneal and help to form nicked hybrid plasmid for the synthesis. The 2nd PCR reaction was set up according to the table (Table 2.16), the amplification of the hybrid plasmid vector was achieved together with the gene of interest. The amplified plasmid vector from the 2nd PCR was incubated with 20 units of DpnI at 37 °C for 1 hr to get rid of the parental plasmid vectors.

Composition	Volume (Reaction volume 50 µl)	Final concentration
5x Phusion HF buffer	2 µl	1x
10 mM dNTPs	1 µl	200 µM
PCR product (megaprimer)	2.5 µl	0.5 µM
Plasmid		50 ng
Nuclease-free water	Final volume to 20 µl	-
Phusion DNA polymerase (2 Units/µl)	0.5 µl	1 unit per reaction

Table 2. 16: The set up for the 2nd PCR-reactions 20 *µl* .

2nd PCR

step	time	temperature	cycle
Initial denaturation	2 min	98 °C	1
Denaturation	30 sec	98 °C	
Annealing	30 sec	55 °C	30
Extension	5 min 30 sec	72 °C	
Final extension	10 min	72 °C	1
Hold		4 °C	1

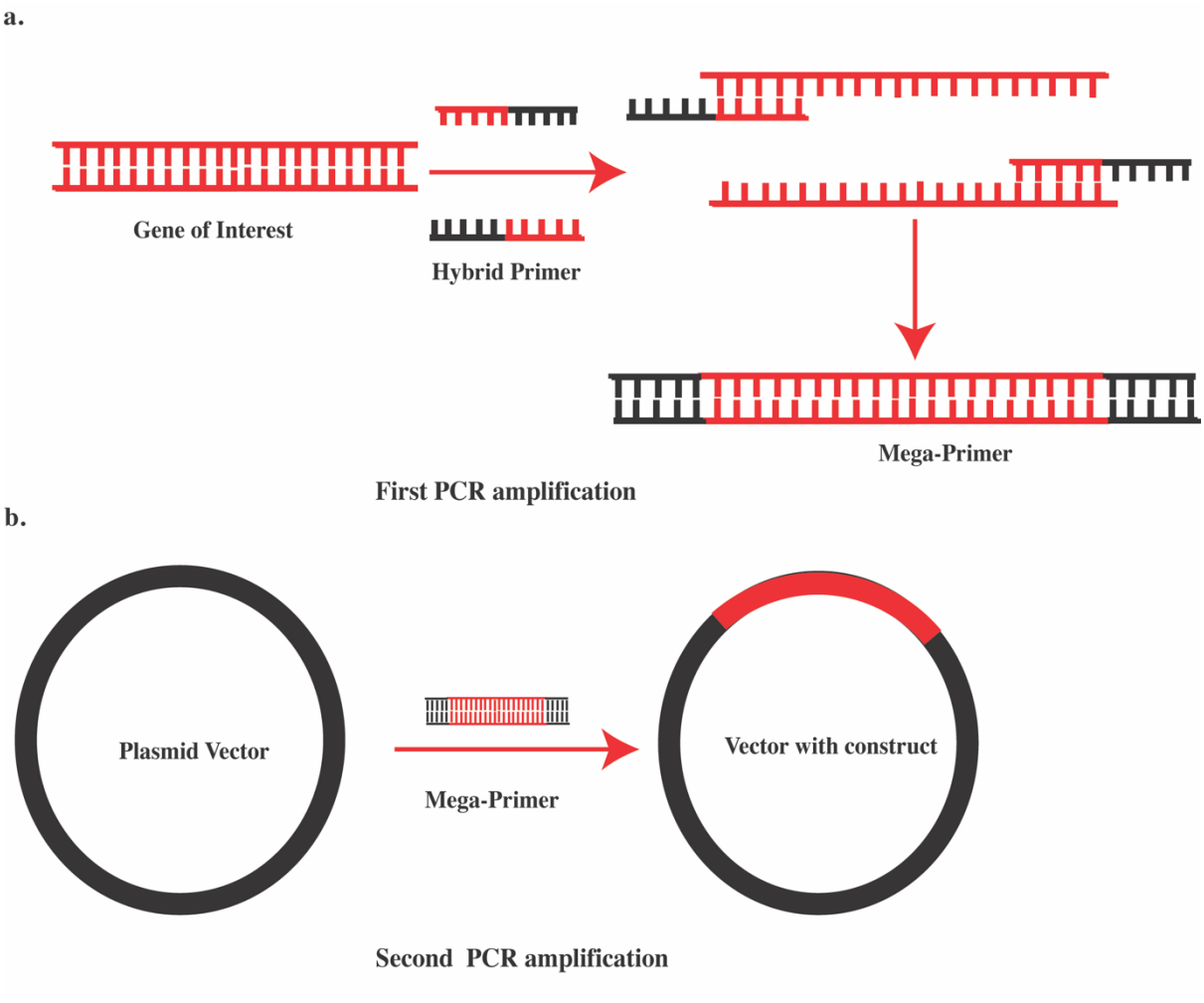

Figure 2.1: Schematic representation of overlapping PCR cloning: The figure shows restriction-free cloning or PCR-based cloning. a) first PCR amplification of megaprimer, b) second PCR amplification constructs into the vectors.

The DpnI digested plasmids were transferred into the commercially available competent *Escherichia coli* DH5α, NEB 10 cell as per section (methods-2.2.2.2).

2.2.2 Working with Escherichia coli (E. coli):

2.2.2.1 *E.coli* culture

A single colony of *E. coli* was picked from an o/n streaked LB-agar plate and used to inoculate 5 ml of LB-media and allowed to grow at 37°C at 200 rpm speed overnight in the presence of the appropriate antibiotics. Overgrown *E. coli* cells were either harvested for further use for plasmid prep or directly used for protein expression.

2.2.2.2 Preparation of competent *E. coli* cells and their transformation

A single colony of *E. coli* (of appropriate strain) was used to inoculate 10 ml of LB-media and allowed to grow at 37°C at 200 rpm speed in the absence of any antibiotics as primary culture. It was grown for 8 hrs under the same condition. It was used at a 1:100 ratio (v/v) as inoculum for starting a fresh culture in SOB medium. The cells were grown at 22°C with vigorous shaking until the O.D. of the culture reached 0.5- 0.8. When it reached the appropriate O.D., the cells were harvested by centrifugation at 4000 g for 30 min. Then the pellet was resuspended in 20 ml of transformation buffer and incubated for 20 min in ice. The cells were harvested again at the same speed for 30 min. The pellet was then resuspended in 8 ml of transformation buffer (per 100 ml of culture) and DMSO was added to the resuspended solution such that its final concentration was 10%. The suspension was incubated in ice for 8 – 10 minutes. 100 ul aliquots were pipetted into sterile Eppendorf tubes. These aliquots were snap-frozen in liquid nitrogen (N_2) and stored at -80°C.

2.2.2.3: Transformation of *E. coli*

The transformation protocol for *E.coli* with the desired plasmid was adopted (Inoue et al., 1990). The frozen competent *E.coli* aliquot was taken from -80°C and kept on ice. The desired DNA was added and the suspension was incubated on ice for 30 minutes. Then the sample was subjected to a heat shock for 45 sec at 42 °C and incubated on ice for 5 minutes. Addition of 1 ml of SOC- media followed and the sample was kept in a shaker for 1 hr at 37 °C. Cells were pelleted and plated on an LB-agar plate containing appropriate antibiotics.

2.2.2.4: Recombinant protein overexpression and purification in *E. coli*

The construct was transformed into *E.coli* BL21 (DE3) cells, and a colony was selected by ist antibiotic resistance (ampicillin or kanamycin). Then the positive colony was inoculated in 10 ml media containing the appropriate antibiotic (1000X stock). The culture was incubated at 37°C and 200 rpm overnight. Then it was transferred to a secondary culture for induction of protein expression. 1 ml of the primary culture was added to 1L of LB-medium with 1ml of

antibiotic. After 3-4 hours of incubation, the absorbance of the culture was measured at 600nm. When the O.D. reached 0.6, induction was started by 1 mM of IPTG for 4-6 hours. The cells were harvested by centrifugation at 6000 rpm at 4°C for 15 minutes. The supernatant was discarded and the pellet was resuspended in 10 ml of TBS with protease inhibitors and 0.5% Triton-X-100. The suspension was kept on ice for 30 minutes followed by sonication for 20 min. The cell lysate was centrifuged at 20,000 rpm for 30 minutes at 4°C. The supernatant was loaded onto a 5 ml His-trap FF column at 4°C for affinity binding. The columns were washed with 20 mM of imidazole in TBS. The protein was eluted with 300 mM of imidazole. The eluted protein was checked on the SDS page and resolved according to their expected molecular weights. All eluted fractions were pooled and dialyzed, and the protein concentration was measured with the BCA assay. The protein was further purified by FPLC.

2.2.3 Working with *Pichia pastoris*

2.2.3.1: *P. pastoris* culture and glycerol stock

Single *Pichia* colonies were picked from freshly plated *Pichia* in a YPD-agar plate and used to inoculate 20 ml YPD medium. Then the culture was grown at 30 °C, 180 rpm for 24 h, and these Pichia cultures was used further for protein expression. For long-term storage of *Pichia* strains, al volume of overnight *Pichia* culture was mixed with an equal volume of 50 % (w/v) glycerol and snap frozen with liquid N_2 and stored at -80 °C.

2.2.3.2: Transformation of *P. pastoris*

Transformation of *Pichia* was achieved via electroporation, as mentioned in the multicopy *Pichia* expression kit (125). A single colony of *Pichia* was picked from the freshly streaked YPD agar plate and transferred into 10 ml YPD media for o/n at 30 °C. On the next day, a secondary culture of 100 ml was grown from this culture with an initial OD600 of 0.1. The yeasts continue to grow until they achieve an OD600 of 1 to 1.5. The culture was then chilled by placing it in an ice bath for 30 minutes, followed by harvesting the cells by centrifugation at

1000 g at 4°C for 15 minutes. To get rid of any extra medium or buffer components, the pelleted *Pichia* cells were washed twice with 100 ml autoclaved and chilled water. Then the *Pichia* cells were pelleted down by centrifuging them at 1500 g at 4°C for 15 min. The pellet was further washed twice with 1 ml of 1M sorbitol and finally resuspended with 200 µl of 1M sorbitol. 80 µl of the resuspended *Pichia* cells were mixed with 10-20 µl (10 µg) of linearized DNA and incubated in a 2 mm electroporation cuvette on ice for 5 min. Electroporation of the yeasts was performed by using the Bio-Rad gene pulser and the Bio-Rad Pulse controller electroporation device with settings of the current at 600 mA, the voltage at 1.5 kV, and capacitance at 25 µF. After electroporation, 1ml of ice-cold YPDS medium was added to the cuvette and the cuvette was incubated at 30°C for 2 hr. Then the culture was plated onto a YAPD-agar plate with various dilutions and incubated for 48-72 h at 30°C until prominent colonies appeared.

*Note: The plasmids were linearized by digesting them with a suitable enzyme (Mostly *PmeI*) followed by purification by phenol-chloroform extraction (section 2.2).

2.2.2.3: Small-scale GPCR expression and membrane preparation

Small-scale membrane preparations from *Pichia* were done by using the methods mentioned (126). For small-scale membrane preparations, the best receptor expression colony was selected (126). The screened colonies from the fresh plate were used to inoculate 10 ml YPD-media and allowed to grow for 1-2 days at 30°C. Then the culture was transferred into a new 100ml baffle flask containing 25 ml BMGY-media with an OD of 0.1 and allowed to grow until OD_{600} of 2 was reached. Then the cells of 12.5 ml of the culture were pelleted using 1000g for 10 min and the cell pellet was resuspended with fresh 25 ml BMMY media to achieve OD_{600} =1. The cell suspension was then transferred into a new 100 ml baffled flask for further growth. For the screening of the expression, two different temperatures, 22 °C and 30 °C, were used. The samples were collected at different time points (6 h intervals). After 24 h of growth 0.25

ml methanol was added to the culture. Cells were collected under different conditions and harvested at 2000g at 4°C for 15 min, snap-frozen in liquid N_2, and stored for future use.

The *Pichia* cell pellets were thawed and resuspended in in double volume of ice-cold breaking buffer (50 mM HEPES,) pH 7.5, 100 mM NaCl, 5% (w/v) glycerol, 1 mM EDTA pH 7.4, 1 mM PMSF). Then nearly 700 µl of the cell suspension was transferred into 2 ml Eppendorf tubes and 1.5 ml of cold glass beads were added to the Eppendorf tubes. The lysis of the cells was achieved by vortexing the 2 ml Eppendorf tube 4-5 times for 5 minutes at 4°C with 5 min intervals with the help of a TurboMix™. Cell lysis was checked under a light microscope at 40X magnification. When more than 90% of the yeast cells had been disrupted, the lysis process was stopped. The beads and cell lysates were transferred into a 5 ml polypropylene column and filtered by centrifuging at 4°C for 10 min. The beads were further washed by adding fresh ice-cold breaking buffer to the beads. The cell lysate was centrifuged for 4.500 g at 4°C for 15 min, to remove unbroken cells and organelles. The supernatant was ultracentrifuged at 100,000 rpm at 4°C for 1hr. The supernatant was discarded and the membrane pellet was flash-frozen and stored at -80 °C for further use.

2.2.2.4: Large-scale GPCR expression in *Pichia* and membrane preparation

After selecting the clone and the conditions for the best expression, the clone was restreaked onto a fresh YPD-agar plate for future use. The clone was used to inoculate 25 ml of YPD media in a 100 ml baffled flask and grown in an incubator at 30 °C and at 180 rpm for 2 days. Then the culture was transferred into a new 100ml baffle flask containing 20 ml BMGY-medium with a final OD_{600} of 0.1 and let them grow to reach an OD_{600} of 6. After achieving this OD_{600}, cells were centrifuged at 1000xg at RT for 10 min. The cells were resuspended in BMMY medium and added equally to six 1L-BMMY media to get a final OD_{600} of 1 in each flask. Then the cells were grown for 48-72 h, at 22 °C shaking at 120 rpm, and supplemented with 1% methanol every 24 h. Then the cells were harvested by centrifuging at 4000xg at 4 °C for 15 min.

The cell pellet was further used for large-scale membrane preparation. The cells were resuspended in 1:3 (v/v) of breaking buffer (50 mM HEPES, pH 7.5, 100 mM NaCl, 5% (w/v) glycerol, 1 mM EDTA, pH 7.5, 1 mM PMSF), and homogenized with the help of an Ultra-Turrax-T15 to make sure that there were no cell clumps. The cells were continuously stirred with a magnetic stirrer which didn't allow the cells to settle. With the help of a peristaltic pump the cells were passed through the disintegrator 6 glass bead mill, 4-5 times, until >90 % cell lysis was achieved. The disintegrator 6 glass bead mill was continuously cooled with the help of a thermostat Fission D8 on the water bath G at 4°C. The breaking of cells was confirmed in a light microscope at 40x magnification. the cell lysate was supplemented continuously with 1 mM of PMSF after every cycle of lysis, to halt any protease activity. The unbroken cell and debris were separated from the cell lysate for 4000 g at 4°C for 15 min. Then the clear supernatant was ultracentrifuged at 100,000xg at 4°C for 90 min. The supernatant was discarded, the membrane was resuspended in membrane buffer, flash frozen and stored at -80 °C for further use.

2.2.4 Working with insect cells (*Sf9*)

2.2.4.1 Insect cell *Sf9* constructs:

All *Sf9* expression constructs were cloned into pOET1 vectors under control by a single polyhedrin promoter (*polh*). The GPCR constructs were cloned with either an N-terminal pre-promelittin signal sequence or a hemagglutinin signal sequence. The protein constructs were tagged N-terminally with a deca-histidine and a flag tag for detection and purification of the protein. The N-terminal tag His10 and the flag tag can be proteolytically cleaved by using the tobacco etch virus (TEV) enzyme. The GPCRs were also tagged C-ly with strep-II for 2nd step affinity purifications.

2.2.4.2 Maintaining insect cell cultures

The *Spodoptera frugiperda* pupal ovarian cell line *Sf9* lab strain was maintained with TNFH-media or insect express (Lonza) media and grown at 27 °C. The *Sf9* cultures were passaged every week twice to maintain a background culture in the T15 flask. For suspension cultures, large-scale insect cell cultures were grown in a glass flask at 130 rpm at 27 °C, until confluence was reached. The suspension culture was grown in TNFH-medium. 0.1% (w/v) Pluronic F-68 was added in order to lessen the shearing of cells during the suspension culture's growth, but it wasn't necessary for the insect express medium.

2.2.4.2: Generation of recombinant baculoviruses

Recombinant baculoviruses were generated using a flashBAC kit following the standard protocol as provided with the kit (FLASHBACGOLD^{TM}, Oxford expression technologies). The Sf9 cells from the confluent flask were seeded into a 6-well plate with $1.28*10^6$ cells per well. The cells were grown in TNFH medium containing 5% fetal bovine serum (FBS), 2 mM glutamine,7.5 nM vitamin B12 and 50 μg/ml gentamicin, ($TNFH^{full}$). Then the cells were washed 3-4 times with TNFH-medium without serum to remove the $TNFH^{full}$ from the wells. Then the transfection mix containing (0.5 μg plasmid DNA, 0.5 μg of baculovirus DNA, and 30 μl of cell-fectin*)* was incubated at RT for 30 mins and added to the 6-well plate slowly along with the TNFH medium $TNFH^{tf}$. The plate was kept in the incubator at 27°C in a humidified chamber for 24 hr. On the next day 1ml of $TNFH^{full}$ medium containing 10 % FBS serum was added to the flask and grown for 5-6 days in a humidified chamber. Then the cells and media were harvested and centrifuged at 4000 g for 10 min. The clear supernatant was stored at 4°C for further use.

2.2.4.3: Determining the virus titters using the endpoint dilution assay

The virus titters were determined by using the endpoint dilution method as mentioned in O'Reilly *et al.* (1993). This assay was performed by using 96 well microtiter plate. Each well of 96 well plates were seeded with a cell density of 10^5 insect cells. Virus-containing

supernatant (section-2.2.3.) was diluted serially to 10^2 until 10^{12}, and 10 µl of the diluted virus stock was added to the 96 well plates for the assays. The first three dilutions (10^2–10^4) were added in triplicate to a well, while the remaining dilutions were added to 12 wells for each dilution. The plate was incubated in the incubator for 7 days in a humidified chamber at 27°C. The plates were screened to determine whether each well was infected or not after a week of incubation in a humidified chamber. The well was considered to be positive when at least one infected cell was observed and negative if there was none. The percentage of infection for each dilution was calculated using this score. The proportionate distance (PD) between the infection dilutions was calculated using this percentage.

$$\boldsymbol{PD = \frac{a-50}{a-b}}$$

a = percentage of infected wells above 50%
b = percentage of infected wells below 50%.

By using the "PD" value I calculated the response of dilution which cause 50% infection called tissue culture infection density at 50% infection ($TCID_{50}$).

log ($TCID_{50}$) = log (dilution of "a") – PD

and

$TCID_{50} = 10^{\log (TCID50)}$

1/ log ($TCID_{50}$) provides the titer of the virus per 10 µl virus used in the assays.

The formula presented below was used to calculate the plaque forming unit (pfu) :

$$\boldsymbol{\frac{pfu}{ml} = \frac{0.69}{TCID50 * 0.01\ ml}}$$

The cells were infected using Pfu as a standard unit to measure various MOIs (multiplicity of infection).

2.2.4.4: Small-scale expression screening using the insect cell system:

A small scale expression screen was done in a 6-well plate to determine the conditions at which the best expression level of the constructs was achieved. A MOI of 1 equates to a virus infection with the same number of Pfu as there are cells in the well. Different MOIs from 1, 5 and 10 along with different infection time periods were tested for the best expression of the proteins. From each condition, nearly 10^5 cells were harvested and used for expression tests. The cells were resuspended with a buffer containing (50 mM Tris/HCl pH 7.4, 1% SDS, Benzonase, and protease inhibitor cocktail), and incubated ine ice for 30 min, for proper lysis. Then the lysate was centrifuged at a high speed of 100000*g for 1 h to remove the cell debris and unbroken cells. The supernatant was used further to run SDS-PAGE gels and immunoblots to detect the protein of interest.

2.2.4.5: Large-scale expression in insect cells:

The expression of GPCRs at a large scale was achieved by growing the *Sf9* cells in suspension cultures at 27 °C and 120 rpm. For the large-scale suspension cultures, we used different sizes of wide-neck Erlenmeyer flasks for our studies. To ensure a sufficient amount of oxygen available for cell growth, we filled the flask only to $1/5^{th}$ of the volume. The cells were grown under continuous shaking in an incubator at 120 rpm. To minimize the shearing forces, we added 0.1% of pluronic F68 to the TNFH media of the suspension cultures. Before infecting the cells with the virus, the cells were centrifuged at 1000g at RT for 10 min and resuspended in fresh TNFH medium at a cell density of $2*10^6$ cells/ml. As mentioned earlier the cells were infected with the baculovirus encoding receptor of interest at 5 MOIs for 72-96 h at 27 °C and 120 rpm. Followed by infection with the virus the cells were harvested by centrifuging at 5000 g at 4 °C for 15 min. The cell pellet was snap-frozen in liquid N_2 and stored at -80 °C for further use for membrane preparation and protein purification.

2.2.4.6: Insect cell membrane preparation

For the lysis of the infected *Sf9* cell membrane, we used the nitrogen decompression method. In this method, nitrogen gas is mixed with the cells, diffuses into the cells, and causes a rupture of the cells as a result of the nitrogen expanding inside upon decompression. In comparison to other lysis techniques, nitrogen decompression lysis of cells is milder and doesn't involve heat or shearing stress. As a consequence, it is the approach that works best with malleable or unstable proteins.

The cell pellets were thawed in ice and resuspended in a buffer containing 50 mM HEPES buffer (pH 7.6, 150 mM NaCl, 10 mM EDTA, 5 µg/ml leupeptin, 1 mM EDTA, 1 µM E64, 2 µg/ml pepstatin A, 10 µg/ml aprotinin, 1 mM PMSF). Cell lysis was achieved by nitrogen decompression (Parr bomb) at 4 °C for 20 min. The unbroken cells and debris were removed by centrifugation at 5000 g at 4 °C for 15 min. The supernatant was ultracentrifuged at 100 000 g at 4 °C for 90 min. Membrane pellets were resuspended in 50 mM HEPES buffer (pH 7.5) containing 150 mM NaCl, 1 mM EDTA, and 5% (w/v) glycerol and were frozen at -80 °C for further use.

2.2.5 Biochemical methods:

2.2.5.1 Polyacrylamide gel electrophoresis (SDS-PAGE)

Proteins can be separated according to their molecular weight under denaturing conditions with the help of sodium dodecyl sulfate-polyacrylamide gel electrophoresis (SDS-PAGE). The sample buffer contains SDS, which binds to the proteins and denatures them. It gives proteins a negative charge that depends on the size of the protein; the larger the protein, the more negatively charged it becomes. However, the charge density per residue remains the same, and no separation would occur upon electrophoresis in aqueous buffers. Separation during PAGE is caused by the fact that large proteins can use fewer polyacrylamide pores than smaller ones, smaller ones thus run faster. DTT was added to the sample buffer 4x NuPAGE™ with 3:1 and

stored at 4°C for further use. The protein sample was mixed with 1X *NuPAGE*™ sample buffer and loaded onto the readymade SDS-PAGE, NuPAGE™ 4-12% bis-Tris gels. Using an electrophoresis power supply EPS 600, gels were run in "xCell SureLock™ Mini-Cell" chambers at 40 mA and 100 V per gel for 1 hour at 4°C in 1x NuPAGE™ buffer containing (50 mM MES, 50 mM Tris pH 7.3, 0.1 % SDS, and 1 mM EDTA). To compare the molecular weights 2-3µl of PageRuler™ prestained protein ladder was run on the side well with the protein sample. After the run, the gel was washed boiled in Mili Q water, and stained for one to two hours with PAGE-blue stain. The gel was then thoroughly washed with water until it was translucent.

2.2.5.2 Immunoblot / western blot.

For immunoblots, the samples were run in SDS-PAGE as mentioned earlier and the protein bands were transferred to the PVDF membrane (commercially available cassette from Invitrogen™) by using a semidry iBlot™ for 6 min at 20 V. Then the blot was transferred to the blocking solution (5% skimmed milk in TBS or PBS buffer) at RT for 1-2 h. After the incubation, the blot was washed thrice with TBS containing 0.5% Tween. The blots were incubated with the suitable antibody conjugated with alkaline phosphatase, with appropriate dilutions in TBS buffer with 3% BSA at 4°C overnight under continuous shaking. On the next day, the blot was washed with TBS with 0.5 % Tween thrice and used for developing the blot. Followed by washing the blot was incubated with AP buffer containing 330 mg/ml nitro blue tetrazolium chloride and 165 mg/ml 5-bromo-4-chloro-3-indolyl phosphate, for AP-staining. Prior to the saturation of the development, the reaction was halted by washing the blot with excess Milli-Q water.

2.2.5.3 Blue Native-PAGE

Blue Native-PAGE separates the protein mixture on the basis of their charge and hydrodynamic radius in the native state (127). With the help of the blue native PAGE, one can separate the proteins in their oligomeric forms and as different complexes. The protein's movement in the

gel is influenced by the native charge on the surface of the proteins (127). The samples were mixed 1: 3 with BN-PAGE sample buffer [50 mM bis-Tris, pH 7.0, 50 mM NaCl.,10% (v/v) glycerol and 0.01% (w/v) bromophenol blue]. The two buffers used for BN-PAGE were 1x cathode buffer (50 mM Tricine, pH 7.0, 15 mM Bis-Tris) and 1x anode buffer (50 mM bis-Tris, pH 7.0). The mixed sample was loaded onto the ready-made NativePAGE™ 4-16% bis-Tris gel which was run in xCell SureLock™ mini-cell chambers, and the cathode buffer was filled into the inner part of the chamber, whereas the anode buffer was filled into the outer part of the chamber. The gel was run at 4°C first at 150 V for 60 min and then at 250 V for an extra 30-60 min. Then the gels were destained with the help of a destaining buffer (???) until the gel became transparent.

2.2.5.6: Fast Protein Liquid Chromatography (FPLC)

After purification of the recombinant protein by affinity chromatography, the protein was subjected to FPLC fractionation for further purification. In FPLC, proteinscan be separated according to their molecular weights. The purified protein via FPLC was further used for electron microscopy and other biochemical assays. The FPLC was performed using Superdex 200 16/60 or Superose-6 (16/60 column preparative and analytic (GE-healthcare) columns. The column was pre-equilibrated with water followed by buffer before injecting a protein. Protein standards (urease, BSA, peroxidase, and lysozyme) were initially injected to check the column''s proper functioning. 500 ulsamples were injected into the column and run at a flow rate of 0.5 ml/min. The absorbance was recorded at 280 nm.

The elution volume fraction of standard protein markers were used to calculate the K_{av} of the protein of interest with the following equation:

$$\boldsymbol{Kav = \frac{Ve - V0}{Vt - V0}}$$

Where V_e = elution volume of the protein. V_0 = void volume of the protein, V_t = total volume of the protein.

The K_{av} of every protein is plotted against the Log10 vs molecular weight (MW) to obtain a standard plot. The K_{av} of unknown proteins was calculated on the basis of the elution volumes. Those were then plotted on the standard XY-plot and the molecular weight was estimated.

The GPCRs were purified by using a size exclusion micro-Äcta or smart system because of low yield. The size exclusion buffer contains (1*CMC) of detergent and reducing agent (TCEP or DTT).

2.2.5.7 Methods for measuring protein concentrations

To measure protein concentration, I used mainly two methods in this work, the colorimetric BCA assay, and the nanodrop spectrophotometry.

2.2.5.7.1 Bicinchoninic Acid (BCA) assay

The protein concentration of both soluble and membrane proteins was determined via BCA assays. Peptide bonds of proteins with more than three amino acids catalyse the Biuret reaction, which reduces Cu^{2+} to Cu^{1+} in an alkaline environment. Then two bicinchoninic acid molecules bind a single Cu^{1+} ion to generate a purple complex with an absorption maximum of 562 nm (128). For our study, we used the Pierce™ BCA protein assay kit, in a 96-well plate according to the manufacturer's instructions. We used BSA as a standard protein and made different dilutions of it to prepare a standard curve. The samples were incubated at 37°C for 30 min before measuring the plate at 562 nm in a TriStar LB 941 instrument. The protein concentration was calculated from a BSA- standard graph.

2.2.5.7.2 Nanodrop spectrophotometry:

Alternatively, the BCA assays nanodrop spectrophotometry is also used to calculate the protein concentration. For the measurements we used the buffer as blank and measured the protein concentration in triplicate and took the average of the three, to consider fluctuations. The protein concentration was calculated using Beer-Lambert's law.

$$A = log\left(\frac{I0}{I}\right) = \varepsilon * c * d$$

A = absorbance,

I0 = intensity of incoming light

I = intensity of the transmitted light

ε = extinction coefficient at the wavelength λ

d= *light path length* (10 mm)

c= protein concentration.

Extinction coefficients (ε) were constant for the same protein which was determined *in silico* by the ProtParama program on the ExPASy server from the protein's amino acid sequence.

2.2.6: Circular dichroism (CD)

The secondary structure of the protein was determined by using far-UV circular dichroism (CD) spectra at RT (25 °C). The spectra were recorded on instruments by using a 0.1 cm cell. 10 µM protein concentration was used for recording the CD spectra. The machine was pre-calibrated with Iolar-grade nitrogen for 1 hr. before starting the actual experiment. The samples were equilibrated at the appropriate condition for at least 4-5 hours before recording the CD spectra. Each spectrum was an average of 3 scans (the width of the slit was 2nm). The values were plotted for molar ellipticity vs the absorbance (from 194 nm to 260 nm) in a 2D graph. The plot was compared with standards to estimate the extent of α- helices, ß-strands, and random coil present in the proteins.

2.2.7: Negative stain electron microscopy

The size exclusion purified GPCRs and G-proteins (section 2.2.11) were directly used for the negative stain electron microscopy. The peak fraction of the protein was collected, the concentration was measured via BCA or nanodrop method, and was negatively labeled with uranyl formate. Protein concentrations of 0.1-0.3 mg/ml were used directly for negative

staining. The protein was diluted before applying it to the grid with the help of a size-exclusion buffer supplemented with 1xcmc, LMNG / GDN detergent. 3 µl of the diluted samples were loaded onto the 300 mesh carbon-coated copper grids which were glow discharged once for 45 sec with the PELCO easi-Glow™ Glow Discharge Cleaning System at 15 mA. With the help of Whatman™ filter papers, the grids were dried as well as extra liquids were removed. The samples were washed with water, followed by washing with 3ul of uranyl formate three times and finally incubated for 30 sec with the last uranyl formate solution for 30 sec.

The negative staining images were collected with either a Tecnai™ spirit or a Tecnai™ Biotwin transmission electron microscope at a nominal magnification of 42,000 at 120 kV. The images were collected at defocus values between -1.5 to 2.0 µm.

2.2.8: Cryo-EM sample preparation and data acquisitions

The sample from size exclusion purified GPCRs and G-proteins (section 2.2.11) were concentrated with a 100 KD Amicon filter and directly used for the cryo-EM grid preparation. Concentrated samples with a protein concentration of 1-2 mg protein/ml were used for vitrification plunge freezing. For freezing the samples in grids, we used C-flat R1.2/1.3 copper grids (400 mesh) which were glow discharged twice for 2 x45 sec with the PELCO easiGlow™ Glow Discharge Cleaning System at 15 mA.

Protein samples of 3-4 ul were loaded onto the grids and vitrified at 4 °C, at a humidity of 100 %, and a with blot force of 5-10 by using the device Vitrobot™ (Thermo Fischer, Netherlands). To get a better particle distribution and better ice thickness various combinations of blot force and blot time from 4-10 sec were tested with the help of a Glacious electron microscope. The grid having the best sample distribution and thinnest ice thickness was further used for data acquisition with the Titan Krios G3i cryo transmission electron microscope. The movies were collected automatically with the help of the EPU software (Thermo Fischer, Netherlands), using electron counting mode.

2.2.9: Functional characterization of GPCRs

Radioligand binding assays for GPCRs in the *Sf9* membrane were performed by incubating the *Sf9* cellular membrane (15-20 µg total membrane protein) with increasing concentrations of [^{3}H]-labeled ligands at room temperature for 60 min. Radioligand binding was terminated by rapid filtration through GF/B glass filters and three wash steps with cold washing buffer (50 mM HEPES, pH 7.6). The remaining radioactivity was measured by scintillation counting (Packard Tri-carb1500) using scintillation liquid (ROTISZINT®eco plus, Roth).

The non-specific binding was determined in the presence of 1000 K_d of unlabeled ligand. The B1R-specific radioligand binding was calculated by subtracting the non-specific radioligand binding X from the total radioligand binding of *Sf9* membranes. The ligand-binding affinity K_d was calculated by fitting the results of our radioactivity measurements to the equation

$$Y = \frac{Bmax*X}{Kd+X}$$

Whereas:
Y= final radioligand binding
X = non-specific radioligand binding
Bmax = maximum binding
Kd = dissociation constant

The inhibition constants Ki were determined by competitive radioligand binding assays. Briefly, *Sf9* membranes were incubated with the radioligand at a concentration of (10xKd) together with an unlabelled peptide ligand of varying concentrations sequentially and incubated at room temperature for 60 min. The membranes were then filtered and washed as mentioned above. The results of the measurements were evaluated with the GraphPad Prism6 software. Half maximal inhibitory concentrations (IC_{50}) were converted to Ki via the Cheng–Prusoff

equation. Data are represented as means ± SD. The value of Ki (IC_{50}) was determined by using the following equation.

$$Y = bottom + \frac{top - bottom}{1 + 10^{X - logIC50}}$$

As: bottom = lower plateau of the curve in the units of the Y axis

Top = Highest plateau of the curve in the units of the Y axis

2.2.10: ACEI and Zinc binding assays:

To determine the effects of Zn^{2+} on the orthosteric binding site of the bradykinin receptor *Sf9* membranes were incubated with buffer (50 mM HEPES, pH 7.6, 150 mM NaCl, 5% (w/v) glycerol) containing 2mM EDTA at 4 °C for 45 min. After the incubation, the membranes were washed twice with EDTA-free buffer to remove any endogenous Zn^{2+} ions from the solution. The EDTA-treated membranes were incubated with different concentrations of zinc chloride (Merck, Germany) from 1 mM- 100 nM for 45- 60 min, and these membranes together with cold peptide ligands were used further for radioactivity assays.

For radioactive assays with ACEIs, we used the commercially available 3-ACEIs enalaprilat, captopril, and lisinopril. Different ACEIs (100nM) were added to the membrane buffer to quantify the radioactive assays of receptor binding kinetics in the presence of ACEIs (129).

We measured the impact of ACEIs on the ligand-receptor binding in the presence or absence of EDTA. The peptide Ki values at different Zn^{2+} concentrations were measured. Our analysis showed some significant variations of the Ki values at low Zn^{2+} concentrations. We maintained similar conditions for hB2R as we did for hB1R.

2.2.11: hB1R Sample preparation for DNP-ssNMR experiments:

To get sufficient protein for each DNP-ssNMR experiment, we required ~4-6 L insect cells which were grown in flasks at 27 °C. The cells were infected with recombinant baculovirus and harvested according to the protocol mentioned in section (2.2.3.4). The *Sf9* cell membranes were prepared according to section 2.2.3.5. Nearly ~100ml of membrane suspended in the

buffer at a protein concentration of 5-10 mg/ml were used for the sample preparation for the DNP-ssNMR experiments. The insect cell membranes were solubilized in a buffer (50 mM HEPES, pH 7.6, 150 mM NaCl, 5% (w/v) glycerol, 1 µM U-[^{13}C,^{15}N]-P8F9 DAKD) supplemented with 1% (DDM, Glucon, Germany) and 0.1% cholesteryl hemisuccinate (CHS, Sigma chemicals, Germany) at 4°C under gentle stirring for 2 h. The non-solubilized fraction of the membrane was separated by ultra-centrifugation at 100,000 g at 4°C for 1 h 30 min. The clear solubilizate was filtered (0.2 um) before loading onto the His-trap column. The samples were loaded with the help of a peristaltic pump at a flow rate 0.2-0.4 ml/min at 4°C. The His-trap column was washed with buffer containing 30 mM and 60 mM imidazole before eluting it with buffer B^{NMR} (300 mM imidazole).

Buffer A^{NMR}	Buffer B^{NMR}	Buffer C^{NMR}
50 mM Hepes-NaOH pH 7.6	50 mM Hepes-NaOH pH 7.6	50 mM Hepes-NaOH pH 7.41
150 mM NaCl	150 mM NaCl	150 mM NaCl
5% glycerol	5% glycerol	5% $^{12}C^{2}H$ glycerol
0.1% DDM	0.07% DDM	In 76% D_2O, 18% HO
0.01% CHS	0.007% CHS	
100 nM ACEIs	100 nM ACEIs	
200 nM DAK^{NMR}	200 nM DAK^{NMR}	
	400 mM imidazole	

Table 2. 2: Composition of buffers used for the purification of B1R for ssNMR studies.

The eluted protein samples were collected and concentrated in 50 kDa cut-off concentrators (Amicon, Merck Millipore, Darmstadt, Germany). The concentrations of the receptors were adjusted by centrifuging the concentrators at 1000g at 4°C to remove excess buffer solution. The receptor solutions were repeatedly diluted every 20 min, to avoid precipitation or aggregation of the samples during centrifugation. The concentrated samples were transferred to buffer C^{NMR}, by repeated dilution and concentration. The receptor was concentrated to 30-40

μl, containing a total amount of ~400 μg for each DNP-ssNMR experiment. The samples were further mixed with nitroxide biradical AMUPol and full $^{12}C^{2}H$ glycerol, for NMR measurement.

Chapter – 3: Results

CHAPTER-3: RESULTS

The thesis aims to characterize the structure and function of the GPCRs from both class-C and class-A families. Therefore, the receptors were heterologously expressed in *Sf9* insect cells or the yeast *Pichia pastoris*. The results section is divided into three parts i) cloning, expression, and purification of a class-C GPCR, namely the calcium-sensing receptor (CaSR), ii) cloning, expression, and purification of G-proteins. iii) Allosteric modulation of the orthosteric binding site of the kinin receptors (B1R and B2R)

i) The first section presents the cloning of different constructs of CaSR, followed by the heterologous production in *P. Pastoris* and insect cells (*Sf9*), furthermore, optimization of the expression and purification conditions in both *Pichia* and *Sf9*, and finally, the biophysical and biochemical properties of CaSR are characterized.

ii) The second section describes the heterologous production and purification of different mini G-proteins in *E. coli.* Also, this section is shown how different chimeric mGα-Maltose binding proteins (MBPs) were heterologously produced and purified from *E. coli.*

iii) The third section presents the heterologous production and purification of class-A peptide receptors (bradykinin receptors). This part also discusses the allosteric modulation of the orthosteric binding site of the kinin (B1R and B2R) receptors and the impact of Zn^{2+} and ACEIs on the orthosteric binding sites of the receptors.

3.1 Cloning and heterologous production of CaSR.

The CaSR is a member of the class-C family of the GPCRs. The molecular weight of CaSR is ~120 kDa with a large (~75 kDa) extracellular domain. Different CaSR constructs were cloned using the cDNA of CaSR into two separate expression vectors, pPICZ or pOET1 vector, using the restriction-free cloning methods mentioned in the earlier section (2.1). The restriction-free cloning approach consists of two PCR steps. In the 1st step, the CaSR gene with tags was amplified from the cDNA of CaSR with the help of a megaprimer, which was 80-90 bp long. In the 2nd step, the modified CaSR cDNA was inserted into the pPICZ or the pOET5 vector by amplifying the entire vector constructs using the 1st PCR product as a primer. DNA sequencing confirmed later the insertion of the CaSR cDNA into the vectors. In addition, the CaSR construct was tagged with an N-terminal flag-tag and C-terminal decahistidine-tag [$(His)_{10}$] for affinity purification and detection of the protein.

3.1.2 Production and expression of the calcium-sensing receptor in *Pichia pastoris*.

Proteolysis and misfolding during heterologous expression might lead to a significant loss of protein. Protease-deficient strains and strains capable of producing various chaperones have been engineered to ensure a maximum yield of heterologously produced proteins. Choosing the right strains for the expression is important for the heterologous over-expression of GPCR cDNA. In order to overexpress CaSR in *Pichia*, I choose four different *P. pastoris* strains based on their expression of specific enzymes, chaperones, or lack of proteases, such as: X33 (wild type), GS115PDI (expresses the protein disulfide isomerase), SMD1163 (lac**k** of proteases like his4**,** pep4**,** prb*)* and HAC (expresses a transcription factor) (130,131).

Two pPICZ constructs (pPICZ_CaSR_H_{10} and pPICZ_ost1app4_flag_CaSR_H_{10}) were used for heterologous overexpression of CaSR in *Pichia*. The construct pPICZ_CaSR_H_{10} contains the native human CaSR membrane signal peptide. It was transformed into the four different *P. pastoris* strains X33, GS-PDI, SMD1163, and HAC. However, I did not observe any protein expression in all four strains that were transformed with pPICZ_CaSR_H_{10}. To improve the

expression of the CaSR receptor, I used an optimized signal peptide of *Pichia* "ost1_app4", a construct created in-house by Dr. Chistoph Reinhart. The construct "pPICZ_ost1app4_flag_CaSR_H_{10}" with ost1_app4 signal peptide was transformed into different *PPichia* strains such as X33, GS-PDI, SMD1163, and HAC. The positive colonies selected from the zeocine plate of these *PPichia* strains were further used to prepare membranes in small scale as mentioned in section (2.2.3). The expression of CaSR in all strains was confirmed by the appearance of a ~140 kDa band in Western blots using an anti-His antibody (Figure 3.2 B). The ~145 kDa band in the Western blot is positioned higher than the expected molecular weight of ~130 kDa of CaSR with tags, which might be due to post-translational modifications. In the Western blot, two bands were observed corresponding to the size of a monomer (~150 kDa) and a dimer (~ 300 kDa) of CaSR.

The best CaSR colonies from all four strains were selected for further standardization of expression conditions like temperature, and time of induction, to improve the expression of CaSR (Fig 3.2 C and D). The cells were grown at two different temperatures, 22 °C or 30 °C after induction with methanol for different time points from 12 h to 72 h. By comparing the intensity of the bands in the Western blot, the best expression strain and duration for induction that supported better expression conditions of CaSR in Pichia strains were selected. The protein expression was maximum in the GS115-PDI strain grown at 22 °C for 72 h. This strain and conditions were further used to purify CaSR from *Pichia*.

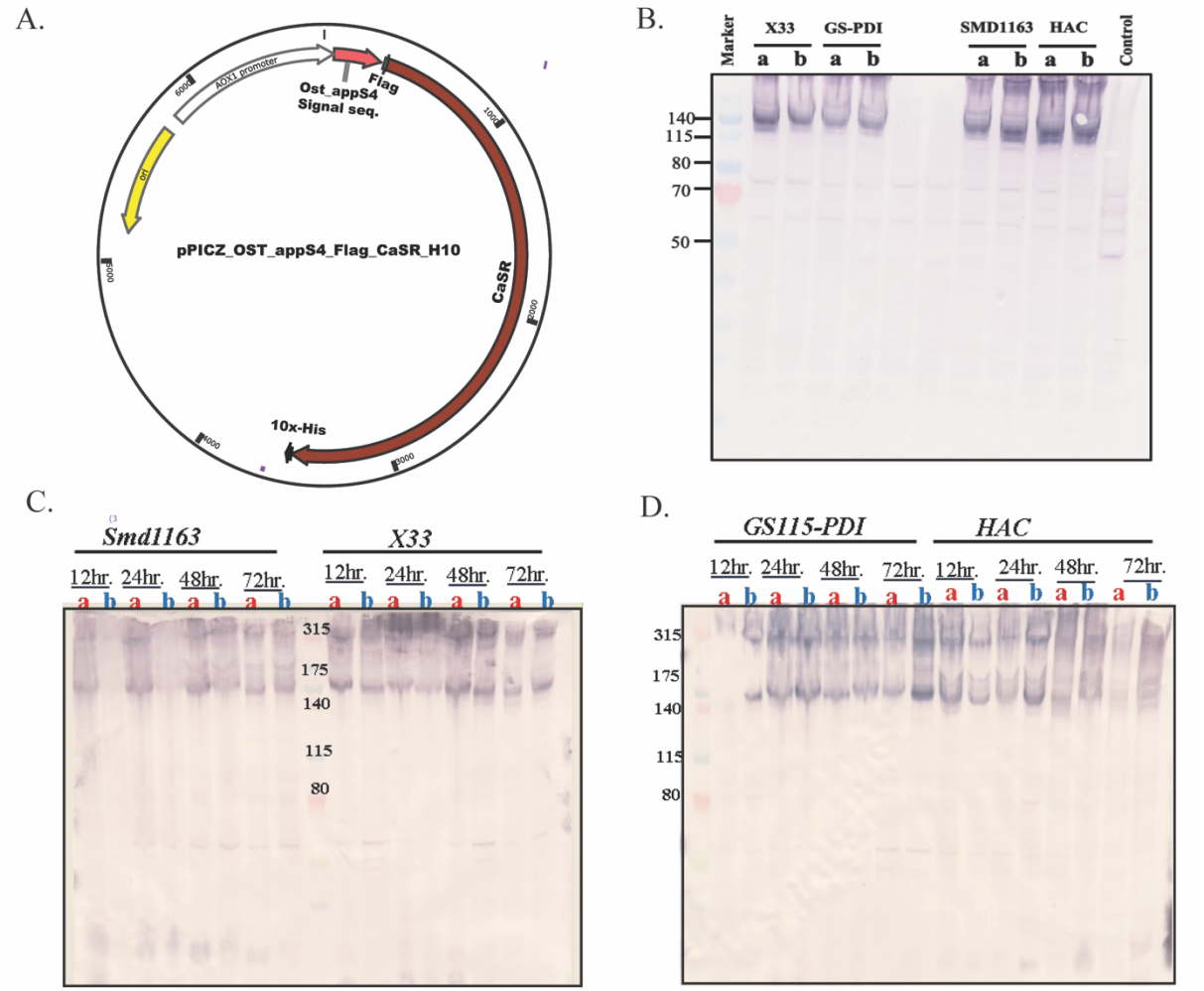

Figure 3.1: Expression and optimization of CaSR in different strains of *Pichia pastoris*: A) Schematic representation of the CaSR with ost1-aap4 signal sequence was cloned into the pPICZ vector. B) Western blot stained with anti-polyhistidine-AP antibody, of small-scale prepared from two colonies (a, b) from each strain (X33, SMD1163, GS115-PDI, HAC). C) Western blot of stained with anti-polyhistidine-AP antibody small-scale purified from CaSR expressed in four strains at a different time and at a different temperature, a = 22 °C and b = 30 °C.

3.1.3 Production and expression of the calcium-sensing receptor in insect cells (*Sf9*)

Both CaSR constructs (pOET1_SS_CaSR_His10 and pOET1_HA_FLAG_CaSR_His10) were cloned into the pOET1 vector under control by the polyhedrin (polh) promoter. In the pOET1_SS_CaSR_His10 construct, the human CaSR- membrane signal sequence was used. Similar to *Pichia*'s case, we did not observe any expression of the CaSR. The construct pOET1_HA_FLAG_CaSR_His10 contains a hemagglutinin membrane signal sequence which

was used for the expression of CaSR in *Sf9* insect cell. The vector pOET1_HA_FLAG_CaSR_His10 was used to generate the baculovirus using the gold speed-vac method as mentioned in section 2.3.2. The generated virus was tested for its functionality and titer to regulate the infection of *Sf9 cells*. In order to optimize the expression conditions of CaSR in *Sf9* insect cells, the cells were infected with different amounts of the virus for different time periods (fig 3.2 B). The *Sf9* cells were infected with the virus at MOIs of 1, 5, and 10 for 3-6 days. The expression of CaSR in *Sf9* is compared with different MOI of virus infection for different time points to find the best expression of CaSR (Fig 3.2). There are two protein bands were observed in the Western blot, suggesting the existence of a monomer and a dimer of CaSR in *Sf9* membrane. By comparing the intensities of the CaSR bands, the best condition for CaSR expression was found to be MOI-5 for a 3-day infection.

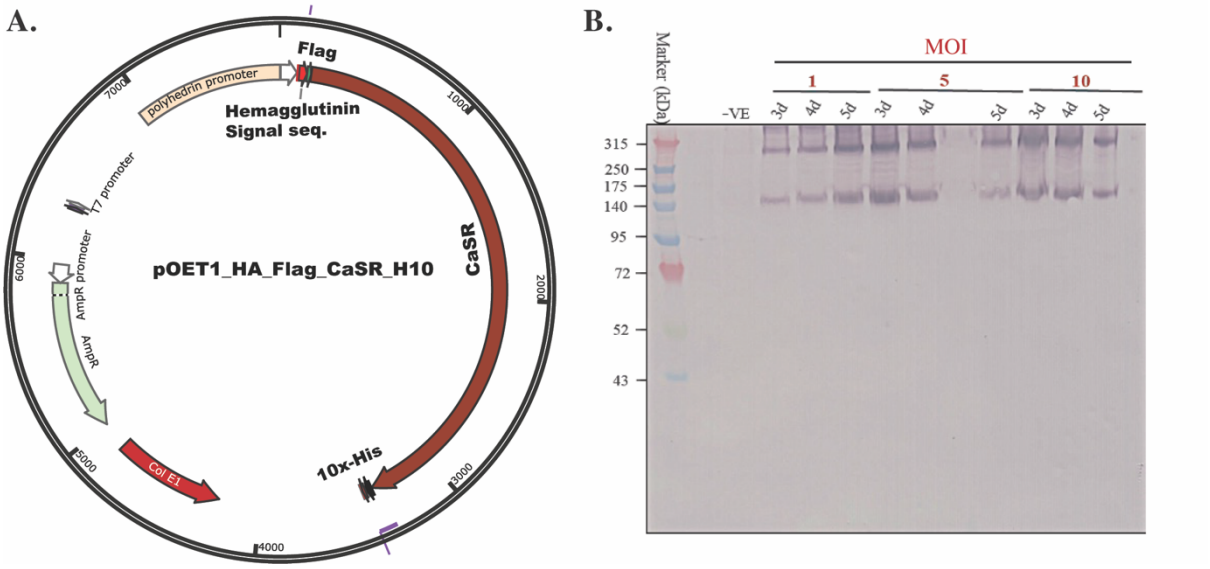

Figure 3.2: Expression and optimization of CaSR in insect cells (*Sf9*): The CaSR constructs were cloned into pOET1 vector under the control of the polyhedrin promoter A) Image showing the pOET1 vector construct with the CaSR cDNA) Western blot probed with anti-flag antibody: -SDS-PAGE gel (4-12% NuPAGE™ Bis-Tris gels) of insect cell membrane proteins. These were later transferred to PVDF membrane to probe with the anti-flag antibody. The insect cells were incubated with different MOIs of 1,5, and 10 of the virus for 3-5 days at 27 °C. the *Sf9* membranes were without infections. Were used as negative controls

3.1.4 Solubilization optimization of CaSR produced in *Pichia pastoris* and insect cells (*Sf9*):

Membrane proteins are solubilized in detergents for downstream purification. For the protein to preserve its structure, stability**,** and function, appropriate detergents have to be found. Detergents tested for the solubilization of CaSR were n-dodecyl-ß-D-maltoside (LM/DDM), n-octyl-ß-D-glucoside (OG), n-Decyl-ß-D-maltoside (DM), N-dodecylphoscholine (FOS), cyclohexyl-alkyl-ß-D-maltoside (CYMAL), and styrene-maleic anhydride (SMA). To check the extent of the solubilization, a small-scale solubilization test was carried out where 200 μg of the isolated membranes **were** treated with each detergent by incubation for ~2h before centrifuging at 100,000g for 1h. The supernatants after ultracentrifugation were run on an SDS PAGE for detection of CaSR in the Western blot by using an anti-His antibody (fig 3.3 A and B).

The efficiency of solubilization of CaSR from *Pichia* membranes in different detergents followed the order: SDS > Fos12 > SMA (300.10) > SMA EF-30p > Cymal-6 > OG > LM (Fig 3.3A). The efficiency of solubilization of CaSR from *Sf9* insect cell membranes followed the order: SDS > Fos12 > SMA (300.10) > Cymal-6 > LM > DM > OG (Fig 3.3B). The CaSR receptor was soluble in all detergents screened, but for our study**,** we solubilized the receptor with SMA, GDN, and LMNG.

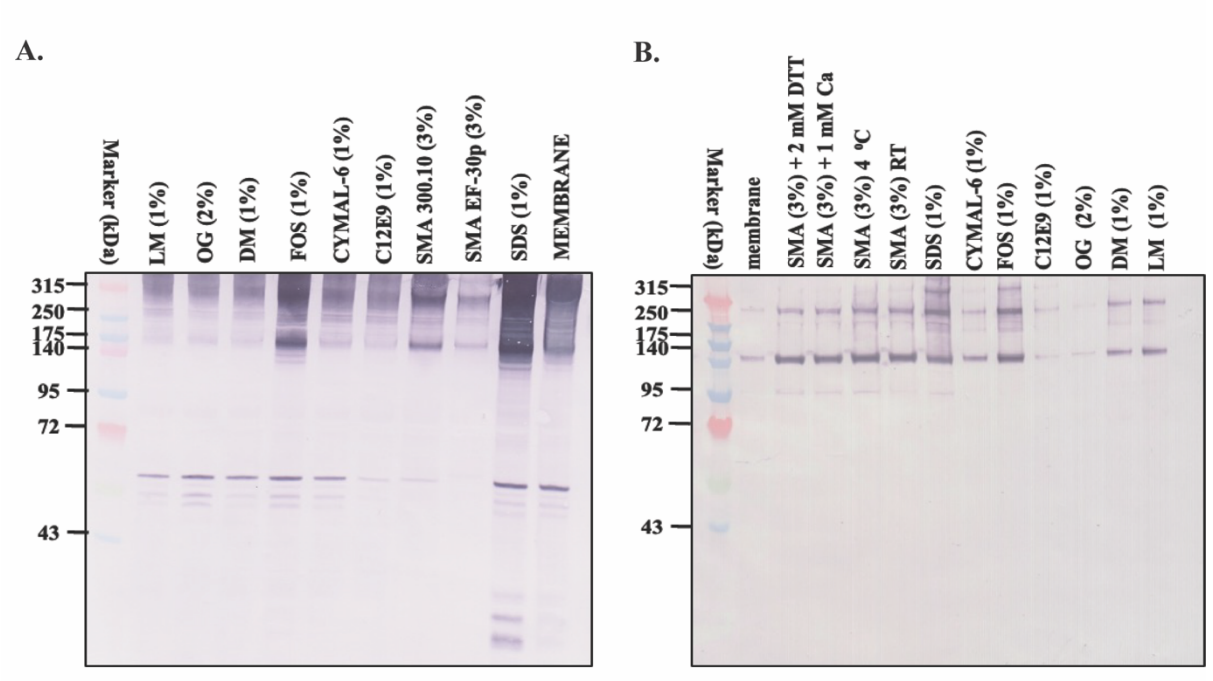

Figure 3.3: Western blots for solubilization screening of CaSR produced in *Pichia pastoris* and insect cells *(Sf9)*: The isolated membranes were solubilized with various detergents and the supernatants were run on SDS-PAGE (4 -12% NuPAGE™ Bis-Tris gels) is the protein bands were later transformed to PVDF membranes to probe with the anti-polyhistidine-AP antibody for detection of CaSR, A) isolated membranes from *Pichia pastoris* GS115-PDI, B) isolated membranes from insect cells (*Sf9*).

3.1.3: Post-translational modification of the CaSR:

In-silico analysis of CaSR predicts that there are 11 potential glycosylation sites in CaSR. To check if there is any post-translational modification in heterologously expressed CaSR in *Pichia* and insect cells (*Sf9*), we incubated the isolated membrane with the enzyme **"**Peptide:N-glycosidase F" (PNAGase F) for ~2h in ice. Then the membrane was loaded onto an SDS-PAGE gel, followed by transferring the protein bands onto a PVDF membrane for Western blot. The Western blot shows a shift in the treated CaSR membrane in comparison with the untreated membrane. This shift indicates that the CaSR expressed in both *Pichia* and *Sf9* is glycosylated (Fig 3.4). The shift in the molecular weight of CaSR suggests that five to six sites might be glycosylated in both cases.

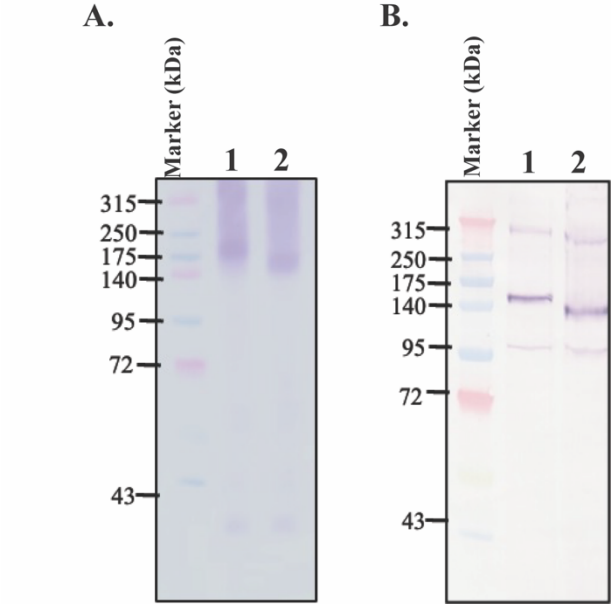

Figure 3.4: Western blots showing the glycosylation state of CaSR produced in *Pichia pastoris* and insect cells *(Sf9):* The CaSR produced both in ***Pichia*** and insect cells was incubated with PNGase F for 1-2 h at RT before loading it onto SDS-PAGE 4-12% NuPAGE™) and transferred it into PVDF membrane for Western blot A) CaSR produced in *Pichia pastoris*, B) CaSR produced in insect cell (*Sf9*), 1- CaSR (control), 2- CaSR treated with PNGase F

3.1.5 Purification of the calcium-sensing receptor (CaSR) in SMA

The CaSR can be solubilized with various detergents as shown earlier. In this part, we purified the CaSR from both *Pichia* and *Sf9* cells by using detergents like SMA.

Purification of CaSR from *Pichia* membranes

The CaSR from *Pichia* was purified by using affinity *HisTrap™ FF* columns. To keep the native lipid composition surrounding the CaSR, SMA (300.10) was used to solubilize the CaSR. The CaSR was solubilized in SMA for 2h at 4 °C with buffer containing (Tris-buffer at pH 8, 200 mM NaCl, 3% SMA, 5% glycerol, and 0.005 mM DTT). The solubilized receptor was separated by ultracentrifugation at 100,000g at 4 °C for 90 min. The soluble fraction was filtered through 0.2 µm Amicon filters before loading onto the *HisTrap™ FF* columns. Then the solubilized CaSR was purified by immobilized-metal affinity chromatography using the His10-

tag at the C-terminus. The protein sample after the His-trap column was found to be pure as can be seen in SDS-PAGE gels (Fig 3.5 A and B). To examine the oligomeric profile of purified CaSR, the protein sample was loaded onto an S-200 column for size-exclusion chromatography. The elution profile indicates that the CaSR was aggregated as seen in the size-exclusion peak as well as in the blue native PAGE gels (fig 3.6 A). Various additives like glycerol, amino acids, reducing agents, and carbohydrates were tested to minimize the aggregation of CaSR protein, but none of the additives prevented the aggregation.

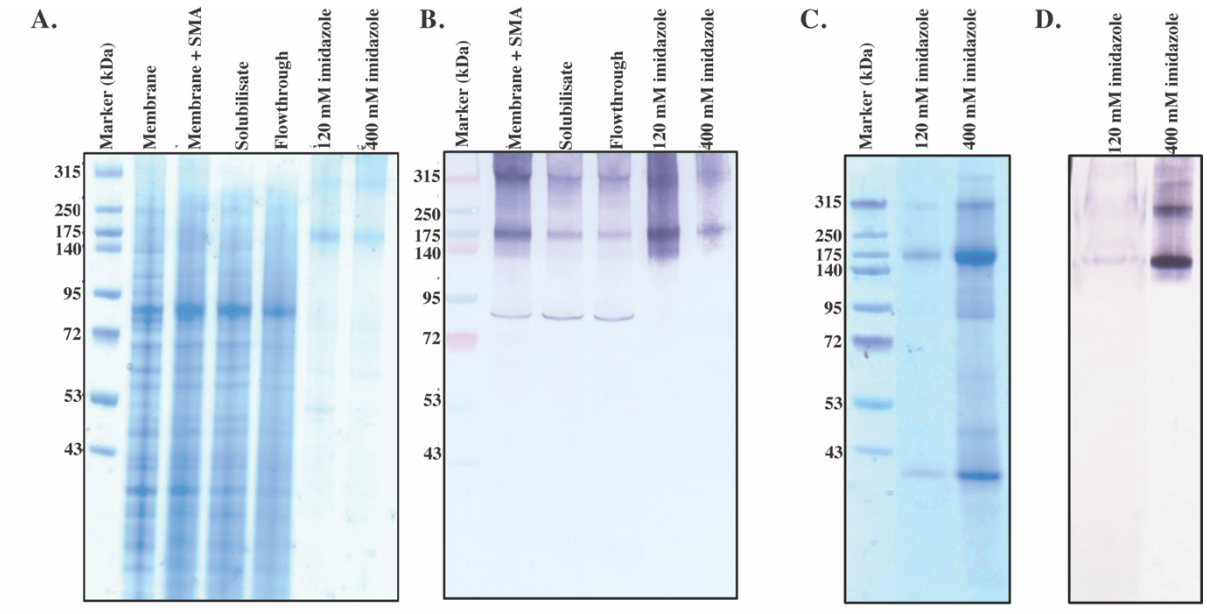

Figure 3.5: SDS-PAGE gels and Western blots showing the IMAC purification of CaSR in SMA from *P. pastoris* and insect cells *(Sf9)* by using His-trap column: IMAC purified CaSR solubilized in SMA from *P. pastoris* membrane A) Coomassie-stained SDS-PAGE gel B) respective Western blot probed with anti-polyhistidine-AP antibody, IMAC purified CaSR, solubilized in SMA from insect cell (*Sf9*) membrane C) Coomassie stained and D) respective Western blot with the anti-polyhistidine-AP antibody

Purification of the CaSR from insect cells

The CaSR was produced in insect cells (*Sf9*) by using the baculovirus system. The infected cells were harvested after four days of infection with MOI_5 and used to prepare the membranes as mentioned in section 2.3.4. The membrane was further solubilized in SMA in buffer-A (Tris-buffer at pH 8, 200 mM NaCl, 3% SMA, 0.005 mM DTT, and 5% glycerol) at 4 °C for 2h.

Then it was centrifuged at 100,000g at 4 °C for 1h and the soluble fraction was loaded onto *HisTrap™ FF* columns with the help of a peristaltic pump. When compared to its expression in *Pichia*, the CaSR can be purified with a high yield. But the purified CaSR was still found to be aggregated (fig 3.6).

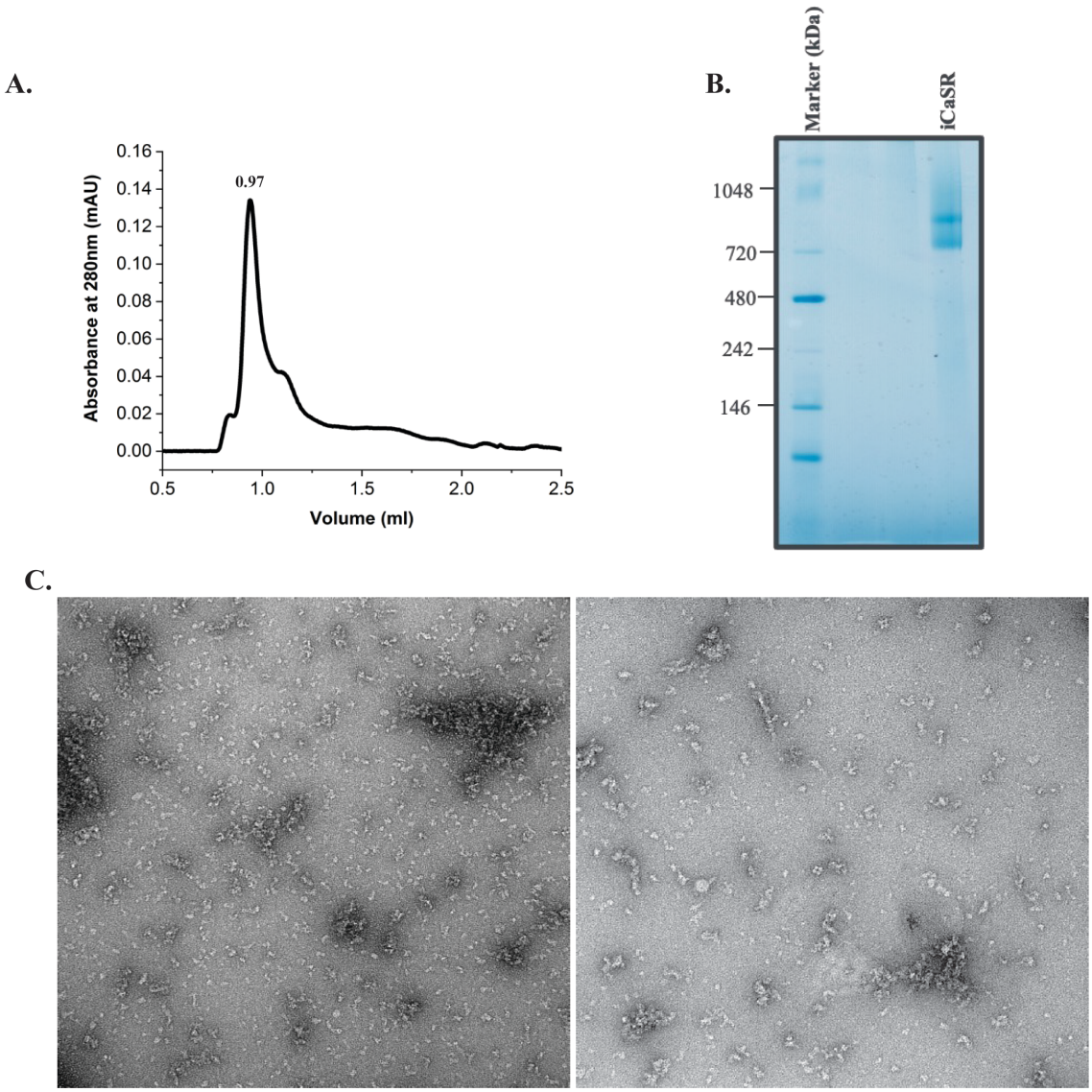

Figure 3.6: Purification of CaSR in SMA from insect cell *(Sf9)* membranes: A) Size exclusion profile of purified CaSR samples, B) Blue native-PAGE gel of CaSR in SMA, C) Negatively stained electron micrographs of CaSR in SMA.

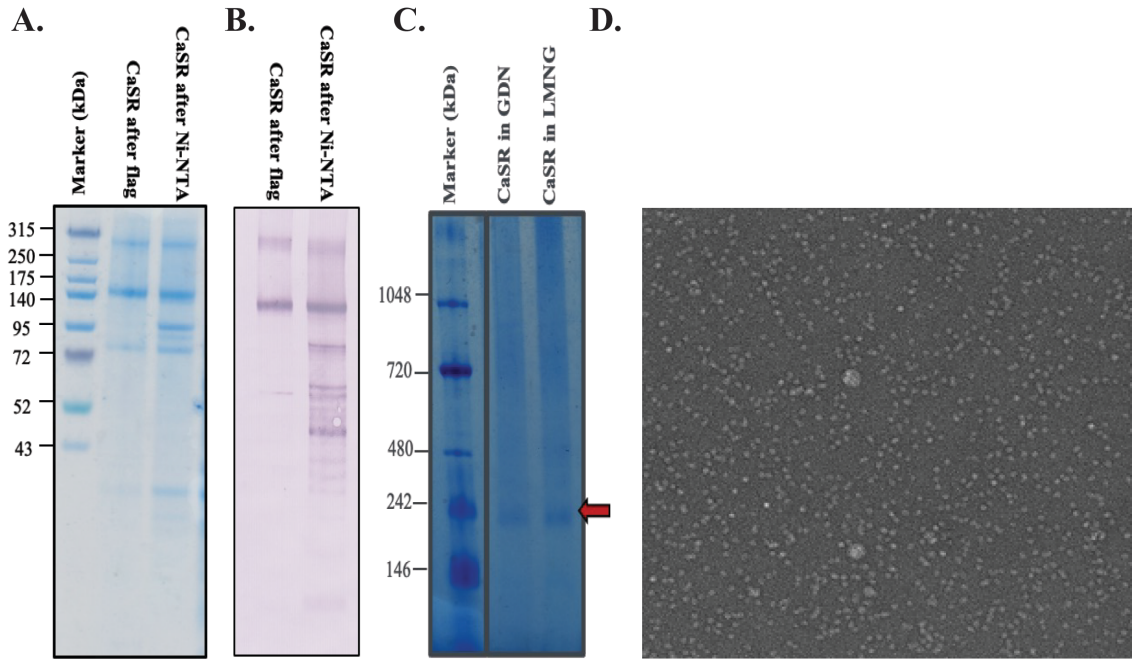

Figure 3.7: SDS PAGE gels, Western blots, and electron micrographs for testing affinity purification of LMNG solubilized CaSR from insect cells *(Sf9)*: The insect cell membranes were solubilized with LMNG and purified both with Ni-NTA and flag-columns. A) 10 ug of purified CaSR from a Ni-NTA column followed by flag-column purified. The Coomassie-stained SDS-PAGE gel (4-12% NuPAGE™ Bis-Tris gels)) D) Representative negative stain image of purified CaSR at a magnification of 42,000 with a pixel size of 2.68 Å.

To prevent aggregation, we decided to test milder detergents like DDM, LMNG and GDN for CaSR purification. The CaSR from insect cells was solubilized with LMNG and purified by using two affinity columns: A His-trap column and a flag-column. We used the additional affinity step for purification via the flag tag as the CaSR sample was not free from contaminations after purification with the His-trap column. The purified sample from the His-trap column was diluted and loaded onto the M2-flag column. The bound CaSR was eluted with the help of 10 mM flag peptide. The purified protein could be seen in the SDS-PAGE gel, identity of protein was further confirmed with the help of an anti-His antibody (fig 3.7 B). The protein was in a monomeric state both in LMNG and GDN, which could be confirmed by the blue native-PAGE or by the negative-stain images (fig 3.7 C and D).

3.1.6 Room temperature transmission electron microscopy of CaSR

After purification with LMNG, the LMNG was exchanged **for** GDN during size exclusion chromatography. The purified samples were diluted to 1-10 μg protein/ml and loaded onto carbon-coated EM-grids and stained with 0.5% uranyl formate for negative stain transmission electron microscopy to examine the homogeneity of the purified CaSR. According to the negative-stain micrographs, the CaSR was uniformly distributed on carbon grids and showed no evidence of aggregation or degradation (fig 3.7 D) and therefore this protein sample was used for structural studies.

3.1.7 Structural analysis of CaSR

For obtaining the structure of the CaSR, single-particle analysis by cryo-electron microscopy (cryo-EM) technique was used. We collected around 700 images and noticed that most of the CaSR were stuck to the carbon edge and were mostly present in thick ice areas of the grids. Due to these issues**,** we could only analyze ~10,000 particles from the micrographs by using Cryo-SPARC software and we could only achieve a low resolution (12-13 Å**)** for the 2D classes. By combining the particles from the best 2D classes, we subjected them to the 3D classification step.

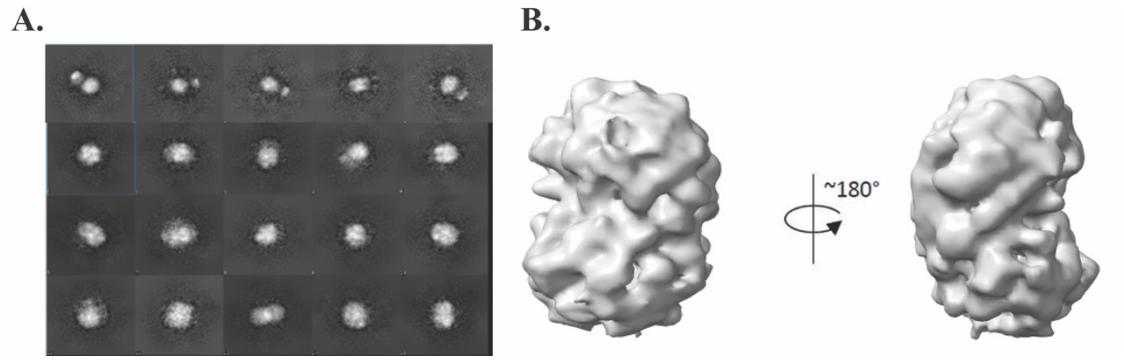

Figure 3.8: 2D classification and initial 3D model of CaSR: A) Representative 2D classes of CaSR obtained from the cryo-sparc analysis B) Side-views of an initial 3D model of CaSR obtained by selecting the best 2D classes.

3.2 Heterologous production and expression of G-proteins

E. coli strains were used for heterologous expression and production of G-proteins. The G_{α}-proteins were codon optimized and their cDNAs were cloned into pET28A as described by Tate et al.(132). These mini-G_{α}-proteins were purified to study the structural and biochemical aspects of the proteins together with their receptors. The mini-G-proteins used in our studies are devoid of their G_{α}-GTPase domains in their C-terminal regions which is crucial for binding to the βγ-proteins and forming heterotrimeric G-proteins. Previous studies showed that the mini-G-proteins can be used to purify active GPCRs for structural studies of GPCRs in their active conformation (55,132,133). In this work, different mini-Gα constructs ($mG_{\alpha s}$, $mG_{\alpha q}$, $mG_{\alpha I}$, and $mG_{\alpha QS}$) were used for production and purification in *E. coli*.

The cDNAs encoding mini forms of the G-proteins (mGαs, mGαq, mGαI, and mGαQS) used in our study were received from Dr. Frank Bernhardt. They were later cloned into the pET28A vector under the control of the T7 promoter and the lac operator. The molecular weights of the mG-proteins are around ~25kDa. The mGs were tagged with N-terminal $(His)_6$.

3.2.1 Production and purification of the mini-G_{α}-protein (mG_{α})

Hexahistidine [$(His)_6$] for affinity purification and detection of protein. The plasmids were transformed into the *E.coli* strain BL21 for the expression of the mG-proteins. Different induction times, temperatures, and IPTG concentrations were tested for each construct to obtain the best conditions for mG-protein expression. After standardizing various induction times and temperatures, mini-G proteins (except $mG_{\alpha q}$) were purified with a high yield (~10mg/1L) from bacterial cultures. The $mG_{\alpha S}$, $mG_{\alpha I}$, and $mG_{\alpha QS}$ were induced with 1mM IPTG for 6-8 h at 28 °C. The mGs were purified with the help of His-trap columns. The purity and oligomeric states were checked by using size-exclusion chromatography. Interestingly, we noted that all four

mini G-proteins are capable of dimerizing in the presence of DTT, suggesting the possibility of disulfide bridge formation between mG-proteins (Fig 3.9).

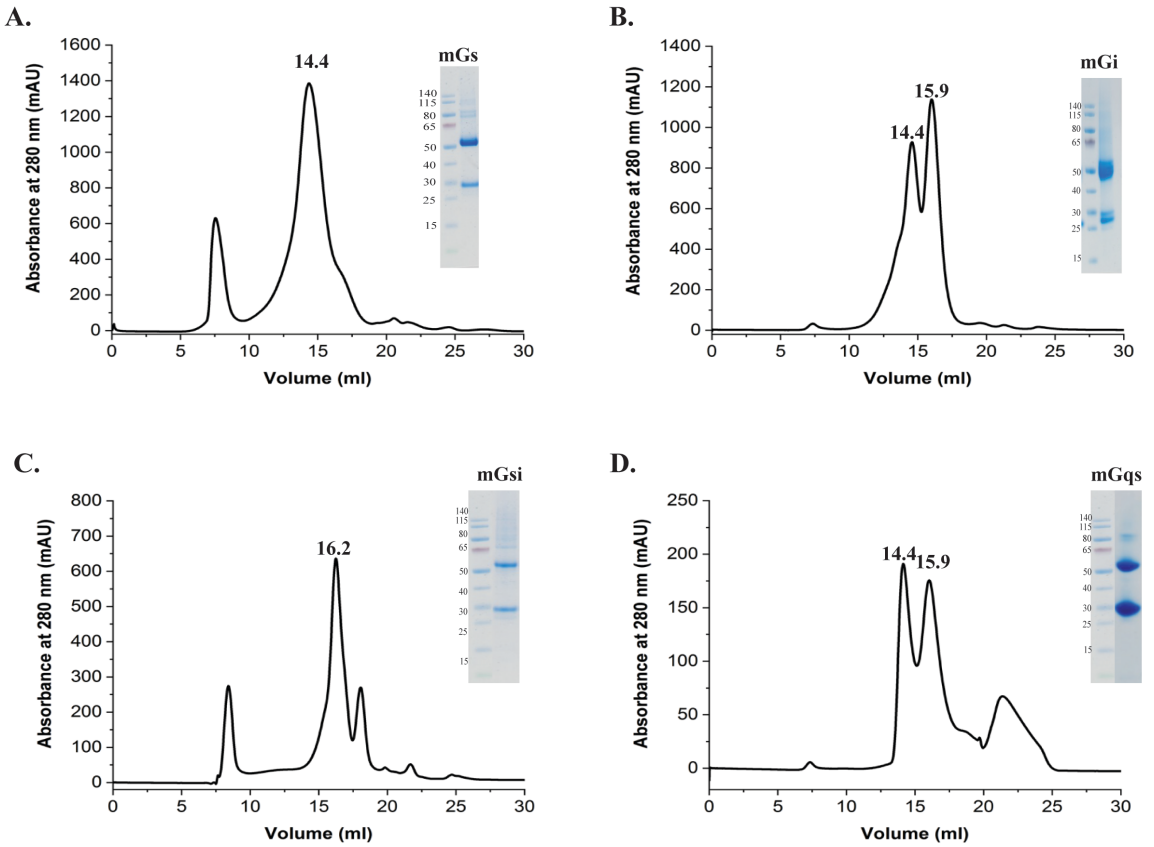

Figure 3.9: Gel filtration profiles and SDS PAGE gels obtained during purification of mini-G proteins from *E. coli*: Size exclusion and SDS-PAGE profile of mini-G protein heterologously expressed and purified from *E. coli*, A) mini-$G_{\alpha s}$ (mGs) B) mini-$G_{\alpha i}$ (mGi), C) mini-$G_{\alpha si}$(mG_{si}), and D) mini- $G_{\alpha qs}$ (mGqs).

The purification of mG was not successful in *E.coli* as it precipitates during cell lysis, likely due to the presence of a hydrophobic surface patch on $mG_{\alpha q}$. $mG_{\alpha q}$ expression was also tested for other BL21 strains expressing different chaperones, but the $mG_{\alpha q}$ expression was unsuccessful.

3.2.2 Production and purification of a mini-Gα-maltose-binding protein (MBP) chimera(mGα-MBP).

Most of the GPCRs are relatively small in size (~45 kDa), especially all class-A GPCRs. Due to the small size of GPCRs, it is challenging to obtain high-resolution cryo-EM structures.

Therefore we decided to increase the size of the GPCR-mG complexes by creating mG-protein-MBP chimeric proteins, which are around ~100 kDa in size. The mG-protein-MBP chimeric complex was designed by adding the MBP construct to the C-terminus of mGα. MBP was not added to the N-terminus as it will interfere with the coupling with the GPCRs. The cDNA encoding the G-protein-MBP construct was cloned into the pET28A vector which was later transformed into BL21 strains for the expression of the chimeric proteins.

In this study, we designed four different mG-MBP chimera constructs (mG_s-MBP, mG_I-MBP, mG_{si}-MBP and mG_o-MBP). Their encoding cDNAs were cloned into pET28a and expressed in the *E. coli Bl21* strain.

The mG_α-MBP chimera protein expression was optimized by testing different IPTG concentrations, induction times, and temperatures. The expression of the mG_α-MBP chimera was best with 0.5 mM IPTG at 28 °C after 4-6 hours.

The chimeric protein was purified with the Ni-NTA purification system by using the His-trap column. The proteins were successfully purified by passing through a His-trap column and the purity was confirmed by the existence of clearly separated monomer and dimer peaks (figure 3.**10**) in the size-exclusion chromatography. The peaks also confirmed the existence of monomer and dimer populations of the protein. All four chimera of mGα-MBP proteins were purified and stored at -80 °C for further use in future experiments. We tried to co-purify the G-protein complex with their receptors, but it led to unsuccessful results due to their low affinity and low yield of the receptor.

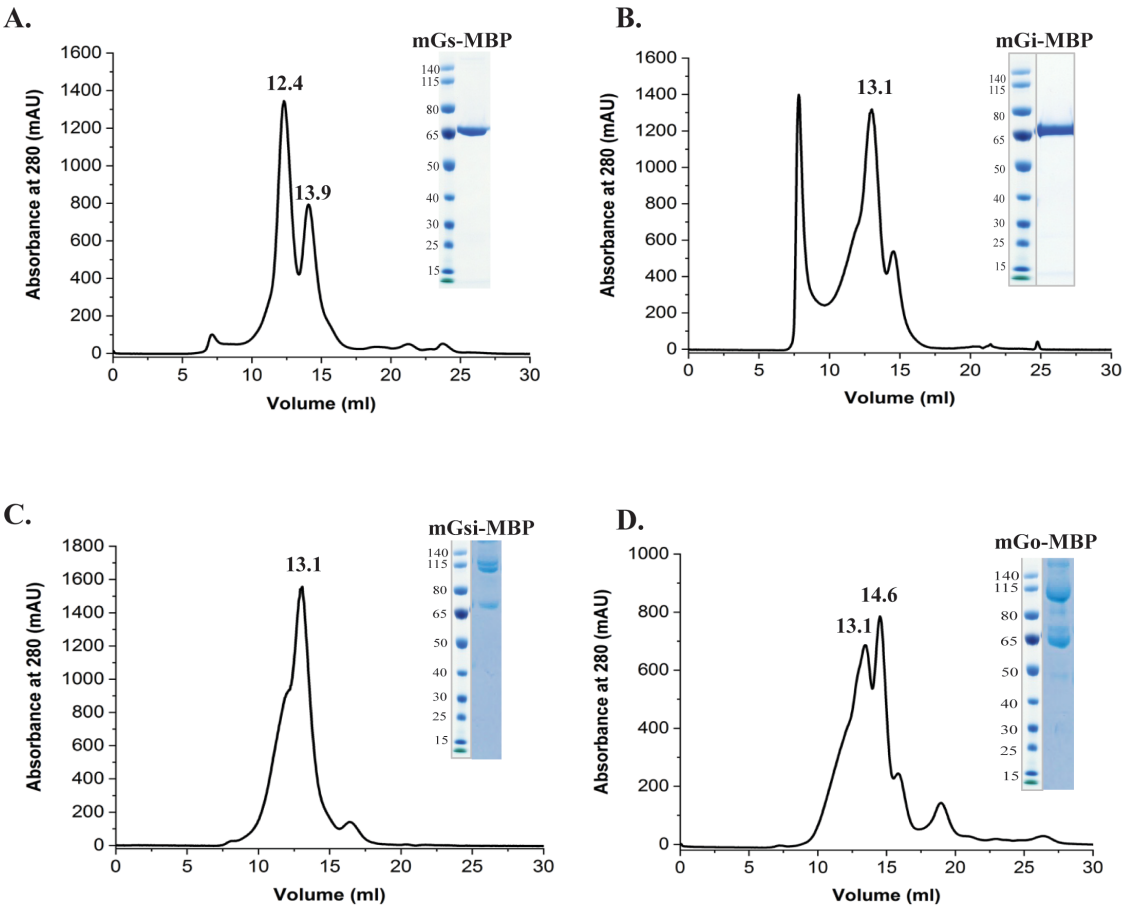

Figure 3.10: Gel filtration elution profiles and SDS PAGE gels during purification of mini-G-MBP chimera proteins expressed and purified from *E. coli*, A) miniG_s-MBP B) mini$G_{\alpha i}$-MBP, C) mini-G-MBP and D) mini-G_o-MBP.

3.3 Allosteric modulation of the orthosteric binding pocket of the bradykinin receptors (BKRs):

The labeled and unlabeled peptides used in this study are listed in table T5

Peptide	Labeling Schemes	Abbreviation	Supplier
DAKD	KRPPGFS-(^{13}C,^{15}N)P-(^{13}C,^{15}N)F	U-[^{13}C,^{15}N]-P8F9 DAKD	Thermo Fisher Scientific
	KRPPGFSPF	$DAKD^{Cold}$	AnaSpec, Fremont, USA
	[^{3}H] KRPPGFSPF	[^{3}H] $DAKD^{Hot}$	
DALK	KRPPGFSPL	$DALK^{Cold}$	AnaSpec, Fremont, USA
	[^{3}H] KRPPGKSPL	[^{3}H] $DALK^{Hot}$	
Bradykinin	RPPGFSPFR	$Brady^{Cold}$	AnaSpec, Fremont, USA
	[^{3}H] RPPGFSPFR	[^{3}H] $Brady^{Hot}$	

Table T5: Peptides used in this study: Peptides used for ssNMR experiments were uniformly labelled with ^{13}C, and ^{15}N at the residue sites P8 and F9, peptides used for radioactivity assays were labeled with [^{3}H].

3.3.1 Heterologous expression and purification of the B1R

The bradykinin receptors (B1R and B2R) belong to the class-A family GPCRs. The cDNAs of both bradykinin receptors were cloned into the pOET1 vector under the control of a polyhedrin promoter. The B1R protein contained a melittin signal peptide plus an N-terminal His10 tag and a C-terminal strepII tag for purification and detection. By using a flashback kit, recombinant baculovirus containing kinin receptors (B1R and B2R) were generated. These viruses were used to infect *Sf9* cells and to heterologously produce kinin receptors in these cells. The expression conditions were optimized by varying the virus quantity and time of infection (Fig 3.11 A). Thereafter, the optimal expression conditions (infection with MOI-5 for 5 days) for B1R were used for protein expression and purification. The B1R membranes were prepared according to the protocol mentioned in section 2.3.4.

The B1R receptor was purified in the presence of detergent micelles containing 1% n-dodecyl-ß-D-maltoside (DDM) and 0.1% cholesteryl hemisuccinate (CHS) (section 2.2.17). The purified B1R receptor exhibited high endogenous ligand (DAKD) binding affinity which was comparable to that of native membranes (Figure-3.11 C). To access the binding affinity of the bradykinin receptor with its agonist and antagonists, we used [^{3}H] labeled DAKD and DALK peptides for radioactive competition studies. We conducted competition binding assays of purified B1R with radioactively labeled DAKD^{hot} which resulted in K_i (Inhibition constant) values of 35 ± 12 nM.

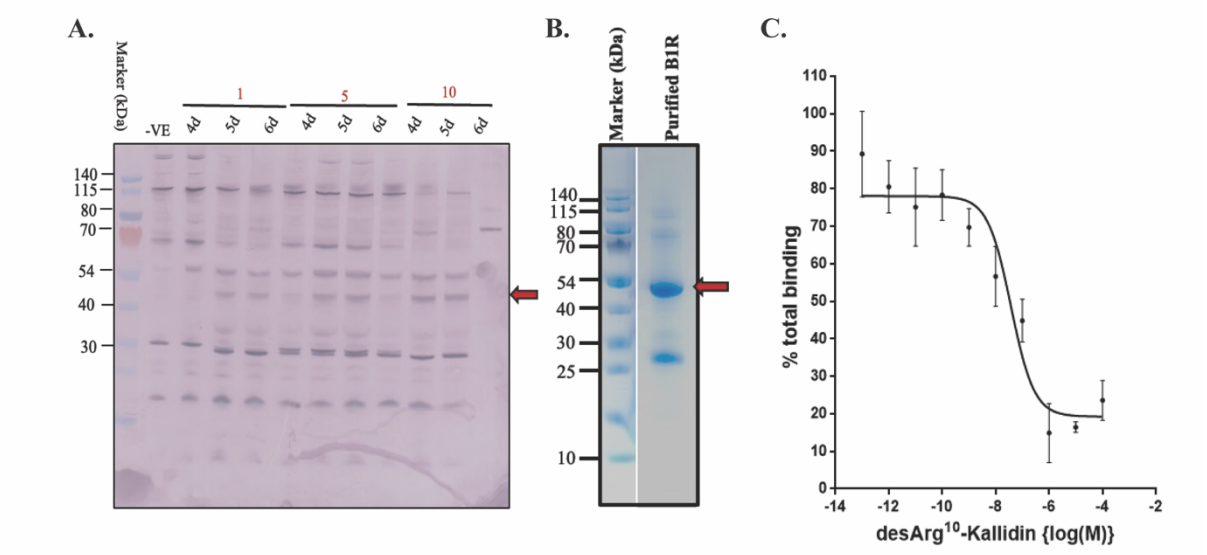

Figure 3.11: Western blots, SDS PAGE gels and binding blots showing expression optimization and purification of B1R in insect cells (*Sf9*): A) The Western blot was probed with anti-His antibody**.** The insect cell membrane was run on SDS-PAGE (4-12% NuPAGE™ Bis-Tris gels) and transformed to a PVDF membrane for Western blot, B) Coomassie blue stained SDS-PAGE of purified B1R (10µg), C) Competition binding assays of B1R in the presence of the radioactive ligand [^{3}H]DAKD indicating that the purified receptors are active.

3.3.2: Biochemical analysis of allosteric modulation by angiotensin-converting enzyme inhibitors (ACEIs) of orthosteric binding sites of bradykinin receptors

The radio-ligand binding approach was used to investigate whether the ACEIs compound can influence the orthosteric binding site of bradykinin receptors. We took advantage of the availability of three widely used ACEI compounds, captopril, enalaprilat, and lisinopril, for our studies. Both human bradykinin receptor (B1R and B2R) was expressed in *Sf9* cells. The purified receptor in the presence of 1% (DDM) and 0.1% (CHS) mixed detergent micelles shows similar ligand binding affinities, as in its native membrane. We used [^{3}H] labeled DAKD and DALK peptides as reporters to determine the binding affinity of the B1R receptor to its agonist and antagonist. The affinities of the bradykinin receptor towards agonist and antagonist were 6.2 ± 0.7 nM and 28 ± 1.8 nM (Fig.3.12 A) respectively. We examined the binding of the [^{3}H] radioactive ligands (DAKD and DALK) to the bradykinin-1 receptor in the presence of 100 nM of various ACEIs such as enalaprilat, captopril, and lisinopril, in order to test the possibility of allosteric modulation of the bradykinin receptors by the ACEIs.

The orthosteric binding pocket of the B1R receptor wasn't affected by the presence of compound captopril significantly. The observed binding affinity of hB1R to the agonist (DAKD) and the antagonist (DALK) in presence of captopril was found to be 3.1 ± 0.5 nM and 5.6 ± 0.6 nM, respectively. Despite the fact that enalaprilat and lisinopril interact with hB1R in a similar way as captopril, they show different agonist (DAKD) and antagonist (DALK) affinities to hB1R. The affinities of the B1R receptor to DAKD and DALK measured in presence of enalaprilat were 984 ± 24 nM and 357 ± 25 nM respectively (Fig.3.12 B and C). This result suggests that the binding of enalaprilat drastically modifies the orthosteric sites of the hB1R and causes a decrease of its affinity to the agonist and antagonist. Surprisingly lisinopril shows a distinct and selective mode of action on DAKD and DALK binding changing the affinities to 124 ± 20 nM and 5.1 ± 2.5 nM respectively. These findings indicate that the

binding of lisinopril stabilizes the antagonist binding conformation rather than the agonist binding conformation.

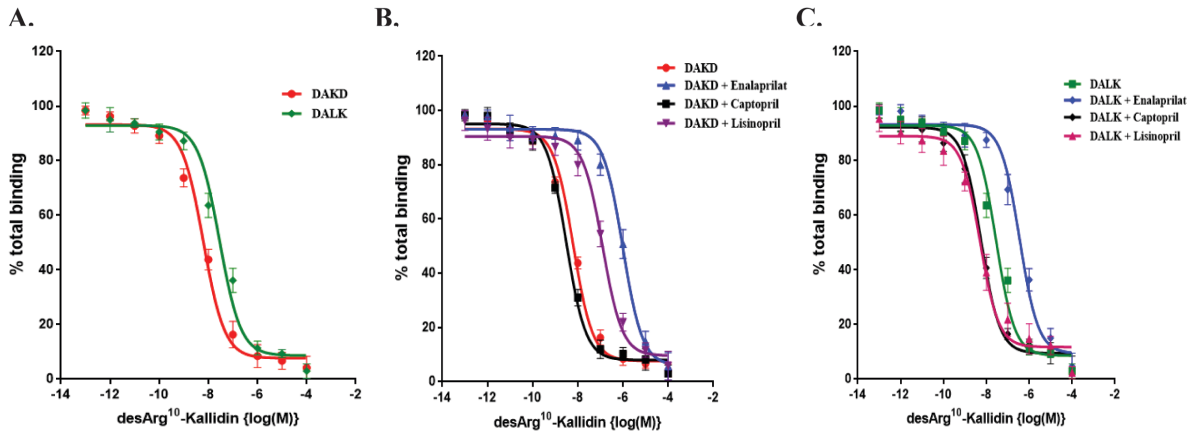

Figure-3.12: Competitive binding of ligands to the bradykinin receptor in the presence of ACEIs": binding of [^{3}H] desArg10-Kallidin ([^{3}H] DAKD) in the presence of the non-radioactive agonist DAKD or the antagonist DALK. A) agonist DAKD and antagonist DALK without allosteric modulators; B) agonist DAKD in the presence of 100 nM enalaprilat, captopril, and lisinopril; C) antagonist DALK in the presence of 100 nM enalaprilat, captopril, lisinopril.

Peptide	ACEIs	Ki.
DAKD	No	6.2 ± 0.7 nM
	Enalaprilat	984 ± 24 nM
	Captopril	3.1 ± 0.5 nM
	Lisinopril	124 ± 20 nM
DALK	No	28 ± 1.8 nM
	Enalaprilat	357 ± 25 nM
	Captopril	5.6 ± 0.6 nM
	Lisinopril	5.1 ± 2.5 nM.

Table T5: Inhibition constants (Ki) of the agonist DAKD and the antagonist DALK in the presence of the ACEIs enalaprilat, captopril, and lisinopril for B1R in the *Sf9* membrane.

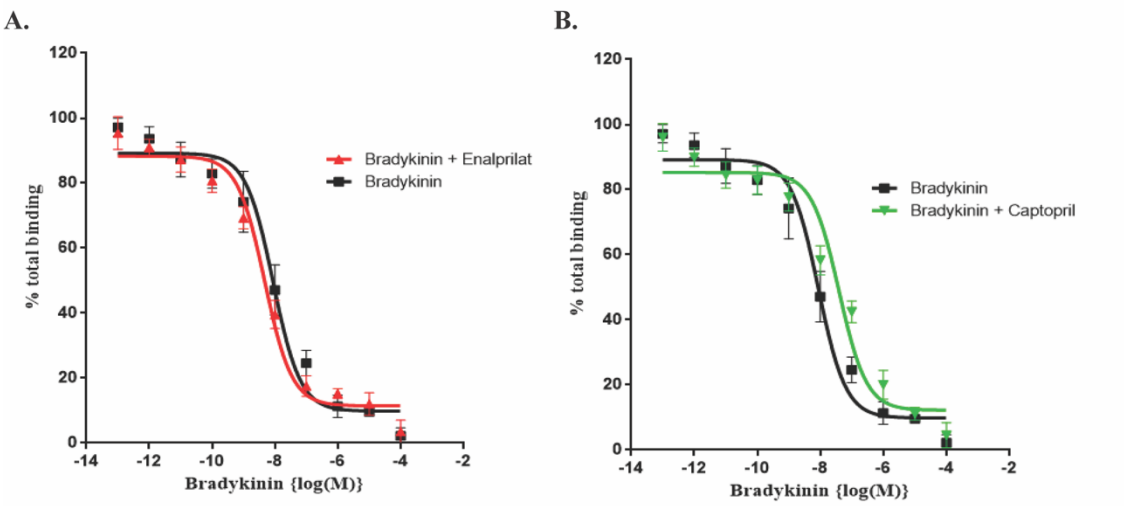

Figure 3.13: Competitive binding of"[^{3}H] bradykinin to the bradykinin-2 receptor (B2R) in insect cell membranes in the presence of ACEIs and the non-radioactive agonist bradykinin. The assay was performed in the presence of A) 100 nM enalaprilat, and B) 100 nM captopril.

3.3.3: Effects of zinc on the kinin receptor (Both B1R and B2R):

ACEI interacts with the B1R through the zinc ion binding site at the extracellular loop 2 (ECL-2) region of the receptor. A previous study suggested that there is a cross-talk between Zn^{2+} and the ACEI on the hB1R receptor (Ignjatovic *et al.,* 2002). We first investigated the impact of Zn^{2+} on the orthosteric binding site of the ligand without ACEI. For our studies, rather than probing the direct interaction of $Zn^{2+}$and B1R, we used an indirect approach to probe the impact of Zn^{2+}on the orthosteric binding site of the receptor, which can be monitored by binding of the radioactive ligand in the presence of Zn^{2+}. To measure the impact of Zn^{+2} on the receptor, we treated the membrane with 2 mM EDTA and measured the binding of DAKD in the presence of different concentrations of $ZnCl_2$. We observed that DAKD- and DALK-binding was enhanced when the concentration of Zn^{2+} was increased. The Kd values for Zn^{2+}-B1R, for DAKD and DALK in Zn^{+2}, are 34 ± 33µM, and 30 ± 2.1µM, respectively. This observation suggests that Zn^{2+} binding to B1R leads to a conformational change in the orthosteric binding site which increases the binding of DAKD and DALK. Ca^{2+} was used as a control to investigate

whether the effect of Zn^{2+} on B1R is unique to Zn^{2+}. As shown in Figure-3.14 B, Ca^{2+} impacts negatively on the ligand binding site at higher concentrations and hence acts as a negative allosteric modulator (NAM) for hB1R.

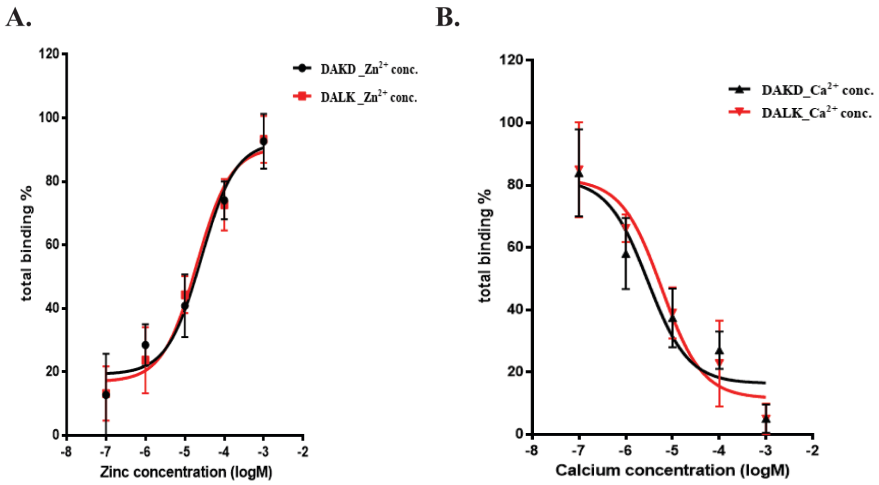

Figure-3.14: Binding of agonist and antagonist to the bradykinin-1 receptor in the presence of divalent metal ions: A) zinc (Zn^{2+}) or B) calcium (Ca^{2+})

To understand the Zn^{2+}-B1R interaction and the impact of Zn^{2+} on the orthosteric binding site of the receptor determined the Kd values of DAKD and DALK in the presence of different concentrations of Zn^{2+}. Interestingly, we observed that the Kd value of the membrane treated with EDTA (DAKD_EDTA) was 57.9 ± 26 nM, the addition of Zn^{2+} increased the affinity of the ligand to the receptor. As seen, the addition of 100 nM of Zn^{2+} increased the Ki value ~2-fold to 35.7 ± 19 nM. The interaction of Zn^{2+} with B1R enhances the DAKD- affinity towards B1R. The binding of DAKD-B1R is increased from 57.9 ± 26 nM at 0 mM Zn^{2+} to 3.6 ± 1.2 nM at 1 mM of Zn^{2+}. Similar enhancements of ligand affinity were also observed in the case of antagonist DALK towards the B1R receptor. The antagonist DALK binding affinity increased from 100.5 ± 40 nM nm to 26.2 ± 16 nM nm in the presence of Zn^{2+}. Surprisingly there was no change in the Ki values of binding of the DALK or DAKD to B2R in the presence or absence

of Zn^{2+}- This observation indicates that there is no impact of Zn^{2+} on the hB2R orthosteric binding site, the effects of $Zn^{2+}$are therefore specific for the hB1R.

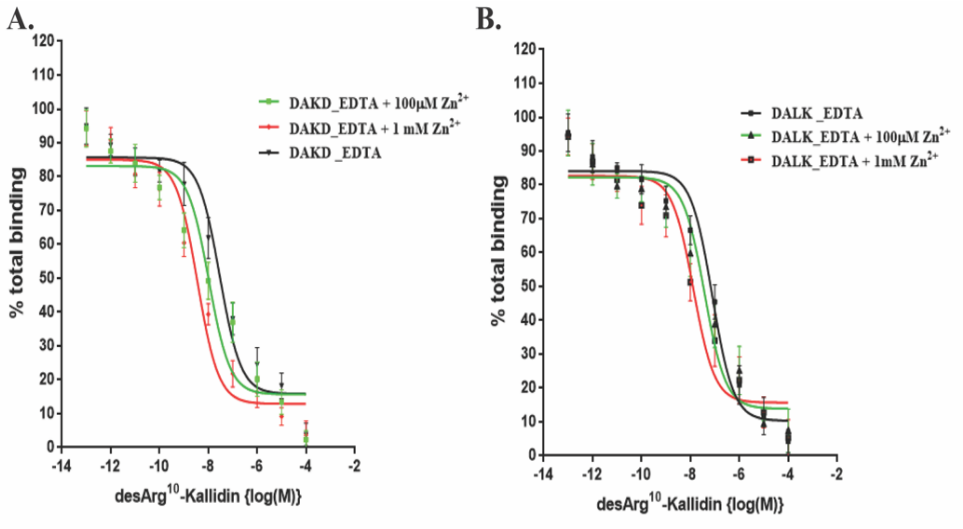

Figure-3.15: The effects of Zn^{2+}/EDTA on the binding of ([^{3}H] DAKD to the bradykinin-1 receptor (B1R) in the presence of the non-radioactive agonist DAKD (A) or the antagonist DALK.

Peptide	concentration of zinc	Ki
DAKD	0	57.9 ± 26 nM
	100 nM	35.7 ± 19 nM
	1 µM	140 ± 156 nM
	10 µM	23.9 ± 14 nM
	100 µM	33.8 ± 35 nM
	1mM	3.6 ± 1.2 nM
DALK	0	100.5 ± 40 nM
	100 nM	434 ± 661 nM
	1 µM	47.3 ± 23 nM
	10 µM	469 ± 782 nM
	100 µM	61.3 ± 37 nM
	1mM	26.2 ± 16 nM

Table T7: Ki values for binding of the of the agonist DAKD or antagonist DALK in the presence of different concentrations of Zinc.

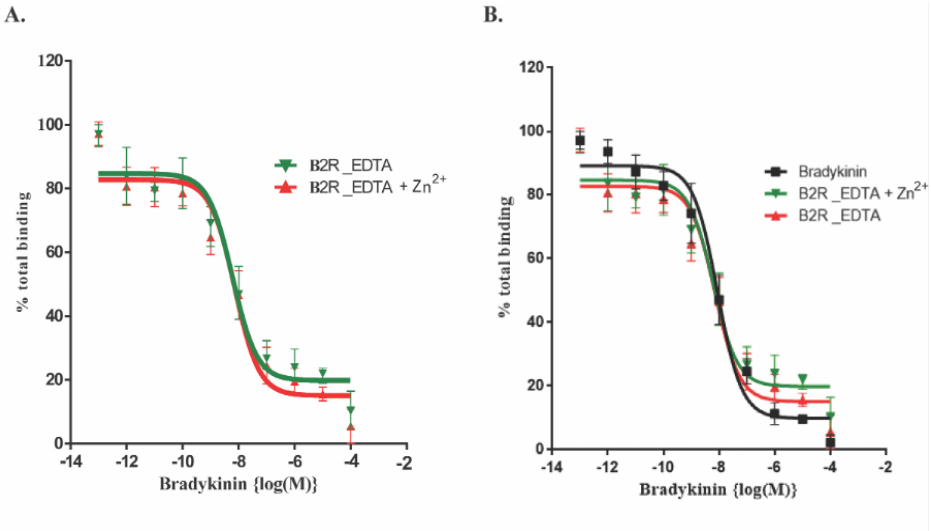

Figure 3.16: Binding of [^{3}H] bradykinin to the bradykinin-2 receptor in the presence or absence of Zn^{2+}: A) no zinc (green line) or 1mM Zn^{2+} (red line) B) the membrane not treated with EDTA (black), no Zn^{2+} (green line) or 1mM Zn^{2+} (red line).

Peptide	Concentration of Zn^{2+}.	Ki.
Bradykinin	0	6.8 ± 3.3 nM
	1mM	5.8 ± 2.7 nM

Table T8: Ki values for binding of bradykinin to B2R in the presence or absence of Zn^{2+}.

3.3.4: Zn^{2+} instructs ACEI binding and amplifies distinct allosteric effect on hB1R

To dissect the interaction between Zn^{2+} and ACEI in regulating the binding pocket of the B1R receptor, and affecting endogenous ligand binding, the EDTA- treated membrane was used for analyzing the impact of Zn^{2+} and ACEI on B1R. Interestingly, the addition of Zn^{2+} and ACEI amplifies the impact on the orthosteric binding pocket of the receptor. We observed that the presence of thee ACEIs captopril, enalaprilat, and lisinopril enhance the binding affinity of DAKD in the absence and in the presence of Zn^{2+} from 13 ± 3.1 nM to 1.4 ± 0.9 nM (captopril), from 17 ± 3.3 nM to 1.4 ± 1.2 nM (enalaprilat) and 115 ± 2.8 nM to 37 ± 4.4 nM (lisinopril).

These results indicate that Zn^{2+} and ACEIs both act as allosteric modulators and act in a coordinated manner in regulating the orthosteric binding site of the receptor. All three ACEI show a distinct allosteric modulation of B1R.

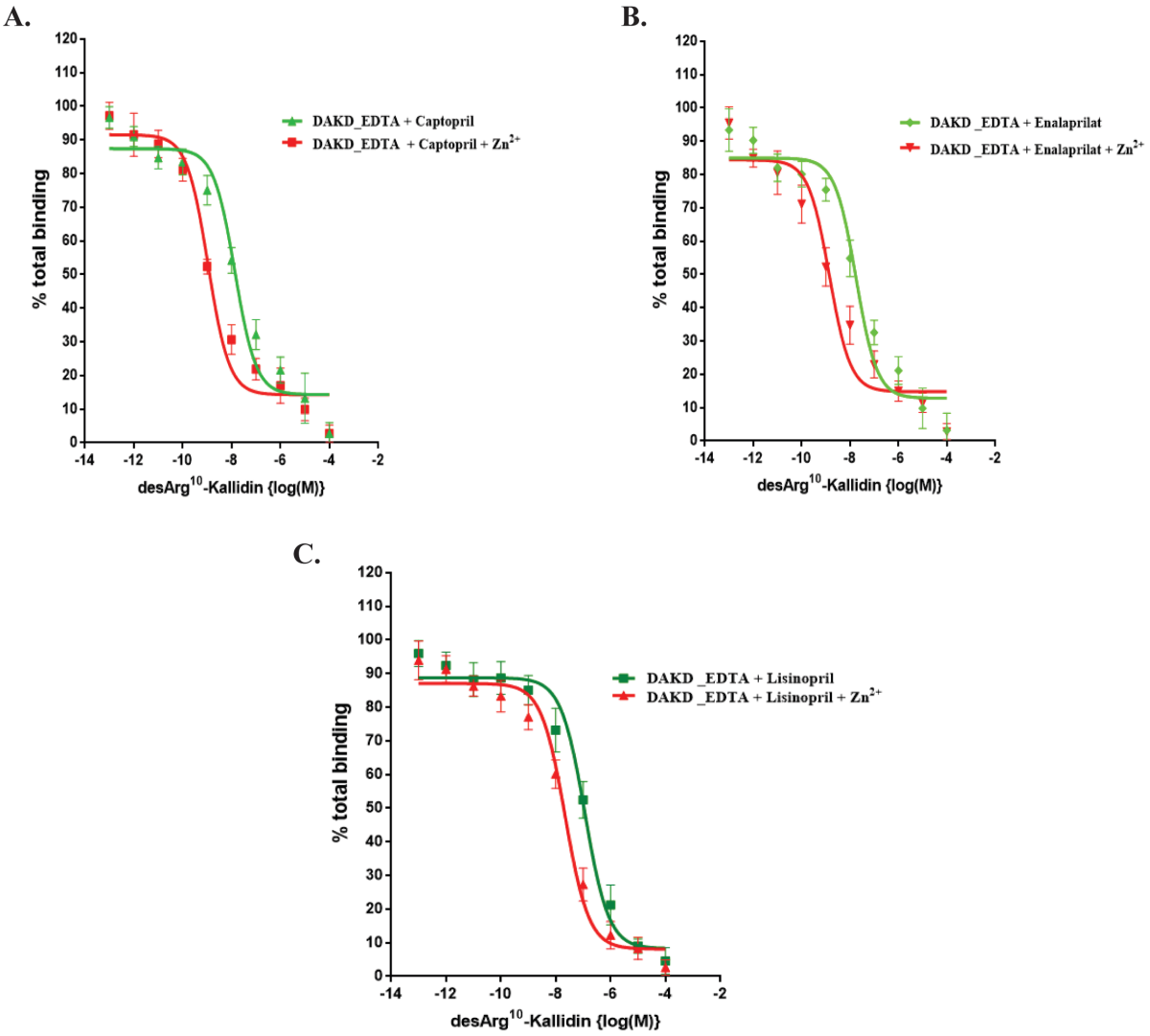

Figure-3.17: Binding of agonists and antagonists to the bradykinin receptor in presence of Zn^{2+}: binding of [^{3}H] DAKD in the presence of the non-radioactive agonist. B1R containing insect cell membranes treated with EDTA (green line) or with EDTA and subsequently with Zn^{2+} (red line) were used. The assay was performed in the presence of a) 100 nM captopril, b) 100 nM enalaprilat, c) 100 nM lisinopril.

Peptide	ACEIs	concentration of zinc	Ki
DAKD	Enalaprilat	0	17 ± 3.3 nM
		1 mM	1.4 ± 1.2 nM
	Captopril	0	13 ± 3.1 nM
		1 mM	1.4 ± 0.9 nM
	Lisinopril	0	115 ± 2.8 nM
		1 mM	37 ± 4.4 nM

Table T-9: Binding of DAKD to B1R containing insect cell membranes in the presence of 100 nM ACEIs supplemented with/without Zinc in the assays.

3.3.5 Molecular docking of Zn^{2+} and ACEIs binding to the bradykinin-1 receptor:

To get a better understanding of the specific binding of Zn^{2+} to the hB1R-DAKD complex and its impact on the orthosteric binding pockets of the receptor. The possible metal ion binding site in both subtypes of the bradykinin receptor (B1R and B2R) were investigated by using an online metal ion binding (MIB) server (Fig-3.18). The MIB server, which predicts binding sites for metal ions and docks metals into these sites, offers a method for utilizing the fragment transformation method to search for the residues contributing to the metal ion-binding sites. A binding score, which is mainly dependent on the sequence and structure, is given to each residue of the protein. A residue is anticipated to contribute to the metal binding if its binding score is higher than a threshold limit. In-silico docking to hB1R-DAKD suggests the existence of multiple potential zinc ion binding sites rather than the primary "HEAWH" region of the ECL2. MIB scores of more than 1.0 were observed in the extracellular part of the receptor at (H195, E196) and (E287, D288) and in the intracellular regions (T321, E325) (Fig 3.19).

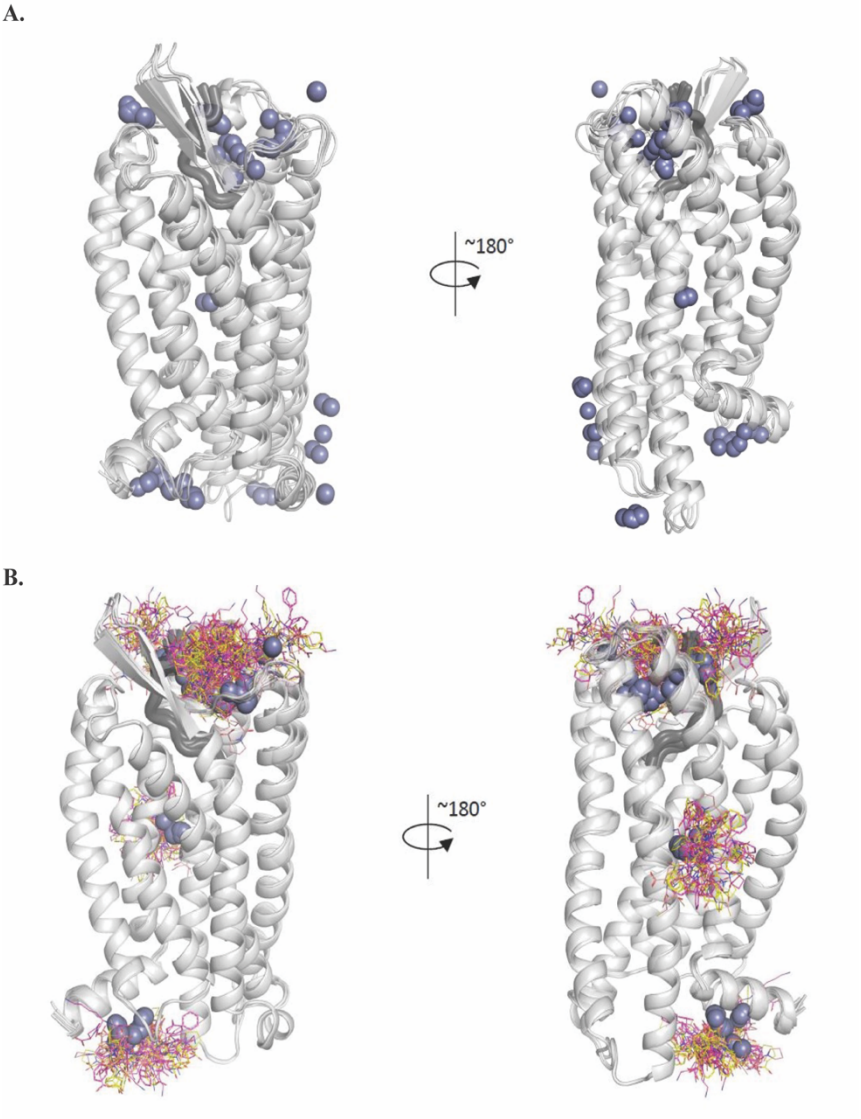

Figure 3.18: Molecular docking of zinc ions and three ACEIs to cryo-EM structure of hB1R (PDB:7EIB): A) docking of zinc ions (which are shown as small ice-blue balls) to the DAKD (thick grey line) containing hB1R receptor. Zn^{2+} mostly binds to the intracellular and extracellular parts of the receptor. B) docking of the 3 different ACEIs together with the zinc ions to the active receptor. Captopril (orange), enalaprilat (yellow), and lisinopril (pink). The three ACEIs primarily bind to ECL2 (H195 and E196) areas of the active hB1R receptor. However, only a small percentage of ACEI binding sites are found at the intracellular part of the receptor compared to the extracellular binding.

According to the earlier study by Ignjatovic *et al.,*2002 the mutation His195 to Ala195 eliminates Zn^{2+}-mediated pharmacological effects of hB1R. Most likely, the receptor's (H195–E196) region, which is found only in hB1R, plays a significant role in the zinc ion binding **(129)**. The majority of the other zinc ion binding sites (from the MIB server) are shared with

the hB2R, therefore it is unlikely that they are the cause of the reported subtype-specific allosteric effect of Zn^{2+} on hB1R.

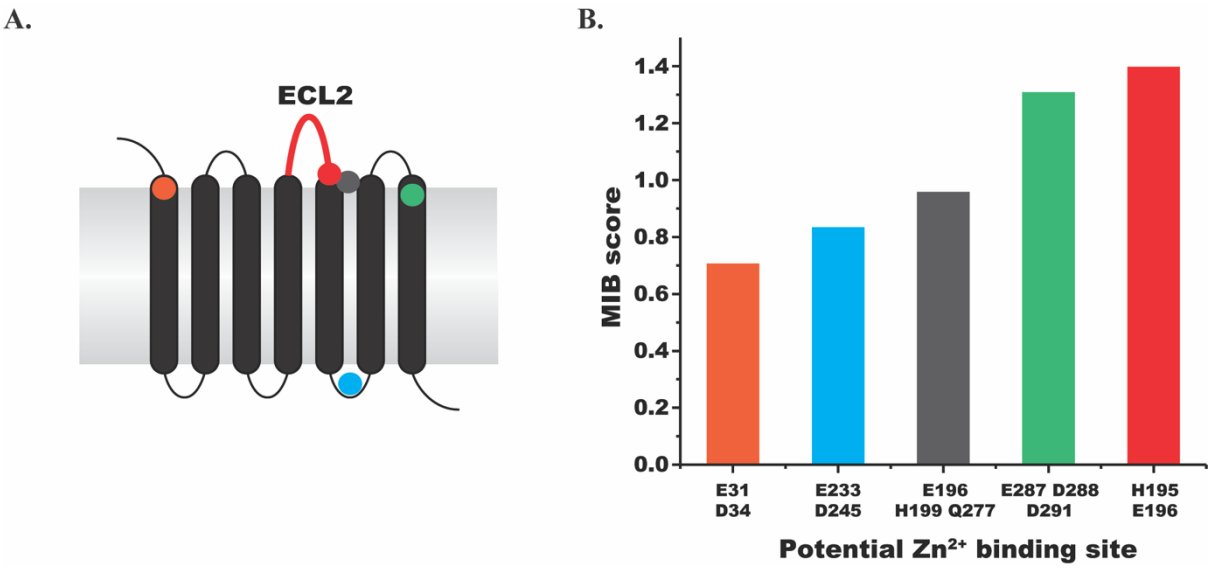

Figure 3.19: Molecular docking prediction of the top five Zn^{2+} binding sites on hB1R: A) small circles are plotted on the topological structure of hB1R, indicating the point of interaction with Zn^{2+}. B) The histogram of the MIB docking score of the top 5- Zn^{2+} binding sites on the hB1R, color coated as the same as those in (A)

By using Rosetta multiple modeling, we docked Zn^{2+} ions and ACEIs into the hB1R-DAKD complex (Fig.-3.20). According to the results of the modeling, the three ACEIs primarily bind to the extracellular region especially the ECL2 regions of the receptor whereas a small percentage of the ACEIs interact with the intracellular domain and the transmembrane part of the receptor. A distinct interaction pattern was observed for all three ACEIs. All three small molecule drugs (ACEIs) target Zn^{2+} binding sites of the ECL2 regions of the receptor via bidentate replacement of water molecules forming a Penta-coordinated environment. All three ACEIs interact with hB1R at the residues H195 and E196 of ECL2. Despite all three ACEIs showing shared binding features the detailed binding chemistry appears to be different. The differences may be due to the size, captopril is smaller, whereas enalaprilat and lisinopril

possess extra phenyl groups. The bigger N-substitution groups in the enalaprilat and lisinopril molecules are mostly responsible for this distinct interaction with the hB1R complex since they sterically inhibit the binding of the thiol group to the zinc ion.

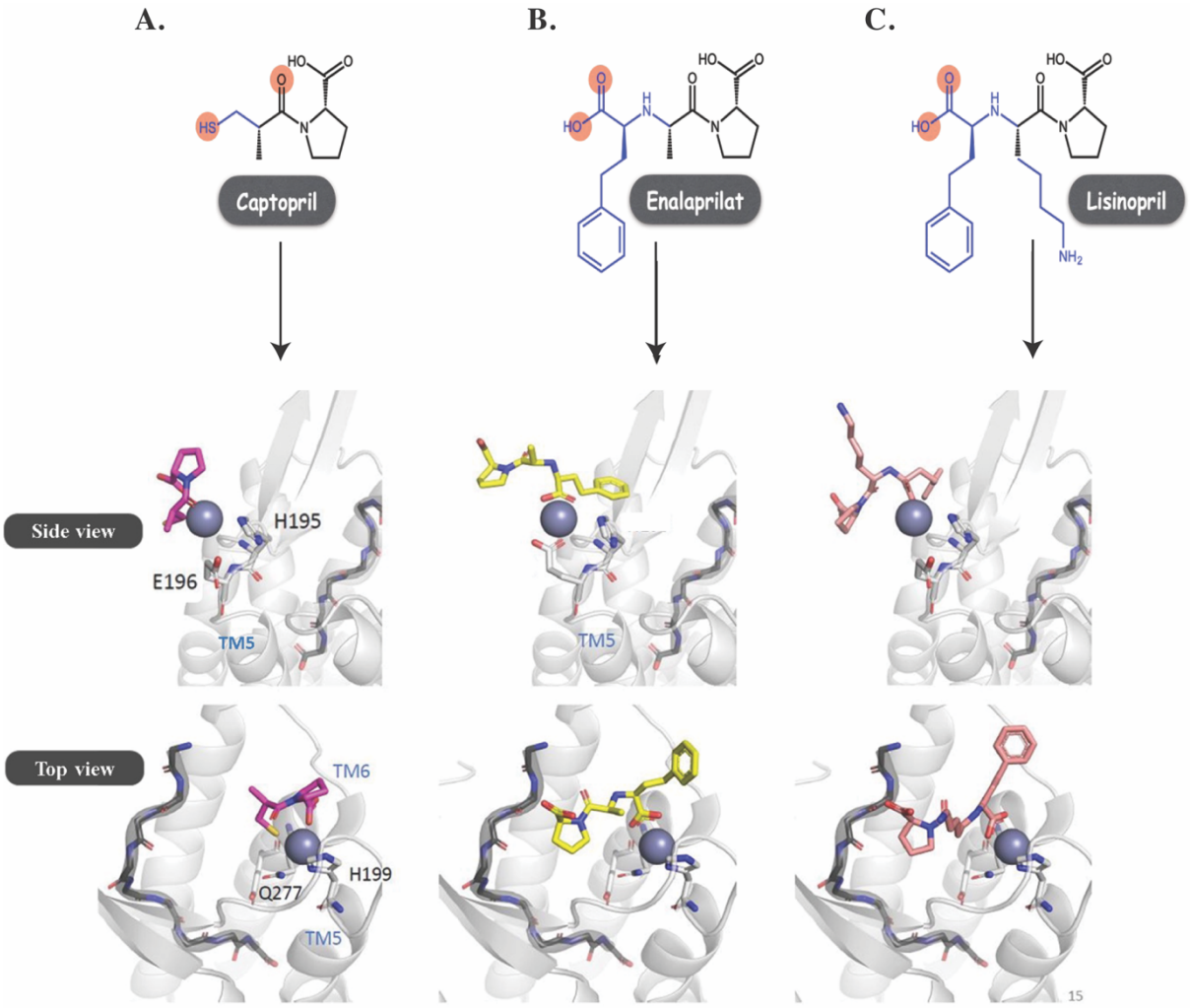

Figure 3.20: Molecular docking of the three ACEIs: Based on the B1R cryo-EM structure (PDB: 7EIB)(1), molecular docking was performed with different ACE inhibitors, in the presence of zinc ions (gray spheres) and the agonist DAKD (gray band). For this purpose, the potential zinc-ion binding site in the extracellular region of the receptor (ECL2) was selected. The top and side views of the ECL2 region show the potential interactions between the agonist DAKD, zinc ions, and ACE inhibitors. A) Captopril (orange), B) enalaprilat (yellow), and C) lisinopril (pink). The interaction between zinc ions and the ACE inhibitors leads to changes in the orthosteric binding sites of the receptor.

3.3.6: DNP-enhanced solid-state NMR of BKR-DAKD complex in the presence of ACEIs.

The biochemical analysis of ACEI on B1R indicates the possibility of a distinct allosteric modulation of the ACEI-B1R-DAKD complex. To get a better understanding of the allosteric modulation we decided to further investigate the structural impacts of three ACEIs on the receptor-peptide complexes. A previous study from our lab and the recent structure of the B1R-DAKD-Gq protein suggest that the C-terminal part of the peptide is responsible for binding to the B1R receptor. Peptides isotopically labeled at the C-terminus can be used as reporters for any changes in the binding pocket of the receptor. So, we choose the U-[13C,15N] P8F9-DAKD labeled peptide for our DNP-ss NMR studies.

13C-13C, double-quantum single-quantum (DQ-SQ) and 15N-13C, transferred-echo double resonance (TEDOR) spectra of U-[13C,15N] P8F9-DAKD bound to the B1R receptor in presence of all three ACEIs (100 nM) drugs captopril (Fig. 3.18A) enalaprilat (Fig 3.18B) and lisinopril (Fig. 3.18C) are shown. We selected DQ-SQ 13C-13C and TEDOR 15N-13C 2D correlation spectroscopy as the primary NMR methods for our research in order to resolve the signal of the peptide. These strategies have been demonstrated to be the most effective for the investigation of membrane proteins using DNP-ssNMR; they both work by removing the naturally abundant 13C signal from detergent and receptor.

Both Pro8 and Phe9 can be seen on 2D-TEDOR, 15N-13C correlation spectra, as shown in (Fig. 3.21). To encourage the dipolar-based 15N-13C magnetization transfer over short distances, we have chosen a short TEDOR mixing time. Therefore, the directly bonded short-distance N-C pairings (backbone amine N - Cα/C'/Pro C) were highlighted in the spectra (figure 3.16). The three ACEI spectra suggest that the DAKD peptide could exist in three distinct structural states when ACEIs are present. Different local conformations of C-terminal residues are indicated by differential NMR chemical shifts, which are consistent with the reported diverse allosteric modulations by various ACEIs.

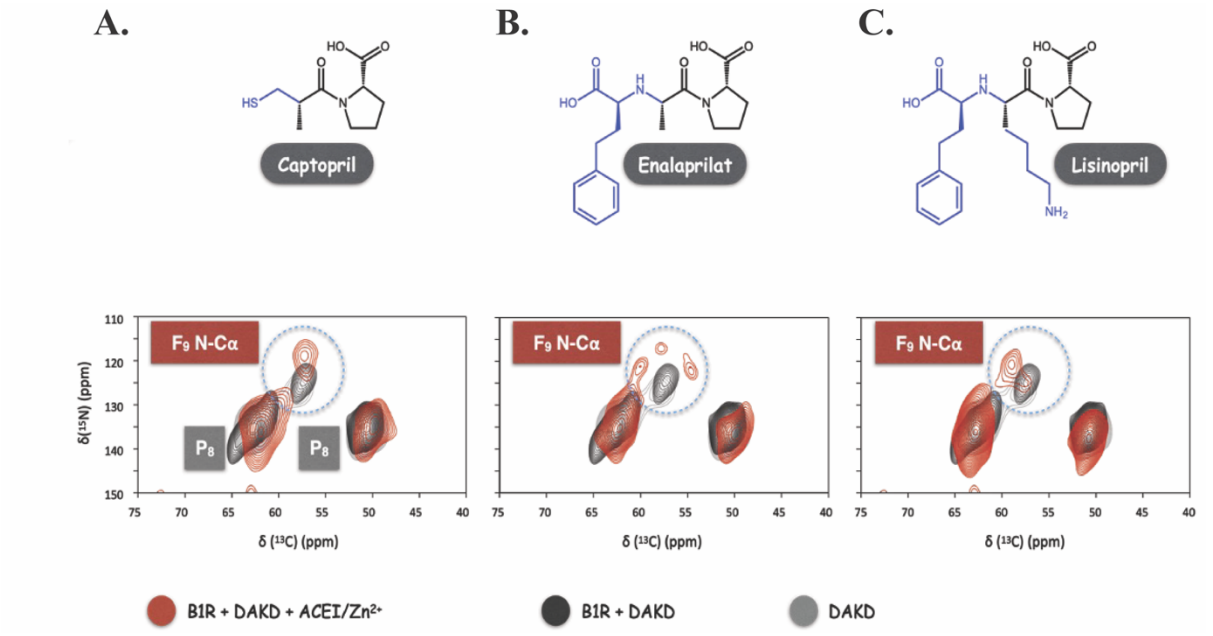

Figure 3.21: DNP-ssNMR spectra of B1R in presence of ACEIs: A sample containing the DAKD–B1R-ACE inhibitor complex doped with the biradical AMUPol is measured via DNP-ssNMR, the DQ/REDOR doubly filtered ^{13}C-spectra of B1R–DAKD-ACEI complex (Red) is observed and compared with B1R-DAKD in (black). A) In presence of captopril, B) enalaprilat, and C) lisinopril.

3.3.7 Molecular dynamic simulation of the active structure of the B1R-DAKD complex

The NMR and biochemical data indicate the structural dynamics of the peptide ligand DAKD in orthosteric binding pockets of hB1R. To explore the structural dynamics of the DAKD we took the help of molecular dynamics (MD) simulation study, as its one of the powerful methods used in the field to depict the structural dynamics of the proteins. The DAKD-bound hB1R complex is highly sensitive to different types ACEIs, so it could complicate the dynamics of the peptide and leads to biases in the interpretation of the structure. Therefore, we performed an MD simulation of DAKD-hB1R without the addition of allosteric modulators. Taking advantage of the cryo-EM structure hB1R-DAKD-Gqβγ complex (PDB: 7EIB), we performed a three independent 3 μs molecular dynamics (MD) simulations (Fig 3.22). The MD

experiments showed that the hB1R-DAKD-Gqβγ complex attains an equilibrium state after 3 μs. The MD simulation study suggests that the ligand (DAKD) can attend diverse conformations within the binding of the hB1R. Various changes in root mean square fluctuations (RMSF) can be observed in the binding pocket, the DRY sequence, and the ECL2 and ICL3 regions of the receptor (The changes observed in the receptor lead to a closed conformation of the orthosteric binding sites enabling close binding of DAKD. The structural polymorphism of the ligand peptide DAKD can be seen by comparing the torsion angles of each residue of the ligands Fig 3.22 B). The torsion angle of the DAKD peptide at Gly5, Phe6, and Ser7 varies a lot suggesting that a rotation of the peptide happens at the middle regions of the peptide. In addition to the middle part of the peptide the C-terminal, at residue phe9 region also exhibits significant dynamics. The COO^- of Phe9 of the DAKD peptide interacts with multiple interacting partners inside the binding pockets of the hB1R. The COO^- of Phe9 of the DAKD primarily interacts with $Arg202^{5.38}$ and transiently interacts with $Lys118^{3.33}$ and $Arg176^{4.64}$ of the peptide. The results from MD-simulation indicate that phe9 of the peptide is more sensitive and can rather tightly interact with the hB1R. Whereas the middle part of the DAKD adopts different structural polymorphisms and is probably responsible for the subtype selectivity and the B1R-G protein coupling.

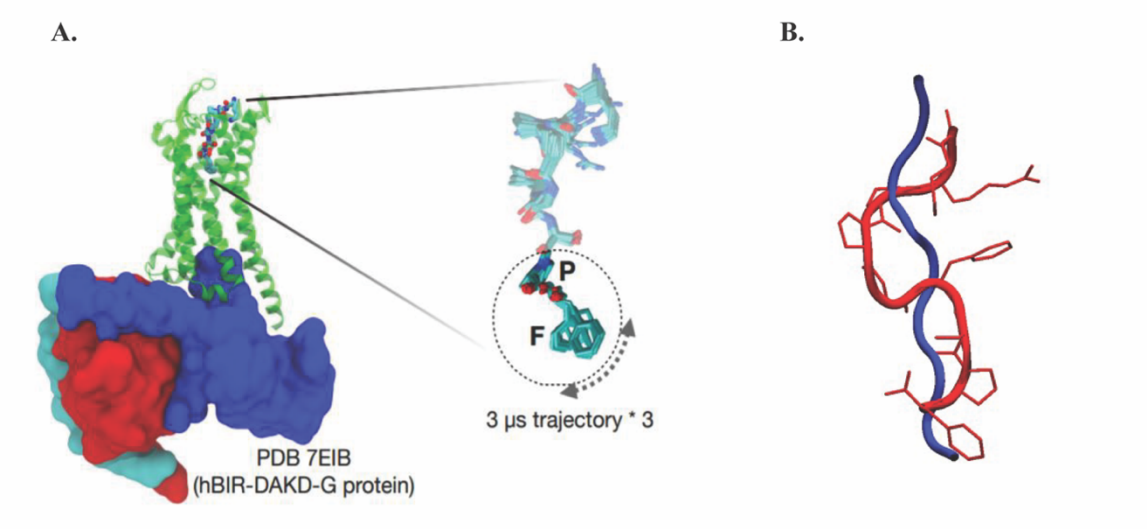

Figures 3.22: Molecular dynamics simulation of the active B1R-DAKD in complex with a G-Protein: Based on the B1R cryo-EM structure (PDB:7EIB) **(1)**, A) hB1R-DAKD with the bound G-protein was equilibrated in the presence of a lipid bilayer for 3µs showing structural changes of DAKD middle part of the peptide. B) conformational change of the peptide DAKD attached to B1R within three µs MD-simulation, showing the dancing motion of the peptide DAKD from an S-shape at the start (red) to a straight state (blue).

3.3.7: Impact of ACEIs on the binding of G-proteins to the receptor:

We tried to understand the effects of ACEIs on downstream signaling inside the cell after binding with the bradykinin receptor (hB1R and hB2R). We used the B2R instead of the B1R because the binding of the agonist to B1R is irreversible which causes difficulties to find the effect of ligand and ACEI binding on the downstream signaling. The bradykinin receptors upon activation bind to either $G_{\alpha q}$ or $G_{\alpha I}$. Both G-proteins activate different downstream signaling pathways. It is known that the bradykinin receptor signal is biased towards $G_{\alpha q}$-pathways rather than the $G_{\alpha I}$ pathways. To find out the impact of the G-proteins on the receptor we used the mG_I protein which we purified earlier. We measured the radioactive (^3H)-bradykinin binding to the B2R receptor in the presence and absence of mG_I. We incubated the B2R-containing membranes with 100 uM mG_I in order to saturate the binding sites of the receptor with mG_I. What we observe is that the affinity of ligand peptide decreases in the presence of mG_I from 8.7 ± 2.8 nM to 65 ± 4.8 nM (Figure 3.23A).

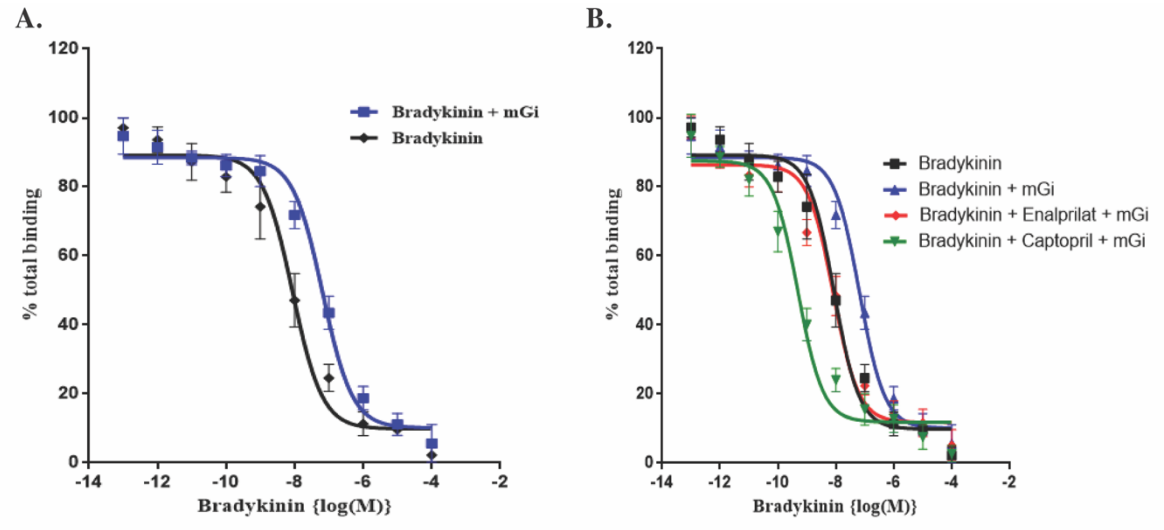

Figure 3.23: Binding of ^{3}H-bradykinin to the bradykinin-2 receptor in the presence of mini-$G_{\alpha I}$ (mG_I) and 2-ACEI compounds A) Binding in the presence of mG_I (blue) and in absence of mG_I (black). B) binding in the presence of two ACEIs, enalaprilat (red) and captopril (green)

To decipher the crosstalk between the ACEI and G-protein binding site we incubated the B2R-bradykinin-mG_I complex with the ACEI compounds enalaprilat and captopril (100 nM). Interestingly, the presence of captopril enhances the binding affinity of bradykinin towards the receptors from 8.7 ± 2.8 nM to 0.48 ± 0.2 nM, whereas enalaprilat increases the affinity slightly to 8.1 ± 2.3 nM (Figure 3.23B).

Chapter – 4: Discussion

Chapter-4: Discussion

The GPCRs form the largest family of cell-surface receptors in higher eukaryotes They are responsible for the regulation of various crucial biological processes of the cells. Any dysfunction in some of the GPCRs can lead to disease conditions in humans. Nearly one-third of the marketed drugs act on GPCRs, which reiterates their therapeutic importance. The objective of this dissertation was to expand structural and functional knowledge of allosteric regulation and ligand binding characteristics of peptide receptors. In this thesis, I describe the heterologous production and purification of CaSR, a member of the class-C family of GPCRs and mention the difficulties associated with the purification of the class-C GPCR. In the 2nd part of thesis**,** I dealt with the heterologous expression and purification of mini G-proteins and chimera of the mini G-protein-MBP (mG-MBP) protein which can be used to get GPCRs for structure studies or activity assays. In the last part**,** the structural and functional mechanisms behind the allosteric modulation of peptide GPCRs and the crosstalk between the allosteric binding sites with the orthosteric binding sites of the receptor are presented. Within the peptide GPCRs molecular insights into PAM and its influence on the orthosteric binding site of the human bradykinin receptor (BKR) are presented.

4.1 Heterologous expression and production of CaSR:

The CaSR is a class-C family GPCR, and it is known for its large extracellular domain. This protein is responsible for the regulation of Ca^{2+} levels in blood. It is predominantly expressed in kidney cells and in parathyroid glands (134,135). In the parathyroid gland, CaSR regulates the production of the parathyroid hormone and its secretion into the blood. In the kidney and bone**,** it regulates the absorption of Ca^{2+} from the blood. Loss of function of CaSR leads to hyperparathyroidism whereas gain of function or overexpression leads to hypocalcemia disease in humans (136). Due to its association with various cellular processes in humans**,** it is an ideal target for drug development.

Since GPCR levels are extremely low in native tissues, over-expression is a more practical method of obtaining the necessary protein amounts for structural research. To study the structural and functional study of the CaSR, it is necessary to express and produce CaSR heterologously. The quantity and functional quality of produced protein greatly depend on the expression system used for protein synthesis. However, low expression levels of the membrane proteins or synthesis of inactive proteins are frequently the result of heterologous membrane protein production. Choosing the right expression system is crucial for obtaining an intact and actives membrane protein expression for structural and functional studies, mainly for three reasons, i)- right chaperones for the proper folding of proteins must be present, ii)- specific post-translational modifications of the protein responsible for certain functions of the protein must occur, and lastly, iii) - the produced protein must be transported into the specific compartments of the cell guided by specific signal peptides of the protein. For a membrane protein to attain its close-to-native structure and therefore suitability to perform its specific function, it is necessary that the protein is transported to the membrane. To get the best result for expressing membrane proteins, it is best to choose an expression system that is evolutionarily close to the host cell. For overexpression of CaSR we choose *Pichia pastoris* and insect cells (*Sf9*) expression systems.

The protein was expressed both in *Pichia pastoris* and insect cells (*Sf9*), with the signal peptide of ost-app4 for *Pichia* expression and of hemagglutinin for *Sf9*- expression. Expression of CaSR can be achieved in both expression systems, *Pichia* and insect cells with a high yield. Fluorescence microscopy was used with anti-CaSR antibodies to locate CaSR both in insect cells and *Pichia*. It is difficult to comment on the localization of CaSR in the cells due to the cross-reactivity of secondary antibodies in fluorescence imaging. Further I investigated the posttranslational modification of heterologously produced CaSR by incubating the CaSR protein with PNAGaseF. The results indicated that the CaSR is glycosylated in both expression

systems (*Pichia* and insect cells). In-silico analysis of the CaSR amino acid sequence suggests, that there are 11 potential glycosylated sites, but in our case, by comparing the shift of the protein bands, I can only suggest the present of 5-6 glycosylations in the CaSR protein.

4.2 Purification of CaSR

To purify the structurally intact and active membrane protein it is necessary to extract it from the biological membrane with the help of amphipathic compounds. Due to the hydrophobic nature of membrane protein, the amphipathic compounds help to solubilize the protein and shield the hydrophobic patch of the protein. The membrane protein can be extracted from the lipid bilayer using an SMA polymer (137), or it can be solubilized using detergent micelles. The proteins extracted with the help of detergents can later be reconstituted into lipid bilayers containing environments such as nanodiscs or peptidiscs. Purifying membrane proteins in lipid environments like SMA, nanodiscs or peptidiscs helps to mimic biological membrane conditions which are close to their native environments. The presence of a lipid bilayer surrounding membrane protein helps to maintain its structural and functional properties (138).

At first, the CaSR protein was purified from *Pichia* membranes using the SMA polymer. The CaSR can be purified with high purity after Ni-NTA affinity purification. But the size-exclusion profile of CaSR in SMA suggests that the proteins form aggregates. During the solubilization and purification of CaSR various substances were added in an effort to reduce aggregation. These substances include reducing agents (DTT, β-ME), glycerol, amino acids, calcium ions (ligands), and trehalose. Unfortunately, these additives did not have any effect on CaSR aggregation.

Then the CaSR was expressed in *Sf9* insect cells using the baculovirus system. The yield of CaSR is higher in this case compared to *Pichia*. The CaSR was purified from the insect cell membranes in the SMA-polymer using a His-trap column. The size-exclusion chromatography

profile of CaSR in SMA from *Sf9* cell membranes shows a higher aggregation peak, indicating aggregation of the purified CaSR. The aggregation of the CaSR was further confirmed by blue native PAGE; the protein ran at ~800 kDa which suggests the presence of a higher oligomeric state of the CaSR. We could also clearly visualize the aggregated CaSR in negatively stained electron microscopic images. The aggregation of CaSR could be seen with receptors from both expression systems, *Pichia* and insect cells, which suggested that the SMA-polymer is not suitable for CaSR purification.

As already shown in the results section (Figure 3.4), the CaSR can be solubilized by various detergents like LM, DM and SMA. For our structural studies the CaSR was solubilized in LMNG and purified using a His-trap column. The first affinity purification did not result in a pure sample as evident from the presence of many other protein bands apart from that of the CaSR protein. Purified CaSR from the His-trap column was not pure enough for functional and structural research, necessitating a second purification step. So second affinity-step was introduced in the form of an M2 -flag column after the Ni-NTA column. The purity of CaSR after the second affinity step was highly satisfactory in comparison to the single-step His-trap purification. Nearly more than half of the protein was lost during the M2-flag column purification. After size exclusion chromatography the purified CaSR protein displayed a monodisperse peak, compatible with the expectation that CaSR is in a homogeneous monomeric state. The blue-native PAGE further supported this expectation. After switching the detergent to GDN the CaSR protein remained in its monomeric state.

The detergent was exchanged from LMNG to GDN by size exclusion chromatography before using it for electron microscopy. In negative staining, a homogenous CaSR was observed, and the protein was uniformly distributed on the grid. But when applied to cryo-grids, the protein either stuck to the carbon edges or was found inside thick ice layers, thus hampering the production of optimal cryo-grids for high-resolution imaging of CaSR samples by cryo-EM.

Despite limitations by the low particle number, we were able to get a low-resolution 3D map by combining 2D classes of the CaSR. During the standardization of the freezing conditions of CaSR, two high-resolution cryo-EM structures of CaSR were published at 3.4 Å resolutions (139,140). The low-resolution map nicely agreed with the extracellular domain of CaSR, PDB number 5FBH (figure - 4. 1).

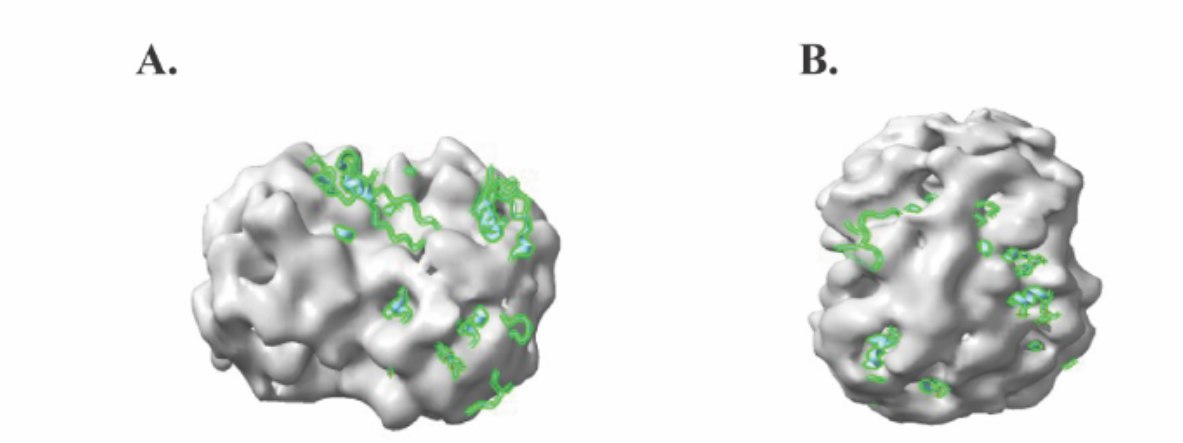

Figure 4.1: Superimposition of the extracellular domain of CaSR (green, PDB number 5FBH) with our low-resolution 3D density from cryoSPARC:

4.3 Heterologous production and purification of G-proteins:

The G-proteins are the cytosolic interacting partners of the GPCR for signal transduction inside cells. The binding of the agonist to the receptor leads to conformational changes in the intracellular loop of the GPCR which facilitate G-protein binding (54). Rhodopsin was the first GPCR which could be co-crystallized with a G-protein (141). Since then there has been a lot of progress in getting high-resolution structures of activated GPCRs with G-proteins, β-arrestin and agonists. Theses structural studies help in understanding the underlying mechanisms of activation of GPCRs and G-protein coupling. It has been observed that the various receptors of the GPCR superfamily show conserved modes of receptor activation and G-protein coupling (142,143). During the last decade, many structures of GPCRs with bound agonists, nearly 1/10th

of the total GPCR structures have been published. It is still challenging to determine the structures of receptors in activated states, due to the instability of activated GPCRs with receptor-bound G proteins.

The first G_α protein was successfully expressed and purified in *E.coli* (144). The crystal structures of human G_α proteins heterologously produced in *E.coli*, like G_i, G_s, and G_t were determined (145-147). The expression and purification of mini-G proteins might serve as a foundation for figuring out the structure of fully activated GPCRs. The mini-G proteins present in the solutions may help to provide biophysical and pharmacological information on receptors in their active state since they are potential binding partners for co-crystallization with the receptor. The usage of mini-G proteins holds a great deal of promise for accelerating the rate at which the structure of GPCRs in their activated states can be determined. The first cryo-EM structures of GPCRs with a bound mini-G_s protein, namely that of the A_{2A} receptor and β2 R were published in 2016 (148). The mini-Gs are genetically engineered and consist of the GTPase domain of G_α, the flexible C-terminal part was deleted. The mini-G protein binds to all $G_{\alpha s}$-coupled GPCRs and the structural rearrangement of the receptor during activation displays a structure resembling that of the GPCR-G_s complex.

As shown in the results section (3.2.1) the mini-G proteins (mG_s, mG_i, mG_o, mG_{qs} and mG_{si}) can be successfully expressed in *E. coli* and purified with the help of a Ni-NTA (His-trap) column. At high concentrations, all G-proteins exist in both monomeric and dimeric states. Mini-G proteins possess no membrane part so they can be purified from the soluble fraction of the bacterial cells after lysis. The purification of mini-G_q was not successful in *E. coli*, the mini-G_q precipitated during cell lysis and centrifugation. Various solubilization conditions were attempted to dissolve the mG_q precipitate with different detergents but were not successful. Different *E. coli* strains (expressing protein disulfide isomerase or chaperones which aid in

protein folding) were used for heterologous expression of mG_q in bacteria. Still, the purification of mG_q from *E. coli* was unsuccessful.

4.3.1 Heterologous production and purification of the chimeric G-protein-Maltose-binding protein (MBP) fusion protein:

One of the most important tools in structural biology is single-particle cryo-electron microscopy (cryo-EM), which can be used to determine protein structures of macromolecular complexes or large protein of sizes higher than 100 kDa. However, at this time, cryo-EM is not able to provide a precise structure determination of proteins that are smaller in size, despite significant advancements in the cryo-EM field. Most of the GPCRs are smaller in size (~50kDa). The size of the mG_α protein is ~28 kDa, the GPCR-mG complex can reach a size of ~80 kDa. The increased chimera protein GPCR-mG size, aids in getting better cryo-EM structures resolution. we designed a chimeric mG_α-MBP protein. In this construct, the mini G-protein is connected to the C-terminal MBP domain by a flexible peptide of 6 amino acids. These extra 6 amino acids after mini G-protein were added to the C-terminal region of miniG proteins to avoid any structural hindrance to GPCR-G protein coupling by the MBP protein. We added the MBP at the C-terminus instead of the N-terminus of the mG-protein because the N-terminal GTPase domain interacts with the GPCRs upon activation.

The DNAs for the constructs mG_s-MBP, mG_i-MBP, mG_si-MBP, and mG_o-MBP were cloned in the pET28a vector and heterologously expressed in the *E.coli* (Bl-21strains). These chimera proteins could be purified with a high yield. The proteins show a monodisperse peak in size exclusion chromatography except for G_{si}-MBP where size exclusion chromatography indicated the existence of monomers and dimers.

4.4 Bradykinin receptor and heterologous production and purification of B1R

Kinins are proinflammatory peptides that are responsible for various cellular processes in humans like inflammation, vasodilation, coagulation, vascular permeability, and pain. In 1970 Regoli and co-workers discovered the existence of two kinin receptors, B1 and B2, which differ by their pharmacology and their expression profiles. B1R and B2R belong to the rhodopsin family (class-A) of GPCRs. They shows ~34% identity in their protein sequence They possess seven transmembrane helices with a conserved orthosteric binding pocket. The B1 receptor is expressed at extremely low levels in healthy tissues but is induced after damage by a variety of proinflammatory cytokines, including interleukin-1beta. In contrast, the B2 receptor is ubiquitously and constitutively expressed. The peptide ligands kallidin (KRPPGFSPFR) and bradykinin are both derived from different kininogen isoforms and differ by the N-terminal additional single lysine residue of kallidin. Each peptide shows a high affinity towards the bradykinin receptors B1R and B2R. Both B1R and B2R upon binding kinin-derived peptides regulate transmembrane signaling primarily through G_q pathways and sometimes via G_i pathways.

The cDNAs of human bradykinin receptors B1R and B2R were cloned into the pOET1 vector under the control of a polyhedrin promoter. The cloned constructs were later used to prepare recombinant baculovirus as mentioned in the methods section (2.3.1). The expression level of the human bradykinin receptors was low and required extensive optimization. The bradykinin receptor (B1R and B2R) was heterologously expressed in insect cells using the baculovirus system. The cells were infected with a recombinant virus containing cDNA encoding the bradykinin receptor together with tags for the detection and purification of the receptor. The receptor showed limited stability, its purification was difficult due to its low expression level.

The B1R displayed a high DAKD binding affinity of ~30 nM, close to that in native membranes, when solubilized in 1% n-dodecyl-ß-D-maltoside (DDM) and 0.1% cholesteryl hemisuccinate (CHS). Therefore, we solubilized and purified the B1R in DDM/CHS and got a yield of 210 ug/1L cell culture. In the previous study from our lab by Joedicke et al.,2018 (120) the mechanism of subtype selectivity of the bradykinin receptors was explored. This study, it was followed up by investigating the subtype selectivity and the characterization of the cross-talk between the orthosteric binding pocket and allosteric binding pocket of the B1R. This study will help to find better drugs to act on the bradykinin receptor.

4.5 Allosteric modulation of the bradykinin receptor

As mentioned earlier, bradykinin receptors are involved in a variety of cellular functions such as inflammation, pain, and blood vessel dilation (149-154). A plethora of studies indicate that antagonists of the B2R receptor act as a potential drug to fight inflammation and chronic epilepsy (155,156). The activity of the bradykinin receptor is terminated by degradation of the peptide ligand at the pro7-phe8 amide bond by the angiotensin I converting enzyme (ACE) (157). ACE inhibitors (ACEIs) are very important therapeutic drugs and are widely used for the treatment of hypertension, congestive heart failure, and diabetic neuropathy (149,151,152,158,159). A plethora of reports emphasize that the clinical success of ACEIs is due to their multiple targets in the cell. They not only prevent angiotensin II release into the blood by blocking its conversion from angiotensin I, but also block the degradation of bradykinin leading to a higher level of active kinin.

It was found that the ACEIs directly stimulate the bradykinin receptor activity by forming an ACEI-BKR complex. It has been reported that captopril, enalaprilat, and lisinopril, thee FDA-approved and widely used clinical ACEIs, target a unique zinc-binding site at the ECL2 of B1R as positive allosteric modulators (PAMs) (129,160). They allosterically modulate B1R and B2R

activation without the action of ACE. However, it is not clear if such a modulation influences the orthosteric peptide binding site of the receptor. To determine the influence of ACEIs on the receptor-peptide complex, and to obtain a better understanding of the molecular mechanism and the structural plasticity of the bradykinin receptors and the allosteric modulators, I used the three commercially available ACEIs captopril, enalaprilat, and lisinopril.

Using these three ACEIs measured the impact of the ACEIs on the orthosteric binding pocket of both B1R and B2R receptors. Enalaprilat and lisinopril both exhibit a negative modulation of the binding affinity of the agonist DAKD. In contrast, captopril had no effect on the binding of DAKD to B**1**R. The binding of enalaprilat somehow modifies the conformation of the orthosteric binding pocket which reduces DAKD binding. The changes of the binding affinity of the antagonist DALK caused by the presence of the three ACEIs showed that captopril and lisinopril both act as positive modulators, whereas enalaprilat acts as a negative modulator. The antagonist binding increases in the presence of captopril and lisinopril whereas it drastically decreases in the presence of enalaprilat. The three ACEIs show highly different effects on the orthosteric binding pocket of the receptor for agonist and antagonist binding.

4.5.1 Zinc acts as a PAM on the bradykinin-1 receptor (B1R).

As previously shown by Ignjatovic *et al*. (160) enalaprilat interacts with the B1R though the zinc-binding site constituted by the 195HEAWH199 region of the receptor. Here, I have led my focus on the influence of Zn^{2+} on the orthosteric peptide ligand binding sites of hB1R, which can be conveniently monitored by binding of the radioactive ligand $DAKD^{hot}$ rather than directly exploring the Zn^{2+} - hB1R interactions.

In B1R, the binding affinity of its endogenous ligands increases nearly 10-20-fold in presence of zinc. This effect can also be observed in the case of antagonist binding to the B1R receptor. This observation suggests that zinc itself acts as a weakly positive (PAM. Zinc was also shown

to be a PAM in other class-A GPCRs like β2AR, GPR39, GPR68, and GPR83 (161-165). Many metal ions like Na^{+} and Ca^{2+} were shown to act as PAMs in some GPCRs. The affinity of Zn^{2+} for B1R was ~30 μM, which is higher than the concentration of zinc in the cells The Zn^{2+} binding affinities of some of the receptors were reported to be in the range of 0.2 μM (GPR68) to about 20 μM (GPR39) (161,163,166). There was no change of the affinity of DALK towards B1R. This result suggests that the conformational change of the orthosteric binding site is not specific for agonists or antagonists.

The Kd of DAKD gradually increases with the increase of Zn^{2+} concentration from 0 mM to 1 mM. The Kd of DAKD in the presence of 100 nM Zn^{2+} is around 30 nM. The strong ligand affinity may be due to the presence of other endogenous ligands or cations in the membrane extracts. The Ki of DAKD at 100 nM Zn^{2+} is closer to the Ki of purified B1R in the presence of DDM/CHS. This observation confirms that there are some other molecules that interfere with receptor binding or act as PAM.

To know if there are other cations that also act as PAMs for the B1R, the binding of DAKD to the receptor was measured in the presence of Ca^{2+}. The results show an inhibitory effect of Ca^{2+} on DAKD binding. Ca^{2+} acts as NAM on the B1R, where it shows a downward curve opposite to the effect of Zn^{2+}onditions (Figure 3.3.3). This observation is different from that with other GPCRs like GPCR-68 where Ca^{2+} and Zn^{2+} also slightly enhance ligand binding or have no effects. To see if there are any effects of Ca^{2+} or Zn^{2+} on the orthosteric binding pocket of B2R or if they are specific to hB1R, the radioligand binding with hB2R was measured. Interestingly there is no impact of Ca^{2+} and Zn^{2+} on the orthosteric binding pockets of the B2R. The affinity of the ligand bradykinin to B2R was not changed by the addition of Ca^{2+} and Zn^{2+}. This result suggests that the divalent cations lead to a distinct allosteric conformational state in class-A GPCRs, which is highly individual for the specific receptor and subtype of the receptor.

4.5.2 Zinc ions and ACEIs act together as allosteric modulators in the bradykinin-1 receptor

As mentioned earlier the ACEIs interact with the receptor at a zinc ion-binding site of the ECL2 region of the hB1R receptor. Both Zn^{2+} and ACEIs act as allosteric modulators of hB1R. Zn^{2+} primarily interacts with the hB1R at residues His195 and Glu196 in the ECL2 region of the receptor. Whenever Zn^{2+} and ACEIs were present together, ligand affinities were higher than when just one of them was present. The zinc ion binding affinity of hB1R may be further enhanced in the presence of ACEIs by forming a penta-coordinated stable complex with the receptor. This feature might further explain the shift of the Zn^{2+} affinity into a regime that is more appropriate for physiological or pathological conditions in humans. For instance, in the synaptic space and in wounded tissues, where B1R is constitutively active, the Zn^{2+} concentration might reach 10 to 30 uM (167). The hB2R shows ~35 % sequence identity with hB1R. Due to the absence of a similar Zn^{2+} binding site on hB2R, ACEIs are recruited to this site on hB1R by Zn^{2+} bound at ECL2, which is specific to hB1R.

The divalent cations exhibit distinct allosteric effects on class-A GPCRs, which are highly individual for the specific receptor and subtype. The Na^{+} binding site in class-A GPCRs, in contrast to that for divalent cations, is highly conserved. The existence of non-conserved divalent ion binding sites in receptors might allow the discovery of allosteric compounds binding to these sites, which are specific modulators for receptors and can be subtype-selective.

The three different ACEIs show a distinct allosteric effect on the orthosteric binding site of the hB1R. These findings suggest, that the three representative ACEIs have different patterns of action on the allosteric modulation of the hB1R, which probably depends on their different modes of binding to the Zn^{2+} site on the ECL2 region of the receptor. In our research, we observed that lisinopril inhibits endogenous ligand binding by functioning as NAM, while enalaprilat and captopril increase the ligand binding affinity of the endogenous ligand and act as PAM.

One common side effect of persistent dry cough linked to kinin receptor activation is a, which is clinically detected in patients. Our in vitro results are consistent with the clinical observations that the incidence of dry cough is higher in the enalaprilat and captopril patient groups compared to the lisinopril group (168).

4.7: Allosteric modulators induce distinct orthosteric-peptide conformations in hB1R

Previously the dynamic nuclear polarization of solid-state NMR (DNP-ssNMR) technique was successfully used to identify the mechanisms behind the subtype specificity of the human bradykinin receptors (BKR). The sample preparation method was modified in order to be able to study the allosteric regulation of GPCRs using the DNP-ssNMR method. Usage of the DNP ssNMR technique helped to overcome the detection sensitivity issues in ssNMR, by enhancing the detection limit by approximately 100fold. To enhance the NMR signal unpaired electrons were used in the form of stable radicals and added to the sample as a polarisation source. Recently developed DNP-enhanced ssNMR with magic angle sample spinning (MAS) emerged as the most important tool in understanding membrane protein structure. Enhancement of the NMR signals enabled us to solve the problem faced previously due to small spin numbers. A better understanding of the trapped intermediate states of receptor-ligand complexes (169-171), subtype selectivity, and ligand-protein interaction on mammalian transporter complexes (170,172) became possible, or direct studies of the receptor in its cellular context (111,173) were enabled. The isotopically labeled agonist peptide (DAKD) was used as the NMR reporter to probe the structural perturbation in the orthosteric binding site of B1R-DAKD complex upon bindings with 3 different allosteric modulators (ACEIs).

The ACEI and Zn^{2+} binding site on ECL2 is rather close to the C-terminal residues of DAKD. The structurally different ACEIs may lead to distinct allosteric modulations of the orthosteric binding pocket of the hB1R receptor. The isotopic labels of DAKD at the C-terminal region of the peptide were used to map the conformational changes of the C-terminal residues of bound

DAKD in response to different ACEIs. The DAKD conformation may be highly sensitive to its receptor environment and so act as a direct reporter of any potential structural alterations to its binding pocket because of the structural complementarity of the peptide and the binding pocket in hB1R. The isotopically labeled peptide at Pro8 and Phe-9 was used for our DNP-ssNMR experiments. The NMR spectra obtained of the three ACEIs show a totally distinct chemical shift of Phe9 suggesting the possibility of three distinct conformational states of the peptide in the presence of the three ACEIs. We compare the spectra of the ^{15}N of Phe9 of DAKD with the Leu9 of the DALK in the earlier study from our lab (120), we find a chemical shift of ^{15}N (Phe9) of the agonist down-field compared to ^{15}N of Leu-9 antagonist, which suggests an increased affinity of DAKD to the hB1R. In the presence of Zn^{2+} and ACEI (captopril and enalaprilat) (PAM of hB1R), the Phe9 N-Cα signal of DAKD in a complex with hB1R moves further towards the down-field direction. This trend aligns well with the enhancing effect of an allosteric agonist by captopril and enalaprilat. In contrast to the drug lisinopril, the downfield chemical shift of Phe9 N-Cα is negligible compared to enalaprilat and captopril. This observation indicates that lisinopril acts as NAM whereas both enalaprilat and captopril act as PAMs.

4.8 Mechanism of allosteric regulation in the bradykinin-1 receptor

By combining our previous knowledge about the subtype selectivity, and the cryo-EM structure of the B1R we can conclude that the residues of the R202$^{5.38}$ and Y266 $^{6.51}$ regions of the hB1R are responsible for the subtype selectivity (1,120). The previous study from our lab suggested that the hydrogen bond between R202$^{5.38}$ and Y266$^{6.51}$ prevents the binding of bradykinin to the B1R (120). Furthermore, the two positively charged pockets at hB1R residues near K118$^{3.3}$ and R202$^{5.38}$ interact with the carboxylic group of phe9 of DAKD. The activation mechanisms of B1R and B2R are conserved, the phe9 of both endogenous ligands DAKD and bradykinin upon binding to the orthosteric binding site leads to a rotameric switch at W263$^{6.48}$. This rotameric

switch of W263$^{6.48}$ further facilitates the toggle switch of residues at F/Y, leading to a rotation of TM6. This interaction between W263$^{6.48}$ and F/Y $^{7.43}$ leads to the activation of the microswitches DRY and NPxxY causing the binding of the G-protein. The mechanisms of activation of hB1R and hB2R are similar as in the case of the angiotensin receptor (AT1R), suggesting also a conserved coupling of Gq leading **to** GPCR activity.

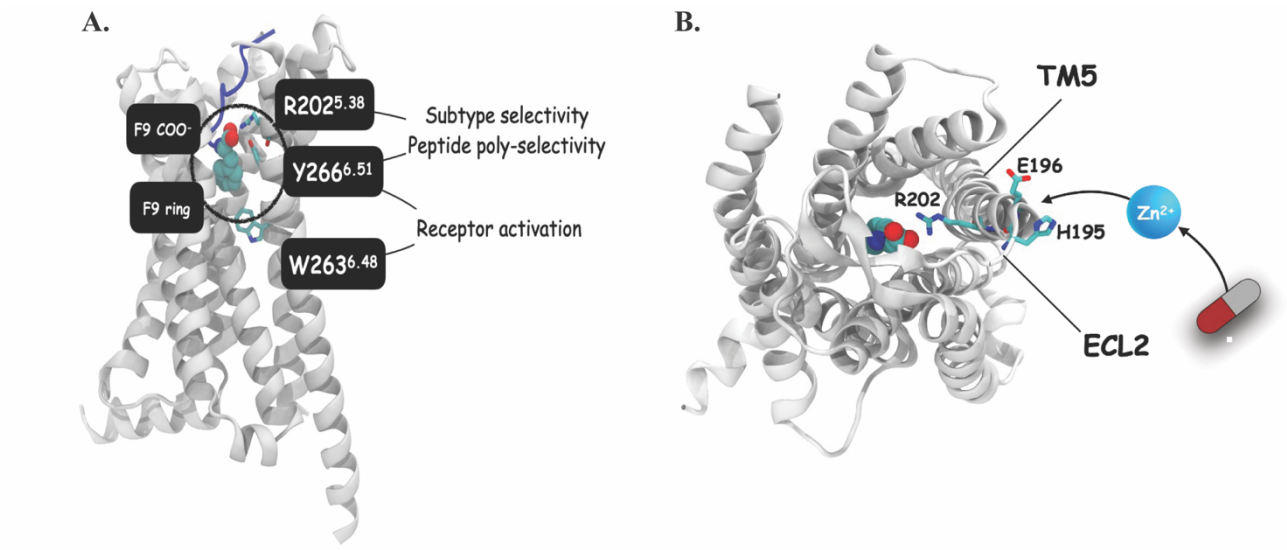

Figures 4.2: Mechanism of ACEI and Zn^{2+} interaction with hB1R: A) Schematic representation of the residues responsible for the activation of B1R and their interaction with ligands. B) Top view of the B1R, depicting the interaction of zinc ions and ACEI at the H195 and E196 position of the ECL2 region of the receptor.

The combination of the results of our biochemical, NMR, and computational studies of hB1R in the presence of allosteric modulators (ACEI and Zn^{2+}) suggests that the strategic sites of the receptor are targeted. The binding of Zn^{2+} and the three ACEIs to B1R at the H195 and E196 positions causes a rotation of TM5, which leads to a conformational change at the R202$^{5.38}$ position. The three different ACEIs differently affect R202$^{5.38}$ leading to a distinct conformational change of the receptor. In Zn^{2+}, enalaprilat, and captopril act as PAM leading to a drastic increase of the affinity of B1R to DAKD.

4.10 Impact of ACEIs on downstream GPCR signaling pathways:

The human bradykinin receptors B1R and B2R are members of the rhodopsin (class-A) family of GPCRs. Both subtypes of the human bradykinin receptors get activated by peptides kallidin and bradykinin. hB1R and hB2R both interact with G_q and G_i, but primarily signal through Gq pathways. The structures of both B1R and B2R coupled with Gq were published last year (**(1)**).

Pre-coupling of GPCRs with Gα- subunits is a common phenomenon of the rhodopsin (Class-A) family of receptors. ACEIs allosterically modulate the hB1R affinity towards the endogenous ligand DAKD. To evaluate the impact of ACEIs on the downstream signaling of the bradykinin receptor upon activation, competition binding assays were conducted in presence of G-proteins. The irreversible binding of the endogenous ligands to hB1R makes it difficult to use competition binding assays to analyze downstream signals. Therefore, we decided to use hB2R instead of hB1R for understanding downstream signaling. The affinity of endogenous ligands decreases in the presence of mG_I, which suggests a signaling bias towards G_q pathways rather than G_i pathways. Activation of G_q leads to the activation of phospholipase C. Similar phenomena were also observed in other class-A GPCRs like NKR and A2AR.

As mentioned earlier in the results section (3.3.5) the affinity of the endogenous ligand bradykinin to hB2R is not altered in the presence of the ACEIs enalaprilat, and captopril. But interestingly addition enhances the affinity drastically. Enalaprilat and captopril show different affinity but both enhance ligand binding. This observation suggests that ACEI binding leads to a conformational change in the intracellular part of the receptor which eventually leads to the binding of G_I rather than G_q. ACEI binding to B2R allosterically modulates G-protein coupling.

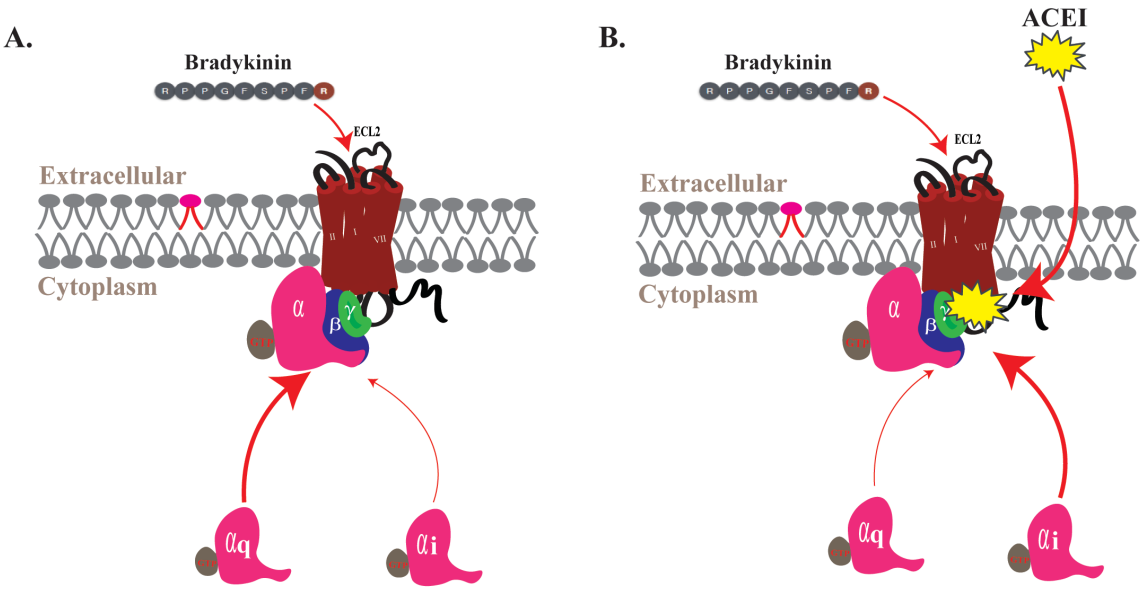

Figures 4.3: Schematic representation of B2R signaling and its preferences: A) The binding of the ligand bradykinin to B2R primarily signals through the G_q pathways instead of G_i pathways. B) In presence of ACEIs the signaling shifts to the G_i-pathways.

Conclusions and Future perspectives

GPCRs are the most important drug targets due to their involvement in various crucial cellular physiological pathways. There are still many GPCRs that are underexplored and their functions are unknown. It is crucial to study the functional and structural properties of GPCRs which is a prerequisite for developing and designing new therapeutic compounds acting on them.

During this thesis work, a successful production and purification strategy for the calcium-sensing receptor (CaSR) was established in both *Pichia pastoris* and insect cells (*Sf9*). The protein purification was standardized for single-particle cryo-EM studies. Further standardization of the CaSR sample is required for getting a high-resolution cryo-EM structure of the receptor. The mini-G proteins and chimera (mG-MBP) proteins were successfully heterologously produced and purified in *E. coli*. These purified mini-G proteins can be further used for co-purification with GPCRs for co-crystallization and cryo-EM studies.

The successful production and purification of the bradykinin 1 and 2 receptors were established in insect cells (*Sf9*). Combining ssNMR and molecular dynamic simulations allowed a better understanding of the ligand-receptor interaction of hB1R. Our findings provide molecular insights into the allosteric modulation of the bradykinin receptors. This study together with the effects of ACEIs on the binding sites of B1R also deciphers the effects of the Zn^{2+} as well as the crosstalk between Zinc ion binding sites and ACEIs on the binding pocket of hB1R. Allosteric binding induces distinct changes of the binding of the endogenous ligands, which might aid in creating new possibilities in the pharmaceutical field. It will be of great interest to determine the structure of ligand-B1R-ACEI complexes by cryo-EM to get a better understanding of the distinct structure of hB1R in presence of ACEIs.

References

1. Yin, Y. L., Ye, C., Zhou, F., Wang, J., Yang, D., Yin, W., Wang, M. W., Xu, H. E., and Jiang, Y. (2021) Molecular basis for kinin selectivity and activation of the human bradykinin receptors. *Nat Struct Mol Biol* **28**, 755-761
2. Mitalipov, S., and Wolf, D. (2009) Totipotency, pluripotency and nuclear reprogramming. *Adv Biochem Eng Biotechnol* **114**, 185-199
3. Singer, S. J., and Nicolson, G. L. (1972) The fluid mosaic model of the structure of cell membranes. *Science* **175**, 720-731
4. Lingwood, D., and Simons, K. (2010) Lipid rafts as a membrane-organizing principle. *Science* **327**, 46-50
5. Pike, L. J. (2009) The challenge of lipid rafts. *J Lipid Res* **50 Suppl**, S323-328
6. Korade, Z., and Kenworthy, A. K. (2008) Lipid rafts, cholesterol, and the brain. *Neuropharmacology* **55**, 1265-1273
7. van Meer, G., Voelker, D. R., and Feigenson, G. W. (2008) Membrane lipids: where they are and how they behave. *Nat Rev Mol Cell Biol* **9**, 112-124
8. Tsirigos, K. D., Peters, C., Shu, N., Käll, L., and Elofsson, A. (2015) The TOPCONS web server for consensus prediction of membrane protein topology and signal peptides. *Nucleic Acids Res* **43**, W401-407
9. Uhlén, M., Fagerberg, L., Hallström, B. M., Lindskog, C., Oksvold, P., Mardinoglu, A., Sivertsson, Å., Kampf, C., Sjöstedt, E., Asplund, A., Olsson, I., Edlund, K., Lundberg, E., Navani, S., Szigyarto, C. A., Odeberg, J., Djureinovic, D., Takanen, J. O., Hober, S., Alm, T., Edqvist, P. H., Berling, H., Tegel, H., Mulder, J., Rockberg, J., Nilsson, P., Schwenk, J. M., Hamsten, M., von Feilitzen, K., Forsberg, M., Persson, L., Johansson, F., Zwahlen, M., von Heijne, G., Nielsen, J., and Pontén, F. (2015) Proteomics. Tissue-based map of the human proteome. *Science* **347**, 1260419
10. Moraes, I., and Quigley, A. (2021) Structural Biology and Structure-Function Relationships of Membrane Proteins. *Biology (Basel)* **10**
11. Cournia, Z., Allen, T. W., Andricioaei, I., Antonny, B., Baum, D., Brannigan, G., Buchete, N. V., Deckman, J. T., Delemotte, L., Del Val, C., Friedman, R., Gkeka, P., Hege, H. C., Hénin, J., Kasimova, M. A., Kolocouris, A., Klein, M. L., Khalid, S., Lemieux, M. J., Lindow, N., Roy, M., Selent, J., Tarek, M., Tofoleanu, F., Vanni, S., Urban, S., Wales, D. J., Smith, J. C., and Bondar, A. N. (2015) Membrane Protein Structure, Function, and Dynamics: a Perspective from Experiments and Theory. *J Membr Biol* **248**, 611-640
12. Overington, J. P., Al-Lazikani, B., and Hopkins, A. L. (2006) How many drug targets are there? *Nat Rev Drug Discov* **5**, 993-996
13. Yin, H., and Flynn, A. D. (2016) Drugging Membrane Protein Interactions. *Annu Rev Biomed Eng* **18**, 51-76
14. Deisenhofer, J., Epp, O., Miki, K., Huber, R., and Michel, H. (1985) Structure of the protein subunits in the photosynthetic reaction centre of Rhodopseudomonas viridis at 3Å resolution. *Nature* **318**, 618-624
15. Boyer, M., and Wisniewski-Dyé, F. (2009) Cell-cell signalling in bacteria: not simply a matter of quorum. *FEMS Microbiol Ecol* **70**, 1-19

16. Cuatrecasas, P. (1974) Membrane receptors. *Annu Rev Biochem* **43**, 169-214
17. Ortells, M. O., and Lunt, G. G. (1995) Evolutionary history of the ligand-gated ion-channel superfamily of receptors. *Trends Neurosci* **18**, 121-127
18. Kobilka, B. K. (2007) G protein coupled receptor structure and activation. *Biochim Biophys Acta* **1768**, 794-807
19. Gether, U., and Kobilka, B. K. (1998) G protein-coupled receptors. II. Mechanism of agonist activation. *J Biol Chem* **273**, 17979-17982
20. Mogensen, K. E., Lewerenz, M., Reboul, J., Lutfalla, G., and Uzé, G. (1999) The type I interferon receptor: structure, function, and evolution of a family business. *J Interferon Cytokine Res* **19**, 1069-1098
21. Pawson, T. (2002) Regulation and targets of receptor tyrosine kinases. *Eur J Cancer* **38 Suppl 5**, S3-10
22. Mangelsdorf, D. J., Thummel, C., Beato, M., Herrlich, P., Schütz, G., Umesono, K., Blumberg, B., Kastner, P., Mark, M., Chambon, P., and Evans, R. M. (1995) The nuclear receptor superfamily: the second decade. *Cell* **83**, 835-839
23. Novac, N., and Heinzel, T. (2004) Nuclear receptors: overview and classification. *Curr Drug Targets Inflamm Allergy* **3**, 335-346
24. Olefsky, J. M. (2001) Nuclear receptor minireview series. *J Biol Chem* **276**, 36863-36864
25. Evans, R. M. (1988) The steroid and thyroid hormone receptor superfamily. *Science* **240**, 889-895
26. Ji, T. H., Grossmann, M., and Ji, I. (1998) G protein-coupled receptors. I. Diversity of receptor-ligand interactions. *J Biol Chem* **273**, 17299-17302
27. Bourne, H. R., Sanders, D. A., and McCormick, F. (1990) The GTPase superfamily: a conserved switch for diverse cell functions. *Nature* **348**, 125-132
28. Takeda, S., Kadowaki, S., Haga, T., Takaesu, H., and Mitaku, S. (2002) Identification of G protein-coupled receptor genes from the human genome sequence. *FEBS Lett* **520**, 97-101
29. Fredriksson, R., and Schiöth, H. B. (2005) The repertoire of G-protein-coupled receptors in fully sequenced genomes. *Mol Pharmacol* **67**, 1414-1425
30. Hauser, A. S., Chavali, S., Masuho, I., Jahn, L. J., Martemyanov, K. A., Gloriam, D. E., and Babu, M. M. (2018) Pharmacogenomics of GPCR Drug Targets. *Cell* **172**, 41-54.e19
31. Attwood, T. K., and Findlay, J. B. (1994) Fingerprinting G-protein-coupled receptors. *Protein Eng* **7**, 195-203
32. Kolakowski, L. F., Jr. (1994) GCRDb: a G-protein-coupled receptor database. *Recept Channels* **2**, 1-7
33. Foord, S. M., Bonner, T. I., Neubig, R. R., Rosser, E. M., Pin, J. P., Davenport, A. P., Spedding, M., and Harmar, A. J. (2005) International Union of Pharmacology. XLVI. G protein-coupled receptor list. *Pharmacol Rev* **57**, 279-288
34. Joost, P., and Methner, A. (2002) Phylogenetic analysis of 277 human G-protein-coupled receptors as a tool for the prediction of orphan receptor ligands. *Genome Biol* **3**, Research0063

35. Miggin, S. M., Lawler, O. A., and Kinsella, B. T. (2016) Palmitoylation of the human prostacyclin receptor. FUNCTIONAL IMPLICATIONS OF PALMITOYLATION AND ISOPRENYLATION. *J Biol Chem* **291**, 19259
36. Escribá, P. V., Wedegaertner, P. B., Goñi, F. M., and Vögler, O. (2007) Lipid-protein interactions in GPCR-associated signaling. *Biochim Biophys Acta* **1768**, 836-852
37. Ponimaskin, E., Dumuis, A., Gaven, F., Barthet, G., Heine, M., Glebov, K., Richter, D. W., and Oppermann, M. (2005) Palmitoylation of the 5-hydroxytryptamine4a receptor regulates receptor phosphorylation, desensitization, and beta-arrestin-mediated endocytosis. *Mol Pharmacol* **67**, 1434-1443
38. Charest, P. G., and Bouvier, M. (2003) Palmitoylation of the V2 vasopressin receptor carboxyl tail enhances beta-arrestin recruitment leading to efficient receptor endocytosis and ERK1/2 activation. *J Biol Chem* **278**, 41541-41551
39. Lohse, M. J., Benovic, J. L., Codina, J., Caron, M. G., and Lefkowitz, R. J. (1990) beta-Arrestin: a protein that regulates beta-adrenergic receptor function. *Science* **248**, 1547-1550
40. Luttrell, L. M., and Lefkowitz, R. J. (2002) The role of beta-arrestins in the termination and transduction of G-protein-coupled receptor signals. *J Cell Sci* **115**, 455-465
41. Harmar, A. J. (2001) Family-B G-protein-coupled receptors. *Genome Biol* **2**, Reviews3013
42. Ohashi, H., Maruyama, T., Higashi-Matsumoto, H., Nomoto, T., Nishimura, S., and Takeuchi, Y. (2002) A novel binding assay for metabotropic glutamate receptors using [3H] L-quisqualic acid and recombinant receptors. *Z Naturforsch C J Biosci* **57**, 348-355
43. Bardwell, L. (2005) A walk-through of the yeast mating pheromone response pathway. *Peptides* **26**, 339-350
44. Nakayama, N., Miyajima, A., and Arai, K. (1985) Nucleotide sequences of STE2 and STE3, cell type-specific sterile genes from Saccharomyces cerevisiae. *Embo j* **4**, 2643-2648
45. Burkholder, A. C., and Hartwell, L. H. (1985) The yeast alpha-factor receptor: structural properties deduced from the sequence of the STE2 gene. *Nucleic Acids Res* **13**, 8463-8475
46. Marsh, L., and Herskowitz, I. (1988) STE2 protein of Saccharomyces kluyveri is a member of the rhodopsin/beta-adrenergic receptor family and is responsible for recognition of the peptide ligand alpha factor. *Proc Natl Acad Sci U S A* **85**, 3855-3859
47. Swaney, K. F., Huang, C. H., and Devreotes, P. N. (2010) Eukaryotic chemotaxis: a network of signaling pathways controls motility, directional sensing, and polarity. *Annu Rev Biophys* **39**, 265-289
48. Othmer, H. G., and Schaap, P. (1998) Oscillatory cAMP signaling in the development of Dictyostelium discoideum. *Comments on Theoretical Biology* **5**, 175-282
49. Malbon, C. C. (2004) Frizzleds: new members of the superfamily of G-protein-coupled receptors. *Front Biosci* **9**, 1048-1058
50. Taipale, J., Chen, J. K., Cooper, M. K., Wang, B., Mann, R. K., Milenkovic, L., Scott, M. P., and Beachy, P. A. (2000) Effects of oncogenic mutations in Smoothened and Patched can be reversed by cyclopamine. *Nature* **406**, 1005-1009

51. Fredriksson, R., Lagerström, M. C., Lundin, L. G., and Schiöth, H. B. (2003) The G-protein-coupled receptors in the human genome form five main families. Phylogenetic analysis, paralogon groups, and fingerprints. *Mol Pharmacol* **63**, 1256-1272
52. Civelli, O., Reinscheid, R. K., Zhang, Y., Wang, Z., Fredriksson, R., and Schiöth, H. B. (2013) G protein-coupled receptor deorphanizations. *Annu Rev Pharmacol Toxicol* **53**, 127-146
53. Kobilka, B., and Schertler, G. F. (2008) New G-protein-coupled receptor crystal structures: insights and limitations. *Trends Pharmacol Sci* **29**, 79-83
54. Rosenbaum, D. M., Rasmussen, S. G., and Kobilka, B. K. (2009) The structure and function of G-protein-coupled receptors. *Nature* **459**, 356-363
55. Manglik, A., Kruse, A. C., Kobilka, T. S., Thian, F. S., Mathiesen, J. M., Sunahara, R. K., Pardo, L., Weis, W. I., Kobilka, B. K., and Granier, S. (2012) Crystal structure of the μ-opioid receptor bound to a morphinan antagonist. *Nature* **485**, 321-326
56. Barak, L. S., Tiberi, M., Freedman, N. J., Kwatra, M. M., Lefkowitz, R. J., and Caron, M. G. (1994) A highly conserved tyrosine residue in G protein-coupled receptors is required for agonist-mediated beta 2-adrenergic receptor sequestration. *J Biol Chem* **269**, 2790-2795
57. Vogel, R., Mahalingam, M., Lüdeke, S., Huber, T., Siebert, F., and Sakmar, T. P. (2008) Functional role of the "ionic lock"--an interhelical hydrogen-bond network in family A heptahelical receptors. *J Mol Biol* **380**, 648-655
58. Cook, J. V., and Eidne, K. A. (1997) An intramolecular disulfide bond between conserved extracellular cysteines in the gonadotropin-releasing hormone receptor is essential for binding and activation. *Endocrinology* **138**, 2800-2806
59. Zhang, D., Zhao, Q., and Wu, B. (2015) Structural Studies of G Protein-Coupled Receptors. *Mol Cells* **38**, 836-842
60. Gilman, A. G. (1995) Nobel Lecture. G proteins and regulation of adenylyl cyclase. *Biosci Rep* **15**, 65-97
61. Wall, M. A., Coleman, D. E., Lee, E., Iñiguez-Lluhi, J. A., Posner, B. A., Gilman, A. G., and Sprang, S. R. (1995) The structure of the G protein heterotrimer Gi alpha 1 beta 1 gamma 2. *Cell* **83**, 1047-1058
62. Hepler, J. R., and Gilman, A. G. (1992) G proteins. *Trends Biochem Sci* **17**, 383-387
63. Taussig, R., Iñiguez-Lluhi, J. A., and Gilman, A. G. (1993) Inhibition of adenylyl cyclase by Gi alpha. *Science* **261**, 218-221
64. Jho, E. H., Davis, R. J., and Malbon, C. C. (1997) c-Jun amino-terminal kinase is regulated by Galpha12/Galpha13 and obligate for differentiation of P19 embryonal carcinoma cells by retinoic acid. *J Biol Chem* **272**, 24468-24474
65. Garcia-Higuera, I., Gaitatzes, C., Smith, T. F., and Neer, E. J. (1998) Folding a WD repeat propeller. Role of highly conserved aspartic acid residues in the G protein beta subunit and Sec13. *J Biol Chem* **273**, 9041-9049
66. Backlund, P. S., Jr., and Aksamit, R. R. (1988) Guanine nucleotide-dependent carboxyl methylation of mammalian membrane proteins. *J Biol Chem* **263**, 15864-15867
67. Tsunoda, S., Sierralta, J., Sun, Y., Bodner, R., Suzuki, E., Becker, A., Socolich, M., and Zuker, C. S. (1997) A multivalent PDZ-domain protein assembles signalling complexes in a G-protein-coupled cascade. *Nature* **388**, 243-249

68. Nobles, M., Benians, A., and Tinker, A. (2005) Heterotrimeric G proteins precouple with G protein-coupled receptors in living cells. *Proc Natl Acad Sci U S A* **102**, 18706-18711
69. Lefkowitz, R. J., and Shenoy, S. K. (2005) Transduction of receptor signals by beta-arrestins. *Science* **308**, 512-517
70. Wilden, U., Hall, S. W., and Kühn, H. (1986) Phosphodiesterase activation by photoexcited rhodopsin is quenched when rhodopsin is phosphorylated and binds the intrinsic 48-kDa protein of rod outer segments. *Proc Natl Acad Sci U S A* **83**, 1174-1178
71. Kim, K. M., Valenzano, K. J., Robinson, S. R., Yao, W. D., Barak, L. S., and Caron, M. G. (2001) Differential regulation of the dopamine D2 and D3 receptors by G protein-coupled receptor kinases and beta-arrestins. *J Biol Chem* **276**, 37409-37414
72. Trester-Zedlitz, M., Burlingame, A., Kobilka, B., and von Zastrow, M. (2005) Mass spectrometric analysis of agonist effects on posttranslational modifications of the beta-2 adrenoceptor in mammalian cells. *Biochemistry* **44**, 6133-6143
73. Bouvier, M., Hausdorff, W. P., De Blasi, A., O'Dowd, B. F., Kobilka, B. K., Caron, M. G., and Lefkowitz, R. J. (1988) Removal of phosphorylation sites from the beta 2-adrenergic receptor delays onset of agonist-promoted desensitization. *Nature* **333**, 370-373
74. Palczewski, K., Buczyłko, J., Kaplan, M. W., Polans, A. S., and Crabb, J. W. (1991) Mechanism of rhodopsin kinase activation. *J Biol Chem* **266**, 12949-12955
75. Zhou, X. E., He, Y., de Waal, P. W., Gao, X., Kang, Y., Van Eps, N., Yin, Y., Pal, K., Goswami, D., White, T. A., Barty, A., Latorraca, N. R., Chapman, H. N., Hubbell, W. L., Dror, R. O., Stevens, R. C., Cherezov, V., Gurevich, V. V., Griffin, P. R., Ernst, O. P., Melcher, K., and Xu, H. E. (2017) Identification of Phosphorylation Codes for Arrestin Recruitment by G Protein-Coupled Receptors. *Cell* **170**, 457-469.e413
76. Palczewski, K., McDowell, J. H., Jakes, S., Ingebritsen, T. S., and Hargrave, P. A. (1989) Regulation of rhodopsin dephosphorylation by arrestin. *J Biol Chem* **264**, 15770-15773
77. Laporte, S. A., Oakley, R. H., Zhang, J., Holt, J. A., Ferguson, S. S., Caron, M. G., and Barak, L. S. (1999) The beta2-adrenergic receptor/betaarrestin complex recruits the clathrin adaptor AP-2 during endocytosis. *Proc Natl Acad Sci U S A* **96**, 3712-3717
78. Hinkle, P. M., Gehret, A. U., and Jones, B. W. (2012) Desensitization, trafficking, and resensitization of the pituitary thyrotropin-releasing hormone receptor. *Front Neurosci* **6**, 180
79. Shenoy, S. K., and Lefkowitz, R. J. (2003) Multifaceted roles of beta-arrestins in the regulation of seven-membrane-spanning receptor trafficking and signalling. *Biochem J* **375**, 503-515
80. Song, X., Coffa, S., Fu, H., and Gurevich, V. V. (2009) How does arrestin assemble MAPKs into a signaling complex? *J Biol Chem* **284**, 685-695
81. Vishnivetskiy, S. A., Hosey, M. M., Benovic, J. L., and Gurevich, V. V. (2004) Mapping the arrestin-receptor interface. Structural elements responsible for receptor specificity of arrestin proteins. *J Biol Chem* **279**, 1262-1268
82. Weis, W. I., and Kobilka, B. K. (2018) The Molecular Basis of G Protein-Coupled Receptor Activation. *Annu Rev Biochem* **87**, 897-919

83. Neubig, R. R., Spedding, M., Kenakin, T., and Christopoulos, A. (2003) International Union of Pharmacology Committee on Receptor Nomenclature and Drug Classification. XXXVIII. Update on terms and symbols in quantitative pharmacology. *Pharmacol Rev* **55**, 597-606
84. Christopoulos, A. (2014) Advances in G protein-coupled receptor allostery: from function to structure. *Mol Pharmacol* **86**, 463-478
85. Khajehali, E., Valant, C., Jörg, M., Tobin, A. B., Conn, P. J., Lindsley, C. W., Sexton, P. M., Scammells, P. J., and Christopoulos, A. (2018) Probing the binding site of novel selective positive allosteric modulators at the M(1) muscarinic acetylcholine receptor. *Biochem Pharmacol* **154**, 243-254
86. Croy, C. H., Schober, D. A., Xiao, H., Quets, A., Christopoulos, A., and Felder, C. C. (2014) Characterization of the novel positive allosteric modulator, LY2119620, at the muscarinic M(2) and M(4) receptors. *Mol Pharmacol* **86**, 106-115
87. Talbodec, A., Berkane, N., Blandin, V., Breittmayer, J. P., Ferrari, E., Frelin, C., and Vigne, P. (2000) Aspirin and sodium salicylate inhibit endothelin ETA receptors by an allosteric type of mechanism. *Mol Pharmacol* **57**, 797-804
88. Gao, Z. G., and Jacobson, K. A. (2013) Allosteric modulation and functional selectivity of G protein-coupled receptors. *Drug Discov Today Technol* **10**, e237-243
89. Lu, S., He, X., Ni, D., and Zhang, J. (2019) Allosteric Modulator Discovery: From Serendipity to Structure-Based Design. *J Med Chem* **62**, 6405-6421
90. Duan, W., Gui, L., Zhou, Z., Liu, Y., Tian, H., Chen, J. F., and Zheng, J. (2009) Adenosine A2A receptor deficiency exacerbates white matter lesions and cognitive deficits induced by chronic cerebral hypoperfusion in mice. *J Neurol Sci* **285**, 39-45
91. Chen, J. F., Sonsalla, P. K., Pedata, F., Melani, A., Domenici, M. R., Popoli, P., Geiger, J., Lopes, L. V., and de Mendonça, A. (2007) Adenosine A2A receptors and brain injury: broad spectrum of neuroprotection, multifaceted actions and "fine tuning" modulation. *Prog Neurobiol* **83**, 310-331
92. Kawakami, N., Miyoshi, K., Horio, S., and Fukui, H. (2004) Beta(2)-adrenergic receptor-mediated histamine H(1) receptor down-regulation: another possible advantage of beta(2) agonists in asthmatic therapy. *J Pharmacol Sci* **94**, 449-458
93. Drake, M. T., Shenoy, S. K., and Lefkowitz, R. J. (2006) Trafficking of G protein-coupled receptors. *Circ Res* **99**, 570-582
94. Insel, P. A., Tang, C. M., Hahntow, I., and Michel, M. C. (2007) Impact of GPCRs in clinical medicine: monogenic diseases, genetic variants and drug targets. *Biochim Biophys Acta* **1768**, 994-1005
95. Li, S., Huang, S., and Peng, S. B. (2005) Overexpression of G protein-coupled receptors in cancer cells: involvement in tumor progression. *Int J Oncol* **27**, 1329-1339
96. Vischer, H. F., Hulshof, J. W., de Esch, I. J., Smit, M. J., and Leurs, R. (2006) Virus-encoded G-protein-coupled receptors: constitutively active (dys)regulators of cell function and their potential as drug target. *Ernst Schering Found Symp Proc*, 187-209
97. Kirshner, J. R., Staskus, K., Haase, A., Lagunoff, M., and Ganem, D. (1999) Expression of the open reading frame 74 (G-protein-coupled receptor) gene of Kaposi's sarcoma (KS)-associated herpesvirus: implications for KS pathogenesis. *J Virol* **73**, 6006-6014

98. Montaner, S., Sodhi, A., Ramsdell, A. K., Martin, D., Hu, J., Sawai, E. T., and Gutkind, J. S. (2006) The Kaposi's sarcoma-associated herpesvirus G protein-coupled receptor as a therapeutic target for the treatment of Kaposi's sarcoma. *Cancer Res* **66**, 168-174
99. Ma, P., and Zemmel, R. (2002) Value of novelty? *Nat Rev Drug Discov* **1**, 571-572
100. Drews, J. (2000) Drug discovery: a historical perspective. *Science* **287**, 1960-1964
101. Vassilatis, D. K., Hohmann, J. G., Zeng, H., Li, F., Ranchalis, J. E., Mortrud, M. T., Brown, A., Rodriguez, S. S., Weller, J. R., Wright, A. C., Bergmann, J. E., and Gaitanaris, G. A. (2003) The G protein-coupled receptor repertoires of human and mouse. *Proc Natl Acad Sci U S A* **100**, 4903-4908
102. Williamson, M. P., Havel, T. F., and Wüthrich, K. (1985) Solution conformation of proteinase inhibitor IIA from bull seminal plasma by 1H nuclear magnetic resonance and distance geometry. *J Mol Biol* **182**, 295-315
103. Bolognesi, M., Gatti, G., Menagatti, E., Guarneri, M., Marquart, M., Papamokos, E., and Huber, R. (1982) Three-dimensional structure of the complex between pancreatic secretory trypsin inhibitor (Kazal type) and trypsinogen at 1.8 A resolution. Structure solution, crystallographic refinement and preliminary structural interpretation. *J Mol Biol* **162**, 839-868
104. Kline, A. D., Braun, W., and Wüthrich, K. (1988) Determination of the complete three-dimensional structure of the alpha-amylase inhibitor tendamistat in aqueous solution by nuclear magnetic resonance and distance geometry. *J Mol Biol* **204**, 675-724
105. Nakane, T., Kotecha, A., Sente, A., McMullan, G., Masiulis, S., Brown, P., Grigoras, I. T., Malinauskaite, L., Malinauskas, T., Miehling, J., Uchański, T., Yu, L., Karia, D., Pechnikova, E. V., de Jong, E., Keizer, J., Bischoff, M., McCormack, J., Tiemeijer, P., Hardwick, S. W., Chirgadze, D. Y., Murshudov, G., Aricescu, A. R., and Scheres, S. H. W. (2020) Single-particle cryo-EM at atomic resolution. *Nature* **587**, 152-156
106. Yip, K. M., Fischer, N., Paknia, E., Chari, A., and Stark, H. (2020) Atomic-resolution protein structure determination by cryo-EM. *Nature* **587**, 157-161
107. Cheng, Y. (2018) Membrane protein structural biology in the era of single particle cryo-EM. *Curr Opin Struct Biol* **52**, 58-63
108. Cheng, Y., Grigorieff, N., Penczek, P. A., and Walz, T. (2015) A primer to single-particle cryo-electron microscopy. *Cell* **161**, 438-449
109. Nwanochie, E., and Uversky, V. N. (2019) Structure Determination by Single-Particle Cryo-Electron Microscopy: Only the Sky (and Intrinsic Disorder) is the Limit. *Int J Mol Sci* **20**
110. Duer, M. J., Friscić, T., Murray, R. C., Reid, D. G., and Wise, E. R. (2009) The mineral phase of calcified cartilage: its molecular structure and interface with the organic matrix. *Biophys J* **96**, 3372-3378
111. Jacso, T., Franks, W. T., Rose, H., Fink, U., Broecker, J., Keller, S., Oschkinat, H., and Reif, B. (2012) Characterization of membrane proteins in isolated native cellular membranes by dynamic nuclear polarization solid-state NMR spectroscopy without purification and reconstitution. *Angewandte Chemie (International ed. in English)* **51**, 432-435
112. Schmidt-Rohr, K., Kulik, A. S., Beckham, H. W., Ohlemacher, A., Pawelzik, U., Boeffel, C., and Spiess, H. W. (1994) Molecular Nature of the .beta. Relaxation in

Poly(methyl methacrylate) Investigated by Multidimensional NMR. *Macromolecules* **27**, 4733-4745

113. Kaflak-Hachulska, A., Samoson, A., and Kolodziejski, W. (2003) 1H MAS and 1H --> 31P CP/MAS NMR study of human bone mineral. *Calcif Tissue Int* **73**, 476-486
114. Cavanagh, J. (2007) *Protein NMR Spectroscopy: Principles and Practice. 2nd Ed (9780121644918)*, Academic Press
115. Laws, D. D., Bitter, H. M., and Jerschow, A. (2002) Solid-state NMR spectroscopic methods in chemistry. *Angew Chem Int Ed Engl* **41**, 3096-3129
116. Hing, A. W., Vega, S., and Schaefer, J. (1992) Transferred-echo double-resonance NMR. *Journal of Magnetic Resonance (1969)* **96**, 205-209
117. Zhang, X. C., Forster, M. C., Nimerovsky, E., Movellan, K. T., and Andreas, L. B. (2021) Transferred-Rotational-Echo Double Resonance. *The Journal of Physical Chemistry A* **125**, 754-769
118. Hartmann, S. R., and Hahn, E. L. (1962) Nuclear Double Resonance in the Rotating Frame. *Physical Review* **128**, 2042-2053
119. Jaroniec, C. P., Filip, C., and Griffin, R. G. (2002) 3D TEDOR NMR experiments for the simultaneous measurement of multiple carbon-nitrogen distances in uniformly (13)C,(15)N-labeled solids. *J Am Chem Soc* **124**, 10728-10742
120. Joedicke, L., Mao, J., Kuenze, G., Reinhart, C., Kalavacherla, T., Jonker, H. R. A., Richter, C., Schwalbe, H., Meiler, J., Preu, J., Michel, H., and Glaubitz, C. (2018) The molecular basis of subtype selectivity of human kinin G-protein-coupled receptors. *Nat Chem Biol* **14**, 284-290
121. Marchanka, A., and Carlomagno, T. (2019) Chapter Nine - Solid-State NMR Spectroscopy of RNA. in *Methods in Enzymology* (Wand, A. J. ed.), Academic Press. pp 333-371
122. Hu, K. N. (2011) Polarizing agents and mechanisms for high-field dynamic nuclear polarization of frozen dielectric solids. *Solid State Nucl Magn Reson* **40**, 31-41
123. Sauvée, C., Rosay, M., Casano, G., Aussenac, F., Weber, R. T., Ouari, O., and Tordo, P. (2013) Highly efficient, water-soluble polarizing agents for dynamic nuclear polarization at high frequency. *Angew Chem Int Ed Engl* **52**, 10858-10861
124. Unger, T., Jacobovitch, Y., Dantes, A., Bernheim, R., and Peleg, Y. (2010) Applications of the Restriction Free (RF) cloning procedure for molecular manipulations and protein expression. *J Struct Biol* **172**, 34-44
125. Wu, S., and Letchworth, G. J. (2004) High efficiency transformation by electroporation of Pichia pastoris pretreated with lithium acetate and dithiothreitol. *Biotechniques* **36**, 152-154
126. Krettler, C., Reinhart, C., and Bevans, C. G. (2013) Expression of GPCRs in Pichia pastoris for structural studies. *Methods Enzymol* **520**, 1-29
127. Schägger, H., Cramer, W. A., and von Jagow, G. (1994) Analysis of molecular masses and oligomeric states of protein complexes by blue native electrophoresis and isolation of membrane protein complexes by two-dimensional native electrophoresis. *Anal Biochem* **217**, 220-230

128. Smith, P. K., Krohn, R. I., Hermanson, G. T., Mallia, A. K., Gartner, F. H., Provenzano, M. D., Fujimoto, E. K., Goeke, N. M., Olson, B. J., and Klenk, D. C. (1985) Measurement of protein using bicinchoninic acid. *Anal Biochem* **150**, 76-85
129. Ignjatovic, T., Tan, F., Brovkovych, V., Skidgel, R. A., and Erdös, E. G. (2002) Novel mode of action of angiotensin I converting enzyme inhibitors: direct activation of bradykinin B1 receptor. *J Biol Chem* **277**, 16847-16852
130. Guerfal, M., Ryckaert, S., Jacobs, P. P., Ameloot, P., Van Craenenbroeck, K., Derycke, R., and Callewaert, N. (2010) The HAC1 gene from Pichia pastoris: characterization and effect of its overexpression on the production of secreted, surface displayed and membrane proteins. *Microb Cell Fact* **9**, 49
131. Weiss, H. M., Haase, W., Michel, H., and Reiländer, H. (1995) Expression of functional mouse 5-HT5A serotonin receptor in the methylotrophic yeast Pichia pastoris: pharmacological characterization and localization. *FEBS Lett* **377**, 451-456
132. Nehmé, R., Carpenter, B., Singhal, A., Strege, A., Edwards, P. C., White, C. F., Du, H., Grisshammer, R., and Tate, C. G. (2017) Mini-G proteins: Novel tools for studying GPCRs in their active conformation. *PLOS ONE* **12**, e0175642
133. Kruse, A. C., Ring, A. M., Manglik, A., Hu, J., Hu, K., Eitel, K., Hübner, H., Pardon, E., Valant, C., Sexton, P. M., Christopoulos, A., Felder, C. C., Gmeiner, P., Steyaert, J., Weis, W. I., Garcia, K. C., Wess, J., and Kobilka, B. K. (2013) Activation and allosteric modulation of a muscarinic acetylcholine receptor. *Nature* **504**, 101-106
134. Grant, M. P., Stepanchick, A., Cavanaugh, A., and Breitwieser, G. E. (2011) Agonist-driven maturation and plasma membrane insertion of calcium-sensing receptors dynamically control signal amplitude. *Sci Signal* **4**, ra78
135. Brown, E. M., Gamba, G., Riccardi, D., Lombardi, M., Butters, R., Kifor, O., Sun, A., Hediger, M. A., Lytton, J., and Hebert, S. C. (1993) Cloning and characterization of an extracellular Ca(2+)-sensing receptor from bovine parathyroid. *Nature* **366**, 575-580
136. Pidasheva, S., D'Souza-Li, L., Canaff, L., Cole, D. E., and Hendy, G. N. (2004) CASRdb: calcium-sensing receptor locus-specific database for mutations causing familial (benign) hypocalciuric hypercalcemia, neonatal severe hyperparathyroidism, and autosomal dominant hypocalcemia. *Hum Mutat* **24**, 107-111
137. Lee, S. C., Knowles, T. J., Postis, V. L., Jamshad, M., Parslow, R. A., Lin, Y. P., Goldman, A., Sridhar, P., Overduin, M., Muench, S. P., and Dafforn, T. R. (2016) A method for detergent-free isolation of membrane proteins in their local lipid environment. *Nat Protoc* **11**, 1149-1162
138. Denisov, I. G., and Sligar, S. G. (2016) Nanodiscs for structural and functional studies of membrane proteins. *Nat Struct Mol Biol* **23**, 481-486
139. Gao, Y., Robertson, M. J., Rahman, S. N., Seven, A. B., Zhang, C., Meyerowitz, J. G., Panova, O., Hannan, F. M., Thakker, R. V., Bräuner-Osborne, H., Mathiesen, J. M., and Skiniotis, G. (2021) Asymmetric activation of the calcium-sensing receptor homodimer. *Nature* **595**, 455-459
140. Geng, Y., Mosyak, L., Kurinov, I., Zuo, H., Sturchler, E., Cheng, T. C., Subramanyam, P., Brown, A. P., Brennan, S. C., Mun, H. C., Bush, M., Chen, Y., Nguyen, T. X., Cao, B., Chang, D. D., Quick, M., Conigrave, A. D., Colecraft, H. M., McDonald, P., and

Fan, Q. R. (2016) Structural mechanism of ligand activation in human calcium-sensing receptor. *Elife* **5**

141. Scheerer, P., Park, J. H., Hildebrand, P. W., Kim, Y. J., Krauss, N., Choe, H. W., Hofmann, K. P., and Ernst, O. P. (2008) Crystal structure of opsin in its G-protein-interacting conformation. *Nature* **455**, 497-502
142. Flock, T., Ravarani, C. N. J., Sun, D., Venkatakrishnan, A. J., Kayikci, M., Tate, C. G., Veprintsev, D. B., and Babu, M. M. (2015) Universal allosteric mechanism for Gα activation by GPCRs. *Nature* **524**, 173-179
143. Venkatakrishnan, A. J., Deupi, X., Lebon, G., Heydenreich, F. M., Flock, T., Miljus, T., Balaji, S., Bouvier, M., Veprintsev, D. B., Tate, C. G., Schertler, G. F., and Babu, M. M. (2016) Diverse activation pathways in class A GPCRs converge near the G-protein-coupling region. *Nature* **536**, 484-487
144. Lee, E., Linder, M. E., and Gilman, A. G. (1994) Expression of G-protein alpha subunits in Escherichia coli. *Methods Enzymol* **237**, 146-164
145. Mou, T. C., Gille, A., Suryanarayana, S., Richter, M., Seifert, R., and Sprang, S. R. (2006) Broad specificity of mammalian adenylyl cyclase for interaction with 2',3'-substituted purine- and pyrimidine nucleotide inhibitors. *Mol Pharmacol* **70**, 878-886
146. Noel, J. P., Hamm, H. E., and Sigler, P. B. (1993) The 2.2 A crystal structure of transducin-alpha complexed with GTP gamma S. *Nature* **366**, 654-663
147. Coleman, D. E., Berghuis, A. M., Lee, E., Linder, M. E., Gilman, A. G., and Sprang, S. R. (1994) Structures of active conformations of Gi alpha 1 and the mechanism of GTP hydrolysis. *Science* **265**, 1405-1412
148. Carpenter, B., and Tate, C. G. (2016) Engineering a minimal G protein to facilitate crystallisation of G protein-coupled receptors in their active conformation. *Protein Eng Des Sel* **29**, 583-594
149. Pfeffer, M. A. (1993) Angiotensin-converting enzyme inhibition in congestive heart failure: Benefit and perspective. *American Heart Journal* **126**, 789-793
150. MADRID, A. H., PENG, J., ZAMORA, J., MARÍN, I., BERNAL, E., ESCOBAR, C., MUÑOS-TINOCO, C., REBOLLO, J. M. G., and MORO, C. (2004) The Role of Angiotensin Receptor Blockers and/or Angiotensin Converting Enzyme Inhibitors in the Prevention of Atrial Fibrillation in Patients with Cardiovascular Diseases. *Pacing and Clinical Electrophysiology* **27**, 1405-1410
151. Heart Outcomes Prevention Evaluation Study, I., Yusuf, S., Sleight, P., Pogue, J., Bosch, J., Davies, R., and Dagenais, G. (2000) Effects of an angiotensin-converting-enzyme inhibitor, ramipril, on cardiovascular events in high-risk patients. *The New England journal of medicine* **342**, 145-153
152. Lever, A. F., Hole, D. J., Gillis, C. R., McCallum, I. R., McInnes, G. T., MacKinnon, P. L., Meredith, P. A., Murray, L. S., Reid, J. L., and Robertson, J. W. K. (1998) Do inhibitors of angiotensin-I-converting enzyme protect against risk of cancer? *The Lancet* **352**, 179-184
153. Burch, R. M., and Kyle, D. J. (1992) Recent developments in the understanding of bradykinin receptors. *Life Sciences* **50**, 829-838
154. Chen, J. J., and Johnson, E. J. (2007) Targeting the bradykinin B1 receptor to reduce pain. *Expert Opinion on Therapeutic Targets* **11**, 21-35

155. Argañaraz, G. A., Silva, J. A., Jr., Perosa, S. R., Pessoa, L. G., Carvalho, F. F., Bascands, J. L., Bader, M., da Silva Trindade, E., Amado, D., Cavalheiro, E. A., Pesquero, J. B., and da Graça Naffah-Mazzacoratti, M. (2004) The synthesis and distribution of the kinin B1 and B2 receptors are modified in the hippocampus of rats submitted to pilocarpine model of epilepsy. *Brain Res* **1006**, 114-125
156. Perosa, S. R., Argañaraz, G. A., Goto, E. M., Costa, L. G. P., Konno, A. C., Varella, P. P. V., Santiago, J. F. C., Pesquero, J. B., Canzian, M., Amado, D., Yacubian, E. M., Carrete Jr., H., Centeno, R. S., Cavalheiro, E. A., Silva Jr., J. A., and Mazzacoratti, M. d. G. N. (2007) Kinin B1 and B2 receptors are overexpressed in the hippocampus of humans with temporal lobe epilepsy. *Hippocampus* **17**, 26-33
157. Sawutz, D. G., Salvino, J. M., Dolle, R. E., Seoane, P. R., and Farmer, S. G. (1995) Pharmacology and structure--activity relationships of the nonpeptide bradykinin receptor antagonist WIN 64338. *Can J Physiol Pharmacol* **73**, 805-811
158. Gaudron, P., Kugler, l., Hu, K., Fraccarollo, D., Bauer, W., Eilles, C., and Ertl, G. (2000) Effect of quinapril initiated during progressive remodeling in asymptomatic patients with healed myocardial infarction. *The American Journal of Cardiology* **86**, 139-144
159. Powell, J. S., Clozel, J. P., Muller, R. K., Kuhn, H., Hefti, F., Hosang, M., and Baumgartner, H. R. (1989) Inhibitors of angiotensin-converting enzyme prevent myointimal proliferation after vascular injury. *Science* **245**, 186
160. Ignjatovic, T., Tan, F., Brovkovych, V., Skidgel, R. A., and Erdös, E. G. (2002) Activation of bradykinin B1 receptor by ACE inhibitors. *Int Immunopharmacol* **2**, 1787-1793
161. Hershfinkel, M. (2018) The Zinc Sensing Receptor, ZnR/GPR39, in Health and Disease. *Int J Mol Sci* **19**
162. Müller, A., Kleinau, G., Piechowski, C. L., Müller, T. D., Finan, B., Pratzka, J., Grüters, A., Krude, H., Tschöp, M., and Biebermann, H. (2013) G-Protein Coupled Receptor 83 (GPR83) Signaling Determined by Constitutive and Zinc(II)-Induced Activity. *PLOS ONE* **8**, e53347
163. Huang, X. P., Kenakin, T. P., Gu, S., Shoichet, B. K., and Roth, B. L. (2020) Differential Roles of Extracellular Histidine Residues of GPR68 for Proton-Sensing and Allosteric Modulation by Divalent Metal Ions. *Biochemistry* **59**, 3594-3614
164. Holst, B., Egerod, K. L., Schild, E., Vickers, S. P., Cheetham, S., Gerlach, L.-O., Storjohann, L., Stidsen, C. E., Jones, R., Beck-Sickinger, A. G., and Schwartz, T. W. (2007) GPR39 Signaling Is Stimulated by Zinc Ions But Not by Obestatin. *Endocrinology* **148**, 13-20
165. Swaminath, G., Steenhuis, J., Kobilka, B., and Lee, T. W. (2002) Allosteric modulation of beta2-adrenergic receptor by Zn(2+). *Mol Pharmacol* **61**, 65-72
166. Huang, X. P., Karpiak, J., Kroeze, W. K., Zhu, H., Chen, X., Moy, S. S., Saddoris, K. A., Nikolova, V. D., Farrell, M. S., Wang, S., Mangano, T. J., Deshpande, D. A., Jiang, A., Penn, R. B., Jin, J., Koller, B. H., Kenakin, T., Shoichet, B. K., and Roth, B. L. (2015) Allosteric ligands for the pharmacologically dark receptors GPR68 and GPR65. *Nature* **527**, 477-483
167. Lin, P.-H., Sermersheim, M., Li, H., Lee, P. H. U., Steinberg, S. M., and Ma, J. (2018) Zinc in Wound Healing Modulation. *Nutrients* **10**, 16

168. Pinto, B., Jadhav, U., Singhai, P., Sadhanandham, S., and Shah, N. (2020) ACEI-induced cough: A review of current evidence and its practical implications for optimal CV risk reduction. *Indian Heart J* **72**, 345-350
169. Becker-Baldus, J., Bamann, C., Saxena, K., Gustmann, H., Brown, L. J., Brown, R. C., Reiter, C., Bamberg, E., Wachtveitl, J., Schwalbe, H., and Glaubitz, C. (2015) Enlightening the photoactive site of channelrhodopsin-2 by DNP-enhanced solid-state NMR spectroscopy. *Proceedings of the National Academy of Sciences of the United States of America* **112**, 9896-9901
170. Maciejko, J., Mehler, M., Kaur, J., Lieblein, T., Morgner, N., Ouari, O., Tordo, P., Becker-Baldus, J., and Glaubitz, C. (2015) Visualizing Specific Cross-Protomer Interactions in the Homo-Oligomeric Membrane Protein Proteorhodopsin by Dynamic-Nuclear-Polarization-Enhanced Solid-State NMR. *Journal of the American Chemical Society* **137**, 9032-9043
171. Mak-Jurkauskas, M. L., Bajaj, V. S., Hornstein, M. K., Belenky, M., Griffin, R. G., and Herzfeld, J. (2008) Energy transformations early in the bacteriorhodopsin photocycle revealed by DNP-enhanced solid-state NMR. *Proceedings of the National Academy of Sciences of the United States of America* **105**, 883-888
172. Lehnert, E., Mao, J., Mehdipour, A. R., Hummer, G., Abele, R., Glaubitz, C., and Tampé, R. (2016) Antigenic Peptide Recognition on the Human ABC Transporter TAP Resolved by DNP-Enhanced Solid-State NMR Spectroscopy. *Journal of the American Chemical Society* **138**, 13967-13974
173. Kaplan, M., Cukkemane, A., van Zundert, G. C., Narasimhan, S., Daniëls, M., Mance, D., Waksman, G., Bonvin, A. M., Fronzes, R., Folkers, G. E., and Baldus, M. (2015) Probing a cell-embedded megadalton protein complex by DNP-supported solid-state NMR. *Nature methods* **12**, 649-652

Acknowledgments

I take this opportunity to thank the people who are directly and indirectly support me in my Ph.D. project. This part consists of my sincere gratitude to all the people, who were part of my Ph.D. journey and make it more memorable. Without these people, I couldn't imagine my Ph.D. work being possible.

First and foremost, I would like to thank Prof. Dr. h.c. Hartmut Michel for giving me this amazing opportunity to work under his supervision and allowing me to finish my Ph.D. under his guidance. He allowed me to work on these challenging and demanding projects, which help me grow both scientifically and intellectually. He provided me the freedom to carry out my own scientific research projects and support me with every scientific decision (whether it's bad or good), and for that, I am grateful. The superb research atmosphere and friendly colleagues who help me to broaden my scientific horizon, which allowed me to grow as a researcher. During my course of Ph.D. in MPI biophysics, I met so many great researchers, who strongly motivated me for my future adventure. Despite his busy schedule, he was always available for scientific discussions. I considered the last few years I spent learning under Prof. Michel's supervision as the golden period of my scientific career.

Secondly, I will also like to express my greatest gratitude to Prof. Dr. Clemens Glaubitz for accepting to register and review my dissertation as my university supervisor. I am very thankful to him for his fruitful collaboration and discussion during my Ph.D. projects.

I am very thankful to Gabi Maul, who helped me with the insect cell (*Sf9*) culture and baculovirus expression system. She was always there for any problems that occurred in the lab. Many thanks to her for all the fantastic technical support during my work.

Many thanks to Dr. Christoph Krettler and Dr. Christoph Reinhart for their help and guidance during the initial stage of my Ph.D. thesis dissertation. I am very grateful for their constant

support and valuable input throughout my dissertation. They helped me with pichia culture as well as introduced me to membrane proteins. I learned many things from them, which will be super helpful in the future. I wish both of them the best and good luck in their future endeavors.

I would like to especially thank Dr. Jiafei Mao for all the DNP-ssNMR measurements and all the fruitful discussions. He played a crucial role in my Ph.D. project. His guidance in both scientific writing and the art of figure-making helped me a lot to grow as a researcher. All the valuable discussions with him regarding science and GPCRs, assists me to grow both scientifically as well as intellectually. Without his encouragement and support throughout my project, it could have been difficult to finish my thesis successfully. I am really grateful and wish him all the best for his future challenges.

I am thankful to the MMB department technical support team including Sabine Buschmann, Cornelia Münke, Hannelore Müller, and Gabriele Maul for their constant love and support. My sincere gratitude to Sabine Buschmann for her unconditional support during my Ph.D. work—both personally and scientifically. I will always remember all the long evening conversations we had about everything including science, non-science, life, politics, snow, and Christmas.

I gratefully acknowledge Birgit Wolff and the media kitchen staff for providing the media for cell culture.

I am truly grateful to Sabine M. Schleker and Tejaswi Kalavacharla for our valuable discussions and the friendly atmosphere at our lab. I will also thank other friends and colleagues like Radhika Khera, Dr. Di Wu, Dr. Jiangfeng Zhao, and Dr. Tamara Grund for all the scientific discussions and coffee breaks. Daily laboratory work may be really frustrating, and stressful therefore I am very thankful to them for all their support. I will also thank my collaborator Samuel Sedl from prof. Glaubitz lab for the solid-state NMR project.

I am grateful to all the new and old members of the Molecular membrane biology department for a friendly and supportive working environment in the lab.

I will also like to thank my friends outside MPI-biophysics like Vijay, Arnab, Praveen, Madhav, Arka, Dushyant, Ayon, and Veera for helping me in surviving during my stressful Ph.D. project life in Frankfurt. I feel fortunate to have met so many wonderful people throughout this time. I will never forget the get-togethers and weekend parties.

Finally, my deepest gratitude to my family members for their unconditional love, support, and guidance throughout my life. I am at a loss for words to thank my parents for their love and emotional support.

Maybe I forgot to mention some important people's names in my acknowledgment, I am really grateful to everyone who has been part of my Ph.D. journey. Thanks a lot to all of you for your kind support and helps.

Thank you so much.

Curriculum Vitae (CV)